Department of Computing

Study of Executive Attention Network using EEG Coherency: A Data-Driven Approach

Tahani A. A. Almabruk

This thesis is presented for the Degree of
Doctor of Philosophy
of
Curtin University

March 2017

Declaration

To the best of my knowledge and belief this thesis contains no material previously published by any other person except where due acknowledgment has been made.

This thesis contains no material which has been accepted for the award of any other degree or diploma in any university.

Signature:

Date: 1.1031.2017.....

Acknowledgements

Firstly, I would like to thank Allah who is the most beneficent and merciful for his blessings to let me completing this thesis. Secondly, it is a great pleasure to thank those who made this research work possible.

I owe my deepest gratitude to my supervisor Dr Tele Tan for his excellent supervision and continuous encouragement throughout the period of this work. I deeply appreciate him for the great support, help and guidance. I also like to appreciate the contribution of my co-supervisor Dr Masood Khan who was always ready to help in times of needs.

I would like to take this opportunity to offer my regards to my family and friends. To my wonderful parents, Almabruk Akream and Akhoera Mohammed, and all my siblings who supported me throughout my PhD studies.

Finally, I would like to thank Professor Mike Anderson, School of Psychology and Exercise Science, Murdoch University, Dr Allison Fox, School of Psychology, University of Western Australia and Professor Corinne Reid, School of Psychology and Exercise Science, Murdoch University for giving me access to the EEG data.

Abstract

In cognitive studies, executive attention is a function that deals with monitoring and resolving a conflict. It is characterised by the ability of concentrating on a particular stimulus and ignoring the surrounding environment. Blocking the distracting information is a required task for response regulation, planning and decision-making. Thus, the study of executive attention has been one of the important research areas in assessing human cognition because its value lies in the discovery of specific biomarkers to identify an abnormality or deficit with pathological populations.

Behavioural metrics including: task accuracy, stimuli recognition, and reaction time show dramatic changes over childhood. In psychology, conflict-related changes in the reaction time (RT) is commonly used to determine the efficiency of the executive attention. In this thesis, we introduce a data-driven approach to detect and localise the conflict process. It utilises Electroencephalography (EEG) coherency analysis as a measure of brain connectivity. EEG coherency quantifies the connectivity between EEG electrode pairs as a function of frequency. The proposed method assesses EEG coherency at two different conditions, which are either with or without the presence of task conflicts. It evaluates and localises the variation in the coherency between these two conditions using an accumulation procedure. In addition, it uses statistical tests to validate the achieved results. Thereafter, coherency measures are passed to a set of the most plausible classifiers in order to examine the power of machine learning algorithms in detecting differences in patterns within the network connectivity with respect to the induced conflict.

We relied on one of the popular theories in neuroscience, which emphasises the relationship between brain regions' integration and cognition. This would allow the further understanding of the relationships between activity in certain brain regions and the specific executive cognitive functions. The bridging of these is important to underpin research in neuro-engineering, cognitive psychology and neuro-rehabilitation.

Measuring the executive attention using this data-driven approach is less expensive compared with other techniques (e.g. ANT). It requires only recording EEG data while performing a task with two different level of difficulties. This technique shows significant results, which to some extent matches the previous reported findings. The results show the capability of EEG coherency in detecting changes in the activity of brain regions regarding the conflict process. Moreover, they show that EEG coherency can be a good data source for classifying brain network connectivity.

List of Peer-Reviewed Publications

Part of the thesis work has been published as listed below.

[1] T. Almabruk, K. K. Iyer, T. Tan, G. Roberts, and M. Anderson, "Investigating Response Conflict Processes in 7 and 9-Year Old Children: An EEG study Using Coherence", in *IEEE Int. Conf. Digital Signal Proc*, Singapore, 2015, pp.813-817.

[2] T. Almabruk, K. K. Iyer, T. Tan, G. Roberts, and M. Anderson, "An EEG Coherence-Based Analysis Approach for Investigating Response Conflict processes in 7 and 9-Year Old Children", in *37th Annu. Int. Conf. IEEE Eng. Med. Bio. Soc. (EMBC)*, Milan, Italy, 2015, pp. 2884-2887.

[3] T. Almabruk, K. K. Iyer, S. Girdler, M. Khan, and T. Tan, "Response Conflict Processes' Classification in 7 and 9-Year Old Children Using EEG Brain Connectivity Measures", in *38th Annu. Int. Conf. IEEE Eng. Med. Bio. Soc. (EMBC)*, Florida, USA, 2016, pp. 704-707.

Contents

List of Figures

List of Tables

Acronyms

ACC	Anterior Cingulate Cortex
ADHD	Attention Deficit/Hyperactivity Disorder
ANT	Attention Networks Task
ASD	Autism Spectrum Disorder
BOLD	Blood-Oxygen-Level Dependent
CBF	Cerebral Blood Flow
EAN	Executive Attention Network
EEG	Electroencephalography
EFs	Executive Functions
ERPs	Event-related potentials
fMRI	functional Magnetic Resonance Imaging
GS	Generalised Synchronisation
ICA	Independent Component Analysis
KDD	Knowledge Discovery from Data
MEG	Magnetoencephalography
ML	Machine Learning
MLP	Multilayer Perceptron
PFC	Prefrontal Cortex
PLV	Phase Locking Value
RT	Reaction Time

SQUID Superconducting Quantum Interference Device

SVMs Support Vector Machines

Chapter 1

Introduction

In the study of brain, there has been a growing interest in investigating cognitive changes that occur in human abilities. Executive attention (cognitive control) is one of the cognitive abilities that is subject to major changes from infancy to late childhood [1]. It describes the attention to a particular part of a stimulus and deals with conflict among competing responses, regulation of thoughts, and emotions [2]. To some extent, it is associated with the executive functions (EFs) which include planning, inhibition, working memory, etc. [3] [4]. The executive attention component was found to be disrupted in many childhood disorders, such as attention deficit/hyperactivity disorder (ADHD), Autism Spectrum Disorder (ASD), obsessive compulsive disorder, and Tourette's syndrome. Therefore, it has become very important topic that received a great deal of research attention [5].

A variety of neurocognitive models and conceptual frameworks were developed to study executive attention. They all relied on inducing conflict among stimuli, responses, or stimulus-to-response mapping [6]. Among these models, Attention Networks Task (ANT) can be regarded as the most popular tool in this area [7]. It has revealed significant information on the development of the conflict process [8] [9]. The ANT measures the efficiency of executive attention as a conflict score by comparing the behavioural data of an incongruent stimulus (i.e. involving a conflict) to that of a congruent stimulus (i.e. involving no conflict). However, when there is a need to study the neuroanatomy of executive attention, the ANT model alone is not

sufficient. Because of this, it is very common in the literature to use the ANT model with either neuroimaging or electrophysiological techniques [10].

In neuroimaging studies, a two-stage process is suggested for resolving the induced conflict [2]. In the first stage (conflict monitoring), the conflict is detected and its difficulty level is evaluated. This process is associated with an activity in the Anterior Cingulate Cortex (ACC). In the second stage (conflict resolving), the conflict is resolved based on the information detected in the earlier stage. This process is associated with an activity in the lateral Prefrontal Cortex (PFC). However, the ACC and the PFC are not the only regions activated by executive attention [11]. Where performing any task was shown to activate multiple regions of the brain[12] [13]. Therefore, effective integration among these regions is assumed for successful task performance. A more comprehensive study has become possible after electroencephalography (EEG) was invented in 1929 by Prof. Hans Berger [14] [15].

EEG is a high-temporal-resolution technique for measuring the brain's electrical signals [16] [17]. It directly captures brain activity throughout both hemispheres by placing an electrode cap on the scalp. The use of EEG in research is more advantageous than other techniques (i.e. functional Magnetic Resonance Imaging (fMRI), Positron Emission Tomography (PET) and Magnetoencephalography (MEG)) for studying brain interactions because it is non-invasive, portable and less expensive.

Event-related potentials (ERPs) are now one of the important EEG areas in intensive brain studies. The ERPs are small changes in the neural activities that occur in tens to hundreds of milliseconds regarding a particular event [18] [16]. In terms of studying the conflict, a number of ERP studies have been conducted on adults [2] [19] [20]. They have associated a particular component of the ERPs called N2 with executive attention. N2 was found to be larger in the frontal and parietal leads when conflict is induced. Although children have not been targeted by many ERP studies, a consistent decline in the conflict level was detected as they mature.

In this thesis, we introduce the use of brain functional connectivity in assessing and localising the cognitive conflict. This approach depends on the same base as the ANT

model in comparing a stimulus's response that induces a conflict to a stimulus's response that does not induce a conflict. The significance of this approach relies on the modern theories of brain function, which suggest that cognition is based on the integration of cerebral areas which can be measured by assessing brain connectivity. As a part of brain connectivity studies, functional connectivity concerns examining the correlation among different regions in the cortex [12] [21] [22] [23] [24] [25].

Coherency is the most commonly used method to determine the synchronisation between two signals. It is a function of frequency that generates a complex value [26]. Two different quantities can be derived from the coherency function. The first is called coherence or magnitude-squared coherence. This quantity has been widely used in the literature to differentiate between normal subjects regarding gender and handedness, etc. (e.g. [27], [28], [29]), and between experimental and normal populations (e.g. [30], [31], [32], [27]). In addition, a number of EEG coherence studies have targeted brain cognition and development (e.g. [33], [34]).

The second quantity is called the imaginary part of coherency and was introduced in [35]. It was proposed to substitute for the coherence because of its power to eliminate the effect of volume conduction. For example, it was found to be successful in presenting clear differences in the cortical synchronisation between autistic and control children in [26] and detecting eloquent regions in patients with tumors in [22].

This thesis explores the use of these two quantities of coherency analysis in studying the cognitive conflict. First, a new method is introduced for evaluating and localising the conflict-related changes in the network connectivity of a group of subjects. Second, the results of the proposed method are statistically validated. We further investigate how effective the classification learning algorithms are in discriminating among the assessed coherency values.

This research is a longitudinal analysis of two EEG datasets of healthy children. The sets were provided by the Neurocognitive Development Unit at the University of Western Australia. The first dataset was collected from the seven-year-old children while performing two stimuli types of Flanker task (i.e. an experimental paradigm for assessing attention). Two years later, the experiment was repeated on the same group

in order to collect the second dataset (at nine years of age). This work relied on several hypotheses, as follows.

1.1 Aims and Hypotheses

Aim 1: Investigating the capability of coherency analysis for capturing changes in brain synchronisation regarding the cognitive conflict; and assessing and localising the conflict across a group of subjects.

Hypothesis 1: Performing a task stimulus that induces conflict causes different changes in brain network connectivity compared to a non-conflict stimulus type.

Hypothesis 2: Conflict level and topography can be assessed by evaluating conflict-related changes in the EEG coherency.

Aim 2: Investigating the use of classification algorithms in categorising coherency values.

Hypothesis 3: The classifiers can distinguish the conflict's effect on brain synchronisation as measured by coherency.

Hypothesis 4: Performing the classification process on the coherency data of different age groups can provide insights into the well-known decline in cognitive conflict.

Hypothesis 5: In terms of categorising coherency data based on age group, implementing the classifiers on coherency data that assess brain synchronisation at conflict task condition will produce better accuracy than that assess brain synchronisation at non-conflict task condition.

1.2 Significance and Contribution

A new approach for studying the function of executive attention and identifying its topography is introduced. The proposed approach is advantageous because it uses the same fundamental base as the ANT model, which is comparing conflict and non-

conflict-related changes. However, no additional neuroimaging or electrophysiological technique is needed to identify the associated cortex regions as with the ANT model. In the current work, the proposed approach was able to detect and localise conflict-related changes in the network connectivity of two age groups (seven- and nine-years-old). The achieved results match the findings of the ANT model in terms of the decline that occurs in the conflict level after seven years of age.

Identifying such particular regions of the brain's neural connectivity, which are associated with solving the problem of cognitive conflict, could result not only in a basic understanding of how the brains of healthy children interact when responding to tasks that elicits executive attention function, but also in the development of specific biomarkers that could aid in the early diagnosis of a number of disorders such as Attention Deficit Hyperactivity Disorder (ADHD) and Autism Spectrum Disorder (ASD). In addition, it could provide a quantitative means of measuring and monitoring the condition while patients are undergoing treatment or using medications.

1.3 Thesis Outline

The thesis is organised as follows.

Chapter 2 provides brief background information on the cognition in human. In particular, it gives details on the function of executive attention and how the ANT model can assess it. Brief background on functional neuroimaging techniques and functional connectivity measures are presented as well. Finally, it considers classification algorithms.

Chapter 3 proposes a new method to detect and localise conflict-related changes in the coherence values across a group of subjects. The achieved results are then statistically validated.

Chapter 4 is a continuation of the study begun in Chapter 3. It investigates the efficiency of the imaginary component of coherency in eliminating volume conduction in the connectivity assessment. It provides information about imaginary coherence and follows the exact same analysing procedure as coherence in Chapter 3.

Chapter 5 proposes mining the coherency data (coherence and the imaginary part of coherency) obtained in Chapters 3 and Chapter 4 in order to obtain meaningful features. Two different experiments are conducted using classification algorithms to investigate the best coherency data, which can be used to discriminate between different network connectivity.

Chapter 6 summarises the research and outlines recommendations for future work.

Chapter 2

Background

As the human brain is the most complicated system in the universe, its anatomy and cognitive functions have been targeted by researchers for investigation [36]. Cognition study is a challenging area of research, which can provide us with knowledge of how the brain deals with our different abilities, such as thinking, talking, remembering, and reasoning. In particular, these cognitive processes are subjected to age-related changes. In the field of developmental psychology, researchers concentrate on studying age-related changes in experience and behaviour [37]. They are concerned with investigating, describing, and explaining the development that occurs from early childhood though adulthood.

The psychologist Jean Piaget made one of the most important contributions to the science of developmental psychology. [38]. The Piaget theory suggested that children's cognitive abilities and critical thinking skills develop at a rapid rate following infancy and in late childhood [39]. This developmental process is defined in four major stages according to approximate age ranges. The sensorimotor stage comprises children from birth to two years of age. In this period, the child depends on his physical interactions with the surrounding environment to construct practical knowledge. The preoperational stage comprises children from two to six years of age. Here, the child begins to learn how to speak a language. However, Piaget observed that the child is not yet able to use the knowledge that was constructed in the sensorimotor stage. The concrete operations stage comprises children from six to 12 years of age. During this stage, the child can perform several operations, such as classification and ordering of different subjects. Additionally, he forms critical abilities to logically and progressively improve in conceptualizing concrete issues.

The formal operations stage comprises children from 12 to 18 years old. This stage is known also as the hypothetical-deductive operations stage where the child becomes capable of dealing with hypotheses. Therefore, development is observed at the level at which the child thinks about abstract concepts.

Attention is one of the major cognitive processes, which are known as executive functions (EFs), such as planning, working memory, and inhibition. These functions underlie our awareness of the surrounding complex environment, our feelings, and our voluntary regulation of thoughts [40]. Attention is widely studied in research to determine human cognitive development [41]. However, in the literature, the study of attention has no unified construct; there is disagreement about whether to consider attention as a single issue or as multiple issues. Because of this, attention has been investigated from different cognitive perspectives. For example, it has been studied in terms of its role in detecting changes that occur under varied conditions in the visual scene where children were found to be less efficient than young adults in detecting the changes in an object's colour. However, as reported in [42], visual change detection is a challenging task even for adults.

Another type of developmental study investigated the amount of time required to shift attention from one object to another, such as is shown in [43]. The reported results revealed differences in the recovery time between two groups of school-aged children (from seven to 22 years of age). The first group was younger than 14 years of age; the second group was older than 14 years of age. The children of the first group had a longer recovery time compared to the children of the second group.

2.1 Executive Attention Network

Michael Posner, one of the founders of the field of cognitive neuroscience [44], has proposed a different approach to studying attention. He suggested that attention is a separate anatomical system that is interrelated with the other regions of the brain [45]. This system consists of different anatomical networks distinguished as three subsystems.

The alerting network involves the frontal and parietal regions of the right hemisphere [46] [47]. It is responsible for producing and maintaining the alert state. The orienting network involves regions in the parietal and frontal lobes [48]. It is responsible for selecting information from sensory input. The executive network (executive control) involves the midline frontal areas (anterior cingulate) and the lateral prefrontal cortex [49] [50]. It is responsible for detecting and resolving conflict among competing responses.

In developmental studies, these three networks have demonstrated different maturational rates [8], where marked development in the alerting network was not observed (particularly between the ages of six to 10 years) before adulthood. While in the orienting network, despite some results that were reported on the early development that takes place before the age of six as in [51] and [52], no improvement was detected in the children from age six to adulthood.

On the other hand, the executive attention network (EAN) shows a more progressive development process starting from infancy (i.e., about the end of the first year of life) to adolescence [8]. Significant changes in the EAN were observed earlier in children between two and three years of age [53]. This development continues up to age seven where the conflict level was found to be decreased at age nine compared to age seven [8] [54]. The EAN development during this period (from about the end of the first year of life to age seven) [9] was found to match the evolution process that is suggested for the fronto-parietal functional connectivity (part of the EAN) [55].

Recently, there has been an increase in research concerning the role of the executive attention process in children's school competence and socialisation, such as [56], [57], and [58]. For example, in [56], questionnaires on temperament, schooling skills, and social status were completed in a school by 69 children who were age 12. Then, they performed the Attention Networks Task (ANT) to assess the executive attention. The results revealed that children with high efficiency of executive attention show better academic outcomes, particularly in mathematics. In addition, the study showed that the executive attention plays an important role in the child's learning and social adjustment at school.

Checa and Rueda in [59] examined brain interaction, which was measured using event-related potentials (ERPs), by performing a combined Flanker-Go/No-Go task (i.e., induces a conflict). They targeted 37 children of 12 years of age. The results showed a level of relationship between the ERPs amplitude and children's performance in mathematics. The ERPs were found to be a significant predictor of grades as a higher or lower general level of intelligence.

Many psychological tasks were introduced to study the efficiency of executive attention. They all rely on the same idea of inducing a conflict. For example in Flanker task (i.e. one of the most common tasks used in this area) [60], the target stimulus is flanked by distracting information. In the case of congruent stimulus, these distractions point in the direction of the target (no conflict is induced), whereas, in the case of incongruent stimulus, they point in the opposite direction from the target (conflict is induced).

2.2 Attention Networks Task

Recently, the Attention Networks Task (ANT) has become the most widely used strategy to study the EAN [7]. It was designed by Fan et al. [7], who adopted the Posner approach to study attention networks (i.e., alerting, orienting, and executive attention). Assessing the efficiency of executive attention in the ANT model depends on comparing brain interactions at two different conditions of the Flanker task (difficulty level of the incongruent stimulus is higher than that of the congruent stimulus). It is operationalized as a conflict score and estimated as the difference in the reaction time (RT) between congruent and incongruent stimuli. The collected data from each subject is divided into two sets based on the stimulus type, either congruent or incongruent. The median of the subject's RT at each condition is calculated. The mean of the RT at the congruent condition is computed across the subjects. The same process is repeated for the incongruent condition. Subsequently, the conflict score of the age group being considered is computed by subtracting the congruent mean RT from the incongruent mean RT [6] [8] [9].

A child-friendly version of the ANT has been used to study EAN in children [2]. As shown in Fig. 2.1, two types of Flanker stimuli are presented on the screen. The stimulus contains five fish. They are pointing in the same direction as the central fish in the congruent condition, while the flankers are pointing opposite to the central fish in the incongruent condition. In both conditions, the child is instructed to feed the central fish by pressing a key with a compatible direction [10].

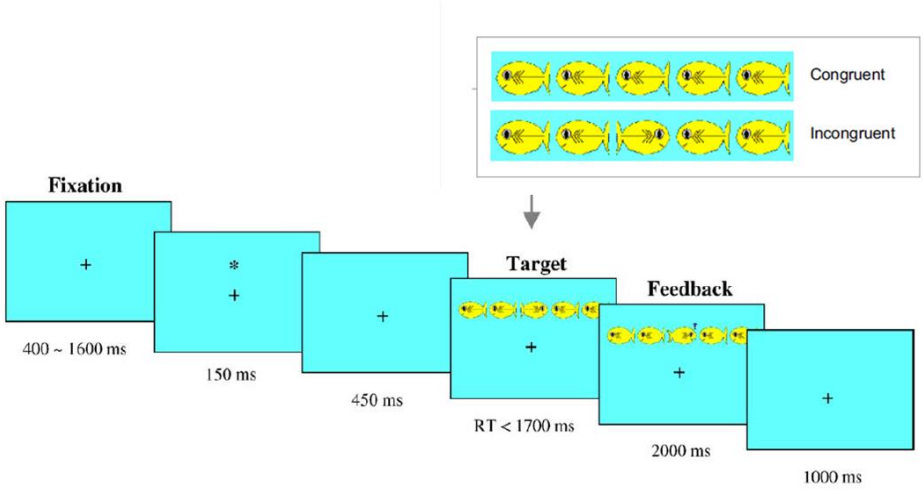

Fig. 2.1 Executive attention trials in the child-friendly version of the ANT [8].

2.3 Functional Neuroimaging Techniques

Non-invasive functional neuroimaging techniques are divided into two classes. First class contains indirect measures of brain function such as functional Magnetic Resonance Imaging (fMRI) and Positron Emission Tomography (PET). They are called hemodynamic techniques because they rely on measuring changes that occur in brain metabolic process. Second class contains direct measures of brain function such as Magnetoencephalography (MEG) and Electroencephalography (EEG). They

are called electro-magnetic techniques because they rely on measuring changes that occur in the neural electromagnetic fields [61].

2.3.1 Functional Magnetic Resonance Imaging

Functional magnetic resonance imaging (fMRI) is a powerful neuroimaging technique with high spatial resolution in localising the neural activity within millimetres. It measures metabolic response via blood oxygenation levels in active neural regions. Where it relies on the fact that when neuronal region is activated, its cerebral blood flow (CBF) increases [62]. fMRI has two principle techniques in mapping the neuronal activity by imaging blood flow-related changes. One is called blood-oxygen-level dependent (BOLD) contrast and the other called dynamic or exogenous technique [63] [64].

2.3.2 Positron Emission Tomography

Positron emission tomography (PET) is nuclear medicine imaging technique that measures blood flow in the brain with a high spatial resolution. It was built on the positron particle, which was discovered in 1928. The positron is a subatomic particle equals in mass and opposite in charge to the electron. It was shown that when positrons collide with electrons they release two photons in almost exactly opposed directions. These photons are picked up by the PET scanner, which then determines where they came from in the brain [65].

2.3.3 Magnetoencephalography

Magnetoencephalography (MEG) is a non-invasive technique for the study of brain function. It has a very high temporal and spatial resolution. MEG measures the magnetic fields that are naturally produced by intracellular postsynaptic currents. These currents are electrically charged ions flow from dendrites to the soma (see Fig. 2.2) [66] [67].

In the modern MEG techniques, several hundred coils (superconducting sensors) called superconducting quantum interference device (SQUID) are used. They are capable in detecting the neuronal magnetic fields in the presence of magnetically shielded room. The shielded room is used to eliminate the effect of the Earth's magnetic field, which is 10 million times larger than the neuronal magnetic field [68].

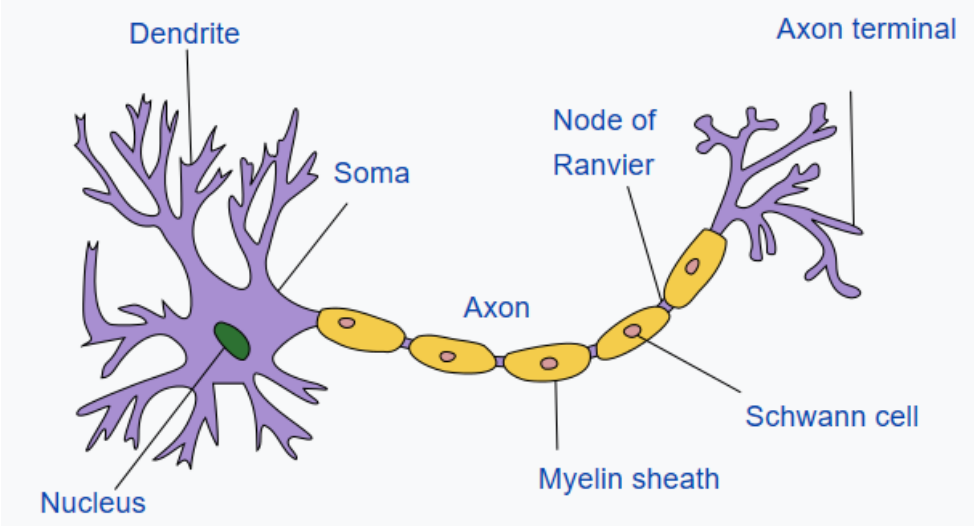

Fig. 2.2 Neuron structure [74].

2.3.4 Electroencephalography

Electroencephalography (EEG) is a high-temporal-resolution technique for measuring the brain's electrical signals. It is portable, non-invasive and less expensive than other techniques (i.e. fMRI, PET and MEG) [16] [17] [69]. EEG is a powerful tool that is very useful in the fields of neurology and clinical neurophysiology because it directly captures brain activity throughout both hemispheres by placing an electrode cap on the scalp's surface [70]. Because of the above mentioned reasons, EEG was chosen to conduct this proposed work.

EEG is generated by the electrical activity of billions of brain neurons. As shown in Fig. 2.2, the neuron structure is divided into three parts: cell body (soma), axon, and

dendrites. Excitation of the cell body produces local current flows along the axon to the synaptic terminal. As the neurons communicate with each other by their dendrites, the currents of large groups of parallel neurons are combined to produce a large electric field that spreads to the scalp's surface and is recordable by the EEG cap electrodes.

EEG, as any other biological signals consists of oscillations. These oscillations represent regular changes in the measured electric potential from the scalp and are called rhythms. EEG rhythms have been the focus of many studies investigating brain dysfunctions. Delta rhythms range from 1 to 4 Hz, theta from 4 to 8 Hz, alpha from 8 to 13 Hz, beta from 13 to 30 Hz, and gamma > 30 Hz. The appearance or the absence of these rhythms depends on the subject's state. For example, delta rhythms appear when the subject is in deep sleep, while theta, alpha, and beta appear when the eyes are closed or the eyes are open when the subject is in a drowsy state, respectively [71].

2.4 Functional Connectivity Analysis

The interest of exploring the complexity of human brain has increased throughout the decades. This interest covers different points of view such as its anatomy, functional connectivity and effective connectivity. In the respect of functional connectivity, the significance of this study underlies on the modern theories of brain function that suggest that human cognition is based on the integration of cerebral areas which can be measured by assessing brain functional connectivity [12] [21] [22] [23] [24] [25].

This approach was initiated in the 1960s and has since attracted the attention of many researchers attempting to achieve a better understanding of brain function integration [72]. In terms of nonlinear interdependency, It has been proven that synchronisation can occur between chaotic systems [73] [74]. This in turn was the principle foundation of the assumption that chaotic systems can be synchronised even if their amplitudes are uncorrelated [75]. The aforementioned assumption is the idea behind introducing two important concepts in the neuroscience studies which are phase synchronisation and generalised synchronisation [76].

On the other hand, many linear connectivity techniques were built on the hypothesis that, EEG signals are linearly dependent. Cross-correlation and coherency are the most common measures in this category. They have shown a great capability in measuring the degree of similarity between EEG signals across a certain range of frequencies [76].

2.4.1 Phase Locking Value

Phase-locking value (PLV) is a nonlinear technique that separates the effect of amplitude and phase in the interrelation between two signals for a given frequency before testing the synchrony hypothesis for brain integration. This measure relies on the fact that coupled chaotic signals can be in phase synchronisation even though their amplitude synchronisation is zero [77] [78]. Its calculation procedure can be described as follows:

1. Extract the frequency of interest by using band-pass filter.
2. Use complex Gabor wavelet centred at frequency of interest to compute the convolution.
3. For the calculated convolution, the phase is extracted for all time-bins t, and for each electrode pair.
4. Take the average of the calculated values from step 3, which is called phase-locking value (PLV).

If PLV is close to 1 then phase difference varies little across the trials. PLV is believed to be a good choice for measuring nonlinear interdependency under the condition of non-stationary [73].

2.4.2 Generalised Synchronisation

Since there is no consensus whether EEG signals are chaotic or not, new approach of measuring synchronisation has been introduced. It is called generalised synchronisation and its underlying idea depends on the capability of signal representation in a phase space to investigate the existence of the nonlinearity characteristics hidden in linear systems [79]. GS deals with non-identical coupled systems and cannot be successful in the case of stationarity [80] [81].

If x and y are two recorded signals, then measuring GS involves the following [82]:

1. Reconstruct delay vectors out of the time serious

   $x_n = (x_n, \ldots, x_{n-(m-1)\tau}), y_n = (y_n, \ldots, y_{n-(m-1)\tau}),$

   where $n = 1, \ldots . N$

   m and τ are the embedding dimension and time lag respectively.

2. Calculate the squared mean Euclidean distance $R_n^{(k)}(X)$ for each x_n .
3. Calculate the conditional mean squared Euclidean distance $R_n^{(k)}(X|Y)$.
4. Calculate interdependence measure by dividing $R_n^{(k)}(X)$ by $R_n^{(k)}(X|Y)$.

GS takes a value between zero (x and y are independent) and one (maximum synchronisation).

2.4.3 Cross-correlation

Cross-correlation modality has been used in investigating brain functional connectivity since 1951. It is principally sensitive to phase and polarity but not to amplitude. Cross-correlation indicates a strong functional relationship when the measured correlation is high. It has been used in several applications such as studying the effect of the drugs and investigating the effect of sensory stimuli on the relation between different cortical regions. [83] [80]. According to [84], the measurement of cross-correlation between two signals can be expressed as follows:

1. Calculate the product of the two signals.
2. Calculate the covariance of the signals, which equals to the average of the calculated product.
3. Calculate the power by dividing the covariance by the square root of the product of the variance of each signal.
4. Repeat the previous steps by making one signal displacement in time with respect to the other by different intervals.
5. Make the covariance independent of the actual amplitude of the signals.
6. Find the maximum of the covariance and specify its displacement, which indicates any time difference between the two signals.

2.4.4 Coherency

Coherency is the measure of interest in this thesis. It is one of the linear dependency techniques which have shown an ability to measure the degree of similarity between EEG signals across a certain frequency range [76]. It is sensitive to both changes in power and changes in phase relationships. Consequently, if either power or phase changes in any one of the signals, the coherency value is affected. The coherency analysis is utilised when the intent is to determine the stability of the relationship between two recording sites, including asymmetries and morphology. As shown in (2.1), coherency is a function of frequency that generates a complex value [26].

$$C_{xy}(f) = \frac{s_{xy}(\mathrm{f})}{\sqrt{s_{xx}(\mathrm{f})\, s_{yy}(\mathrm{f})}}, \qquad (2.1)$$

where s_{xy} is the cross spectrum of signals x and y, while s_{xx} and s_{yy} are the auto spectrum of signals x and y, respectively.

Auto (s_{xx}, s_{yy}) and cross spectrum (s_{xy}) can be estimated by several methods [85]. These methods are classified either as parametric (e.g. Yule-Walker Method, Least Squares Method and Two-Stage Least Squares Method) or non-parametric (e.g. Bartlett Method, Daniell Method and Welch method). The former category is chosen when adequate knowledge on the signals being considered are available otherwise the latter category is chosen. Welch method from the nonparametric category was selected to implement the spectral analysis in the current research.

Welch Method

Welch method is a form of non-parametric method introduced to estimate the spectral power of time series signals. It is based on the concept of splitting the targeted signal to several segments, estimating the power spectrum of each individual segment and then averaging them [86]. It requires less computational expenses compared to the other methods of spectral power estimation. These computations begin with partitioning the signal x to q segments of length M.

$$x_1(t), x_2(t), \ldots\ldots, x_q(t), \qquad t = 0, \ldots M-1 \qquad (2.2)$$

The segments may be sectioned with D overlapping windows.

A window w of length M is applied to this sequence of segments.

$$x_1(t)w(t), x_2(t)w(t), \dots\dots, x_q(t)w(t), \qquad t = 0, \dots M-1 \qquad (2.3)$$

Finite Fourier transform is then applied to each segment to calculate the modified periodogram such as $A_1(n), A_2(n), \dots., A_q(n)$. This is shown in (3.4) below, where $i = \sqrt{-1}$.

$$A_q(n) = \frac{1}{M} \sum_{t=0}^{M-1} x_q(t)w(t)e^{-\frac{2qitn}{M}}, \qquad (2.4)$$

By averaging these q modified periodograms $(A_1(n), A_2(n), \dots., A_q(n))$, power spectra s_{xx} of signal x is then estimated.

The cross-spectrum s_{xy} of two signals x and y is estimated in the same way. After sectioning each signal into a sequence of q segments overlapped by D data points as

$$x_1(t), x_2(t), \dots\dots, x_q(t) \text{ and } y_1(t), y_2(t), \dots\dots, y_q(t), \qquad t = 0, \dots M-1$$

Welch method treats these two sequences as pairs such as $x_q(t), y_q(t)$. Each pair of the segments $x_q(t)$, $y_q(t)$ is windowed by w and Fourier transformed. This subsequently produces q modified cross periodograms which are averaged to achieve the cross-spectra of signals x and y.

2.4.4.1 Coherence

Coherence is the real part of the coherency (i.e. magnitude-squared coherence) (utilised in Chapter 3). It is defined as the modulus of coherency equation (2.1) and it can be calculated as follows [87].

$$Coh_{xy}(f) = \frac{\left|\langle s_{xy}(\mathrm{f})\rangle_z\right|^2}{\langle s_{xx}(\mathrm{f})\rangle_z \langle s_{yy}(\mathrm{f})\rangle_z}, \qquad (2.5)$$

As shown in (2.5), coherence value is calculated by taking the magnitude of the coherency and squaring it. This results in a real value bounded between zero and one; if phase difference $(\theta_x - \theta_y)$ between signals x and y is consistent, coherence function produces a value equal or close to one otherwise it produces a value equal or close to zero.

Coherence Smoothing

In order to calculate the coherence, signals x and y have to be segmented to z epochs. This step is required because of the coherence bias to the epoch count, which can be illustrated as follows. Suppose that, signals x and y are used to calculate the coherence without segmenting them (i.e. one epoch are used from each signal) and the spectral periodograms are estimated by another simple equivalent formula [88]. In this formula, the auto-spectra of signal x is estimated as:

1. Calculating its Fourier transform X(f).
2. Computing the dot product between X(f) and its conjugate X^*(f) as shown below.

$$S_{xx} = X(f).* X^*(f)$$

This can be written as:

$$\begin{aligned} S_{xx} &= (a_1 + ib_1)(a_1 - ib_1) \\ &= a_1^2 + b_1^2 \end{aligned} \tag{2.6}$$

The power spectra of signal y is estimated in the same way:

$$S_{yy} = Y(f).* Y^*(f)$$

$$\begin{aligned} S_{yy} &= (a_2 + ib_2)(a_2 - ib_2) \\ &= a_2^2 + b_2^2 \end{aligned} \tag{2.7}$$

While the cross-spectra is computed as follows:

$$\begin{aligned} \left|S_{xy}(f)\right|^2 &= |X(f).* Y^*(f)|^2 \\ &= |(a_1 + ib_1)(a_2 - ib_2)|^2 \end{aligned}$$

$$= |(a_1a_2 + b_1b_2) - j(a_1b_2 - a_2b_1)|^2$$

$$= (a_1a_2 + b_1b_2)^2 + (a_1b_2 - a_2b_1)^2$$

$$= {a_1}^2{a_2}^2 + {b_1}^2{b_2}^2 + {a_1}^2{b_2}^2 + {a_2}^2{b_1}^2 \quad (2.8)$$

Substituting (2.6), (2.7) and (2.8) to (2.5) we get:

$$Coh_{xy}(f) = \frac{{a_1}^2{a_2}^2 + {b_1}^2{b_2}^2 + {a_1}^2{b_2}^2 + {a_2}^2{b_1}^2}{(a_1^2 + b_1^2)(a_2^2 + b_2^2)}$$

$$= \frac{{a_1}^2{a_2}^2 + {b_1}^2{b_2}^2 + {a_1}^2{b_2}^2 + {a_2}^2{b_1}^2}{a_1^2a_2^2 + b_1^2b_2^2 + a_1^2\,b_2^2 + a_2^2b_1^2}$$

$$= 1 \quad (2.9)$$

As shown in (2.9), coherence measure between any pair of signals always equals to unity when only one epoch from each signal is involved in the calculation. This resulted in recommendations to use epochs count (z) as large as possible [89]. Therefore, when the coh_{xy} is calculated between the segmented (z epochs) signals x and y at frequency f, the auto and cross spectrum are first calculated for each epoch pair (x_i, y_i) where $i = 1,2, \ldots . z$ and then averaged before substituting them into (2.5).

In the literature, coherence can be smoothed across adjacent frequency intervals as well [90]. This technique facilitates representing the correlation of signals x and y of several frequencies $(f_1,\ f_2, \ldots, f_c)$ by individual values.

Coherence Matrix

To study brain interaction changes associated with performing a cognitive task in terms of the network connectivity, coherence has to be estimated for all possible combinations of the recorded EEG signals. If m electrodes were used to record the EEG of subject k, then a network connectivity of $m \times m$ values have to be

investigated. Representing this as a $m \times m$ matrix can facilitate the visualisation and analysis of information related to the network connectivity [16]. Fig.2.3 shows how each electrode pair (x, y) is placed at the corresponding intersected pixel (x, y) in the matrix. For example, the second value located in the first row represents coherence value between EEG signals FP1 and FP2.

In practice, computing the connectivity matrix is restricted to the upper right triangular because of its symmetry to the lower left triangular. In addition, another exclusion is applied to the diagonal elements because coherence measure between any electrode and itself is always equal to one.

	FP1	FP2	PO9	PO10	F7	F3	FZ	...	FT10
FP1	0	0.4773	0.0381	0.0360	0.2824	0.1985	0.3519	...	0.0707
FP2	0	0	0.0116	0.0470	0.1483	0.1022	0.2381	...	0.1308
PO9	0	0	0	0.0434	0.0385	0.0554	0.0286	...	0.0227
PO10	0	0	0	0	0.0472	0.0757	0.0770	...	0.1151
F7	0	0	0	0	0	0.2328	0.1796	...	0.0610
F3	0	0	0	0	0	0	0.6125	...	0.0662
	.	.	.	.	.	.	.	...	.
	.	.	.	.	.	.	.	...	.
	.	.	.	.	.	.	.	...	0.0224
FT10	0	0	0	0	0	0	0	...	0

Fig. 2.3 Illustration of the $m \times m$ connectivity matrix of subject k produced form m channels.

2.4.4.2 Imaginary Part of Coherency

Coherence was the only measure that represented the coherency until 2004, when the imaginary part of coherency (utilised in Chapter 4) was proposed. The calculation of the imaginary component of coherency is very similar to the coherence calculation.

As seen in (2.10), the measure between signals x and y at frequency f is assessed over z epochs. The spectrums s_{xy}, s_{xx}, s_{yy} are calculated for each pair of the segmented epochs as (x_i, y_i) where $i = 1,2, \ldots . z$. Then they are averaged over the z measures before substituting into (2.10). The last step is extracting the imaginary part of the coherency.

$$icoh_{xy}(f) = \text{imag}\left(\frac{\langle s_{xy}(\text{f})\rangle_z}{\sqrt{\langle s_{xx}(\text{f})\rangle_z \langle s_{yy}(\text{f})\rangle_z}}\right), \tag{2.10}$$

2.4.4.3 Coherency Applications

Coherency analysis (i.e. coherence and the imaginary part of coherency) has been developed as an important tool in studying the functional connectivity between EEG signals. It relies on the hypothesis that a high correlation indicates a strong functional relationship between EEG signals [91].

A number of coherence applications have concentrated on differentiating between normal populations regarding gender and handedness, etc. (e.g., [27], [28], and [29]). For instance, in [28], the coherence analysis was calculated for a group of 37 males and 46 females to investigate gender differences. As each gender group comprised dextrals and sinistrals, handedness differences were investigated as well. In terms of gender, females showed higher interhemispheric synchronisation compared to males. The correlation within the right hemisphere at the beta band in the sinistral group was observed to be higher than that in the dextral group.

Coherence has been successful in determining variations in the network connectivity of some neurodevelopmental disorders, such as Autism Spectrum Disorder (ASD). ASD has attracted researchers because it affects social interaction, communication, and behavioural flexibility [92]. Many studies such as [93] and [94] were built on the hypothesis that ASD is a condition of different brain functional connectivity. In [93], EEG coherence was calculated at the delta band for two groups: 10 healthy adults and 10 adults with ASD. Compared to the control subjects, a decrease in the long-distance connections was observed in the ASD subjects, especially in fronto-occipital

connections. Additionally, ASD subjects showed an increase in the short-distance connections (particularly in lateral–frontal electrodes).

A similar experiment was conducted in [94] where functional connectivity was also assessed with EEG coherence between pairs among 18 adults with ASD and 18 control adults in an eyes closed resting state. The results revealed that, in the theta (3–6 Hz) band, high interhemispheric coherence was evident for the ASD group, especially within the left hemisphere frontal and temporal regions. In the alpha band (8–10 Hz), low intrahemispheric coherence was evident for the ASD group within the frontal regions and between the frontal and all other scalp regions.

EEG coherence was utilised in investigating cognitive issues, such as in the study of networks involved in working memory operations (e.g., [95], [96], and [97]) and linguistic functions and binding (e.g., [98], [99], and [100]). As there is increasing evidence that executive functions rely on a complex fronto-parietal network connectivity [101] [102] [103], in [95] for instance, coherence was used to assess the connectivity of the fronto-parietal network during a visuospatial working memory task at two conditions of different levels of difficulty. The results showed the involvement of prefrontal areas in executive functions as reflected by the observed increase in the coherence of the fronto-parietal within the alpha band.

Regarding language processing, EEGs were recorded in [98] from 21 healthy adult subjects as they uttered the sound [a:] (talking condition) and as they heard these recorded sounds played back (listening condition). Gamma band coherence was used to investigate the communication between the frontal lobes (i.e., speech generator) and temporal lobes (i.e., speech perceiver) when a subject was talking. The frontal-temporal coherence at the gamma band was found to be capable of differentiating between talking and listening conditions; it was higher during talking than during listening.

Various studies have confirmed the usefulness of the coherence analysis of EEG signals in brain development and cognition, such as [104], [34], and [105]. One prominent study in this area is reported in [104] where coherence measures were analysed for the eyes-closed EEG data of 577 normal subjects ranging from two

months to 26 years of age. The study demonstrated the efficiency of EEG coherence in capturing significant differences between age groups that were compatible with the popular cognitive development stages of the Piaget theory (previously addressed in this chapter).

Developmental studies have utilised maturation patterns of coherence to discriminate between normal and pathological populations. In [34], for example, age-related changes in coherence were studied in two different groups at rest. This study targeted 98 normal and 54 learning-disabled (LD) children that were 6.0 to 16.8 years of age. In the normal group, a significant increase with age was found in the coherences between the posterior regions and the vertex (Cz). In the LD group, no age-related effect was found. These results indicated the existence of differences in brain organisation (particularly myelogenesis and synaptogenesis) between the two groups.

The imaginary part of coherency has also been involved in number of studies that investigated network connectivity in different conditions (e.g., [26], [22], and [106]). It has contributed to the study of ASD as reported in [26]. Like coherence, the imaginary part of coherency relies on the hypothesis that an ASD child's brain processes the information differently compared to an age-matched control. In [26], they conducted an experiment on 103 children (from two to five years of age) using an attention to faces exercise. A total of 72 children were diagnosed with autism, while the remainder (31) were deemed to be developing normally. The imaginary coherence was successful here in presenting clear differences in the cortical synchronisation between autistic and control children at a wide range of frequencies, locations, and times.

The imaginary part of coherence also has shown a great capability in defining functional topography in and around a brain tumor required resection. In [22], imaginary coherence was computed for MEG, recorded at resting state, from 57 patients with focal brain tumors. An increase in imaginary coherence was observed in the areas that comprised the tumors.

2.5 Machine Learning algorithms

Machine Learning (ML) is a fast-growing field successfully applied in many areas such as business, intelligence, defence, bioinformatics and finance. This field concentrates on extracting information from the data. Because of this reason, it is known as data mining or knowledge discovery from data (KDD) [107].

The nontrivial patterns found in the data can be used to make useful predictions on new data [107] [108]. There are different kinds of patterns that can be investigated in the data. Each of which is associated to a particular functionality in the data mining tasks such as characterisation, discrimination, cluster analysis, classification and regression.

The progression of Machine Learning (ML) algorithms and tools has made data mining more accessible supporting further understanding of the level of information content that are available in the data [109]. Research's goal defines which data mining functionality is appropriate to be applied [110]. As we aim to investigate the ability of the machine learning algorithms in detecting the effect of the conflict in the coherency data, classification is the functionality we are looking for. The classification task is defined as the process of distinguishing data classes. As it is performed under the supervision of the class labels of the data being known [111], it is often characterised as a supervised learning functionality. In this instance, machine learning algorithms were designed to be applied to a class-labelled data (i.e. class labels of the data are known during training) to build and train the classifier. The trained classifier can then classify new data to predict its class label.

2.5.1 Data Classification

Classification as a Two-Step Process

In order to use classification algorithms, data should be organised in a particular form, namely a table [107]. The rows are known as instances (examples, data points, or objects). Each row comprises values as measures of number of variables known as

attributes (features). In addition, the raw comprises a designated attribute known as a class (i.e. label). The attribute values are generally categorised to be either continoues (i.e. numeric) or categorical (i.e. nominal, binary, ordinal) [108].

In the first step of the classification process (i.e. training step), the classifier is trained on a labelled dataset (i.e. class labels of the data instances are known). Consequently, it learns how to predict class labels for new unlabelled instances.

In the second step of the classification, the model's accuracy is evaluated on a new dataset usually referred as 'testing set or previously unseen set'. Class labels of the testing set are not provided. Therefore, the percentage of the instances classified correctly is assigned as a measure of accuracy to the constructed classifier.

2.5.2 Weka Software

Weka is a comprehensive open source platform supporting many data mining functionalities like classification, clustering, regression, association rule mining, and attribute selection. It is distributed under the terms of the GNU General Public License [111]. Within Weka, an extensive set of machine learning methods can be applied flexibly through a common interface.

In this research, we used the Weka classification algorithms to test our objective, which is discriminating the coherency data (coherence, imaginary coherence) regarding the effect of the task conflict. The different classifiers and algorithms used in this study are naïve Bayes, support vector machines (SVM), multilayer perceptron (MLP) decision tree, random forests and random tree.

NaiveBayes

The Naïve Bayes classifier adopts a class conditional independence assumption that instance attributes are independent [107] [111]. It is based on Bayes' theorem in predicting class label probability of a given instance X. This is done as presented in (2.11) by estimating the posterior probability of H conditioned on X **(**i.e. P(H|X)).

$$P(H|X) = \frac{P(X|H)P(H)}{P(X)} \quad , \tag{2.11}$$

Assume that X is unknown-label instance and we want to predict its class. Let H be a hypothesis that instance X belongs to a specified class E. Therefore, (2.11) is looking for the probability that the hypothesis H holds given the instance X (i.e. $P(H|X)$).

To solve the classification problem using the Naïve Bayes technique, we need to estimate P (H), P (X|H), and P(X). Where P (H) is the prior probability of H, P (X|H) is the posterior probability of X conditioned on H, and P(X) is the prior probability of X.

Multilayer Perceptron

The Multilayer Perceptron algorithm found in the Weka software is based upon the backpropagation algorithm, which operates on a multilayer feed-forward neural network (see Fig. 2.4) [112].

The backpropagation algorithm is the most popular algorithm in neural network [107]. Fig. 2.4 represents topology for a basic multilayer feed-forward neural network. It is composed of three layers, each of which has a number of nodes. The input layer consists of number of nodes corresponding to the instance's attributes (i.e. features) of the training dataset. These nodes are called input units. The hidden layer can arbitrarily be more than one layer, consists of nodes called output units. They receive inputs from the input units (the previous layer) and modify them by some weights. Then the results are passed to the last layer (output layer). The output layer receives the information from the hidden layer and applies a nonlinear function to weight them. After that, it emits the outputs as class labels' prediction for the given instances.

The backpropagation algorithm predicts instances' class labels by repeating the learning process on a set of weights. These weights are initialised randomly. Therefore, if the prediction of the multilayer feed-forward neural network is not acceptable, the weights of each instance are adjusted in the backward direction. This

means it starts from the output layer back down through all hidden layers. This process is repeated till the prediction error is minimised within a predetermined level.

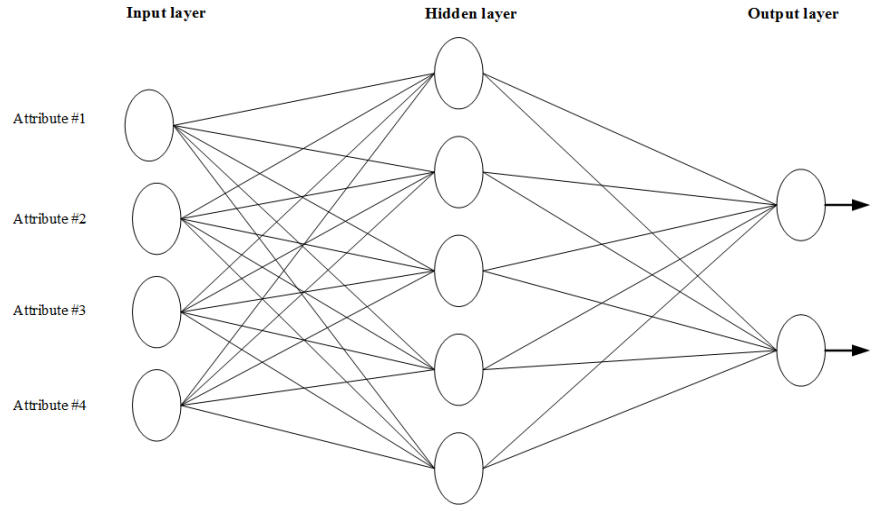

Fig. 2.4 Basic multilayer feed-forward neural network.

LibSVM

Support vector machines (SVMs) are one of the more popular algorithms that are used for classification and numerical predictions [113]. They have been applied in many areas such as handwriting recognition, speech recognition and object recognition.

The SVMs is based on the statistical learning theory for classifying linear and nonlinear data [107]. It transforms the input instances to a higher dimension by nonlinear mapping. With the two-class problems, the nonlinear mapping searches for the appropriate hyperplane to perform the separation of the data classes. Data instances that are located close to the decision boundaries (see Fig. 2.5), known as support vectors, distract the classification task. The SVM algorithm uses these vectors to separate the instances by building a linear discriminant function [111]. The basic idea is maximising the margin that separates the two classes as widely as possible.

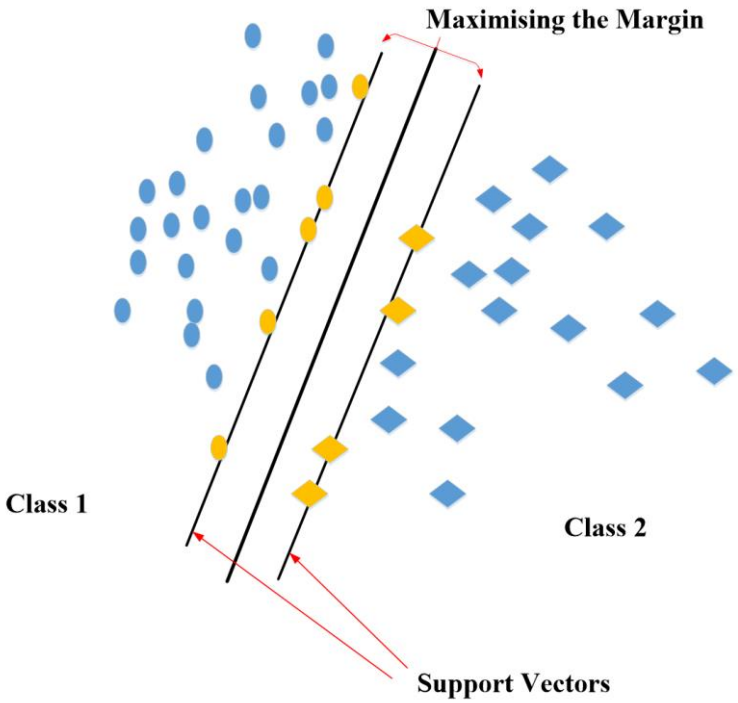

Fig. 2.5 Support vector machines.

J48

The J48 classifier implementation in Weka is an improved version of the original C4.5 algorithms [114], which is one of the most popular decision tree induction algorithms. The J48 algorithm is based upon a standard top-down decision tree. It consists of internal nodes, branches and terminal nodes as presented in Fig. 2.6.

The internal nodes represent a testing process performed on the instance's attributes. This testing process can be described in general as a series of questions [115] [116]. Each question tests a particular attribute value. Based on the result of each question, the node (i.e. the one being tested) may end up with a terminal node (i.e. class) or branch to a subtree. The testing process continues with the subtree until it terminates with the predicted class.

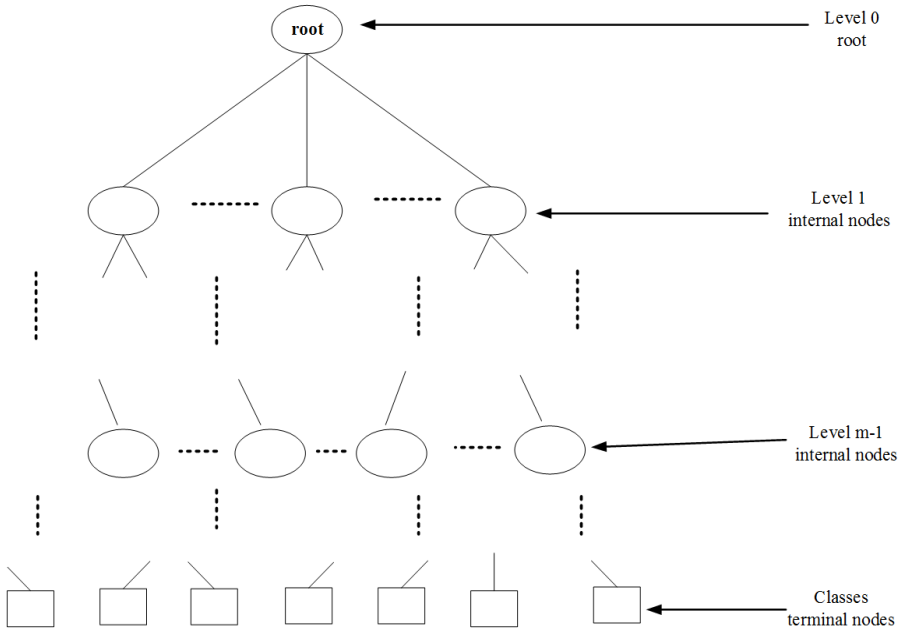

Fig. 2.6 Flowchart for a simple decision tree.

RandomTree

In Weka, the induction scheme of the J48 classifier was utilised in building one more classifier, which is called RandomTree. The difference between these classifiers is simply concentrated in the data attributes that are involved in building the decision tree. In contrast to the J48 classifier, the RandomTree classifier constructs its decision tree based on a subset of the given attributes [111]. This subset is randomly selected from the training data attributes.

RandomForest

As the base of the decision tree technique depends on selecting attributes to discriminate the training dataset [117] [118]. Over many years, it was observed that using a classifier that relies on a single decision tree might miss some useful attributes

that can give better partition into the training dataset. Because of this, number of algorithms such as random forests, adopted the idea of building many decision trees and then combine them into one model.

Random Forests is a well-known classifier which has shown a significant improvement in the classification accuracy [119]. Its algorithm often relies on a large number of the decision trees that range from 100 to 500 [117]. In order to generate sufficient datasets for these trees, the randomness is applied in two levels. Initially, it is applied on the instances and then on the attributes. To produce an overall model, all decisions of the generated trees are equally treated. A vote then is performed over class predictions that are achieved from the trees per instance. The most popular class predication is assigned to the instance being classified.

2.6 Summary

Attention is a significant component of several key mental processes (e.g., planning, working memory, and inhibition) called executive functions. It has been associated with three anatomical networks: alerting, orienting, and executive attention. The executive attention is widely used in developmental studies because of its progressive development process. It describes attention on a particular part of a stimulus. This ability greatly influences our cognitive, social, and psychological lives, which particularly affects children's school competence and socialisation.

ANT is the most widely used model for studying the EAN. It assesses a conflict score based on the subject's behavioural changes (i.e., reaction time) when responding to a task that induces a conflict.

Research into brain functional connectivity using EEG coherency analysis has provided insights into a number of aspects, such as cognitive processes (e.g. working memory and language), disorders (e.g. ASD), and cognitive development (i.e. Piaget stages). Therefore, it will be useful to assess the executive attention using the EEG coherency analysis especially it has shown a success in associating brain interactions to particular regions in the cortex. This topic will be covered in the next Chapter.

Chapter 3

Cognitive Conflict Detection using EEG Coherence

In cognitive neuroscience, the ability to measure the efficiency of executive attention network is critical to develop a better understanding of the attention function [10]. It describes the attention to a particular part of a stimulus and deals with conflict among competing responses, regulation of thoughts, and emotions [2]. Such a cognitive process may be a challenge to perform with respect to the conflict level generated by the surrounding activities or noise. For example, people suffering from obsessive compulsive disorder or attention deficit disorder have observable impairment in their executive attention functions [5].

In this study, we introduce a new data-driven approach in measuring the efficiency of the executive attention. This method as indicated in Chapter 1 (Section 1.1) relies on two hypotheses as follows.

1. Performing a task stimulus that induces a conflict causes different changes in brain network connectivity compared to a non-conflict stimulus type.
2. Conflict level and topography can be assessed by evaluating conflict-related changes in the EEG coherency.

The EEG coherence analysis was selected to measure the network connectivity. It has been reported in the literature to be successful in detecting age-related changes as in [104], [34], and [105]. In particular in [104], EEG coherence has demonstrated a great efficiency in capturing significant differences between children age groups (577

normal subjects with age ranging from two months to 26 years) which were basically compatible with the popular cognitive development stages of the Piaget theory (see Chapter 2).

The success of the EEG coherence in detecting the age-related changes was very promising which leads to the current study to assess the conflict related-changes. Thus, this study proposes that the difference in EEG coherence between the two task conditions (i.e. B minus A) can represent the level of the conflict induced by the B condition (B is more difficult to perform than A), and at the same instance define the regions of brain where these changes take place.

This chapter is organised as follows. A proposed method to assess coherence variation between two task conditions is explained in Section 3.1. Section 3.2 presents complete details on the conducted experiment such as targeted EEG dataset, EEG pre-processing treatment, experimental procedure, results and discussion. Validating the achieved results by a statistical test is shown in Section 3.3. Lastly, Section 3.4 summarises the Chapter.

3.1 Accumulation Method

In this section, we propose a new method, which assesses the conflict between tasks by utilising the concept of coherence matrix. It adopts the same idea of the ANT model (Chapter 2 Section 2.2) of measuring the variation in the response reaction times (RTs) between two different task conditions. Therefore, the proposed method requires the connectivity network to be measured by the coherence at two task conditions A and B associated with two different level of difficulties. Assume that B stimulus induces a cognitive conflict. Consequently, performing A stimulus is easier than B stimulus.

The first stage of the proposed accumulation method measures the changes occurring in the network connectivity at B condition (the one induces the conflict) compared to that at A condition. This is executed as shown in Fig. 3.1 by subtracting the coherence matrix of A stimuli from that of B stimuli per subject k.

In the second stage, simple inspection process is implemented on the connectivity variations that were assessed in the earlier stage. It replaces the n difference coherence matrices (i.e. associated to the n subjects) with one accumulation matrix summarises conflict-related changes on the coherence across the n subjects.

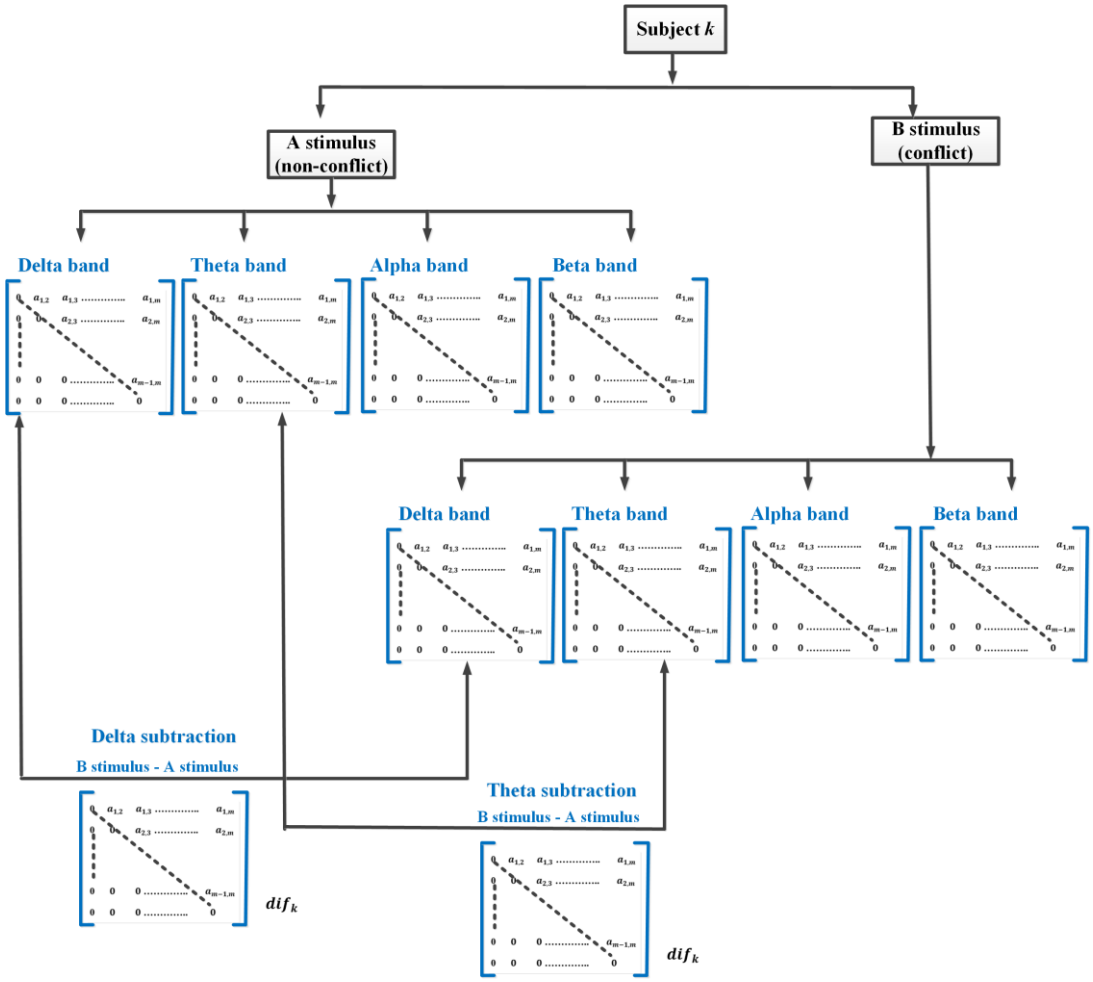

Fig. 3.1 Illustration of the main steps in accumulation method's procedure.

3.1.1 Procedure

The procedure starts by evaluating coherence increments regarding the conflict per subject k (see Fig. 3.1). For each subject k, subtraction operation is performed on the $m \times m$ coherence matrices (matrix (B) minus matrix (A)). This is repeated for all n subjects.

Implementing such procedure produces n difference matrices (dif), corresponding to the n subjects as illustrated in Fig. 3.2. The multidimensionality of each pixel (x, y) represents conflict related-changes on the coherence of the corresponding electrode pair (x, y) across the n subjects. Therefore, summarising this amount of information in one matrix is needed to ease the analysis task. Because of this, stage two of the proposed method was introduced.

In this stage, a new $m \times m$ matrix, called accumulation matrix(cum), is generated (see Fig. 3.1). It is initialised with zeros and later, integer values equal or less than n are assigned. The value assigned to each pixel (x, y) in the accumulation matrix represents the count of subjects who encountered significant increments at the electrode pair (x, y) while responding to the B stimuli compared to the A stimuli.

Therefore, an inspection procedure is implemented at the level of the matrix's pixels. This procedure can be explained as follows. Consider Fig. 3.2 which shows n difference matrices (dif) associated to n subjects. Let us say, the inspector procedure is to check the coherence variations occurring at pixel (x, y) across the n subjects. It starts with the first difference matrix say dif_k which is associated to subject k. It examines whether the value of pixel (x, y) is significant or not. If it is significant, a value of 1 is added to the current value of the corresponding pixel (x, y) in the new matrix (i.e. the accumulation matrix).

The procedure continues with checking all pixels of the same indices (x, y) in the rest of the difference matrices (i.e. dif_k where $k = 1,2,3, \ldots . n$). If pixel value of any difference matrix dif_k has a non-significant coherence variation, then nothing is added to the corresponding pixel (x, y) in the accumulation matrix as shown in (3.1).

$$\forall\, x,y\ \in [1\ m]\ \ cum_k(x,y) = \begin{cases} cum_{k-1}(x,y) + 1 & ,dif_k(x,y) > \sigma \\ cum_{k-1}(x,y) & ,dif_k(x,y) < \sigma \end{cases} \tag{3.1}$$

As can be seen from (3.1), σ represents the threshold that is used to refine the trivial changes in the coherence. It is a statistical measure that evaluates coherence significance based on epochs count and adjacent frequency interval that were involved in the calculation. This parameter of coherence deviation can be calculated as shown in (3.2) [120].

$$\sigma = \frac{1}{\sqrt{(\text{number of epochs}) * \ (\text{number of frequencies})}} \tag{3.2}$$

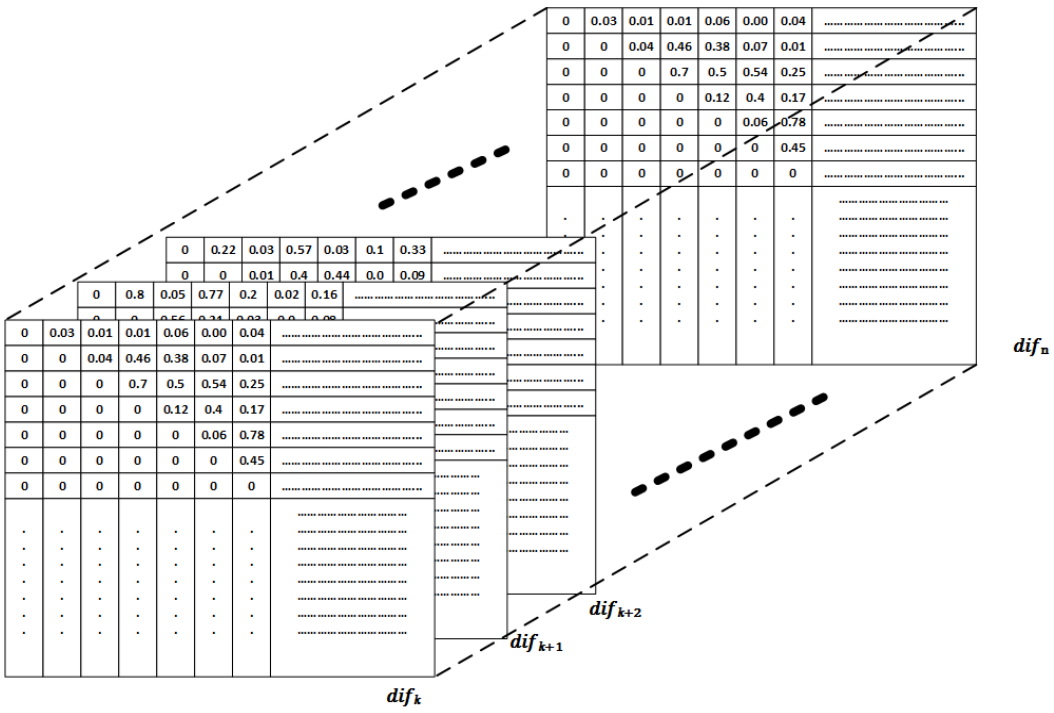

Fig. 3.2 Illustration of the multi-dimensionality of the coherences across n difference matrices.

3.1.2 Visualisation

Thresholding the Accumulation Matrix

Graph theory is a common tool used to represent the EEG connectivity in the form of matrices or graphs [16]. The basics of utilising the concept of $m \times m$ matrix in the graph theory were introduced in Section 2.4.4.1. When the accumulation matrix is depicted as colour-scale intensities, specific information on the network connectivity are expected to be achieved. In particular, the accumulation matrix's pixels of the highest intensities are supposed to be distinguished easily by visual inspection. These pixels are of special interest to us in the present study. They represent the neural connections that are encountered with common changes in the coherence across the n subjects. From Section 3.1.1, recall that, pixel intensity (x, y) in the accumulation matrix expresses the count of subjects who experienced changes in the coherence measure between task conditions at the corresponded electrode pairs (x, y).

The nature of the noise level presents in the accumulation matrix may influence the determination of the electrode pairs of interest. For instance, Fig.3.3 (a) shows the colour-scale figure that associated to $m \times m$ accumulation matrix. In this example, comparing the intensities and defining subset of the highest intensity locations is difficult to achieve. Therefore, the accumulation matrix needs to be refined by implementing a threshold on the pixels' intensities (i.e. by subject count) as shown in Fig.3.3 (b). In this figure, only three electrode pairs were extracted by thresholding Fig.3.3 (a).

Thresholding the connectivity matrix has no statistical effect on the connection itself. Because of this reason, in graph theory, it is highly recommended to pick up a liberal threshold as required in your experiment conditions. Consequently there is no constraints on the way we should threshold the coherency matrix [16]. In this current work, as we concentrate on defining electrode pairs of common coherency changes across the N subjects, then the accumulation matrix can be thresholded with a value represents 70% of the population (N).

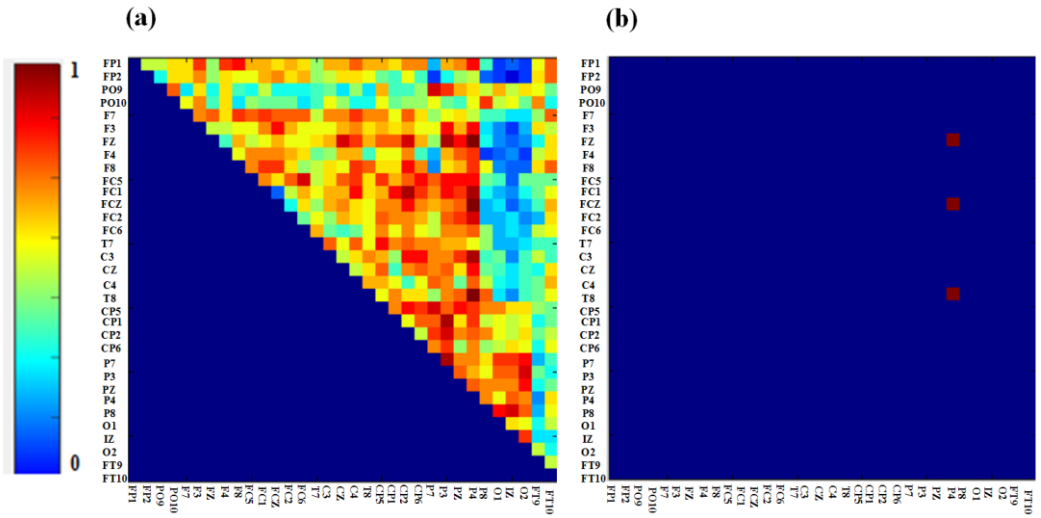

Fig. 3.3 (a) Colour-scale graph associated to the accumulation matrix of coherence variations. (b) Colour-scale graph of the high intensity pixels that derived from part (a) by the thresholding.

Topographical Map Representation

As shown in Fig. 3.3 (b), coherence increments are represented as a colour-scale figure. Thresholding the connectivity matrix as discussed above produces pixels' subset of the areas of interest. This small set facilitates the use of another interpretation tool in the graph theory namely topography map. With the topography map, spatial information on the electrode pairs' locations associated to the accumulation pixels can be visualised. As an illustration, Fig. 3.4 represents a topography map of the three electrode pairs derived in Fig. 3.3 (b).

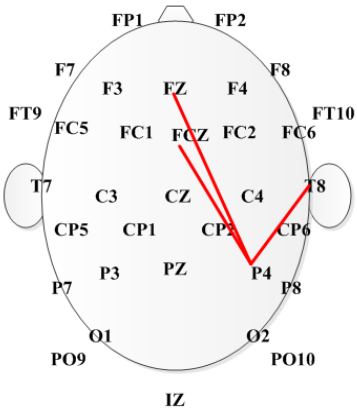

Fig. 3.4 Topography figure represents electrode pairs that corresponding to the pixels extracted in Fig. 3.3 (b).

3.2 Experiment

3.2.1 EEG Dataset and Experimental Protocol

This research made use of an existing data set that was provided by the Neurocognitive Development Unit (NDU) at the University of Western Australia. Written informed consent was requested from children and their parents. In addition, an approval was provided by the ethics committee of the School of Psychology, University of Western Australia.

Subjects

Two datasets of healthy children were used in this study. In the first dataset, EEG recordings were collected from a group of children aged 7 years (n=45; 23 females; 22 males; mean=7.5 years; STD= 0.27) while performing Flanker task. Afterward, this task experiment was repeated on the same group of subjects two years later in order to produce a second dataset (n=45; 23 females; 22 males; mean=9.56 years; STD= 0.26), allowing for longitudinal analyses.

Task Procedure

As described in [121], a friendly model of Flanker task was introduced to the subjects as a game, where a set of five fish are presented on the computer screen. In order to respond to the task, children were asked to concentrate on the direction of the central fish. By manipulating the flanking fish directions, three different trial types were produced:

1. Congruent, the stimulus contains five green fish pointing to the same direction (Fig.3.5 (a)).
2. Incongruent, the stimulus contains five green fish and the direction of the central fish is opposite to the flank fish (Fig.3.5 (b)).
3. Reversed, the stimulus contains five red fish pointing to the same direction (Fig.3.5(c)). This type of stimuli were not involved in the present work.

In order to ensure that children have fully understood how to perform the task, instructions and practice trials for each trial type were administered.

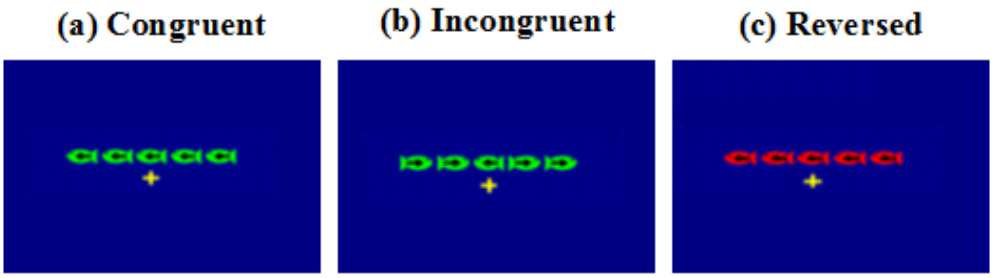

Fig. 3.5 Flanker task conditions where the crosshair at the middle of the screen is the fixation point.

Data Acquisition

Data were collected using an Easy-Cap^{TM} and electrode impedance level was kept below 5kΩ. The signals were amplified with a NuAmps 40-channel amplifier and

sampled at 250 Hz using a linked-mastoid reference. Thereafter, zero phase shift band-pass filter from 0.05 to 30 Hz was digitally performed [121].

3.2.2 EEG Data Pre-processing

In the EEG coherence computation, attention is usually paid to issues such as choices of reference electrode, volume conduction, and epoch sample size. These issues have been proven to have a significant impact on the coherence calculated from the scalp potentials compared to that calculated from the underlying neural sources [89]. Regarding the reference electrode and volume conduction, separating distance between EEG electrodes tends to have less effect on the scalp coherencies compared to the intracranial coherencies. Therefore, as the distance between EEG electrodes increases, intracranial coherence decreases. On the other hand, no such drop was encountered with the scalp coherencies which in turn may refer to its influence by the volume conduction. Assessing the error resulted from the reference electrode and volume conduction remains a challenge, as this requires an extensive knowledge of the brain sources' location.

Nunez et al. in [89] conducted a study to compare coherence measures obtained using different referencing methods like (a) conventional reference, (b) average reference, and (c) Laplacian. Averaged mastoid reference (i.e. M1, M2), which was used in this study, was one of the suggested references to minimise the effect of the volume conduction. This was implemented by subtracting $((M1 + M2)/2)$ from each electrode signal.

Fig. 3.6 shows the pre-processing stages of the EEG data before computing the coherence. Within the stage of bad data rejection, eye channels (i.e. VEOGL and VEOGU) and the unconnected channels (i.e. CPZ, X7 and X8) were removed. Consequently, the EEG connectivity was assessed on the remaining 33 electrodes (i.e. Fp1, Fp2, F7, F3, FZ, F4, F8, FT9, FT10, FC5, FC1, FCZ, FC2, FC6, T7, C3, CZ, C4, T8, CP5, CP1, CP2, CP6, P7, P3, PZ, P4, P8, PO9, PO10, IZ, O1, and O2). Afterward, inspecting the data in depth revealed that some of the participants' keypress responses to stimuli were detected to be either too early ($< 500ms$) or too late ($> 2000ms$). These

situations, which possibly relate to participants not following task instruction correctly were defined as cognitive artifacts. These artifacts were subsequently detected and the EEG data removed from further analysis.

In general, performing cognitive task causes changes in the EEG data which are linked to either stimulus-related changes or response-related changes [16]. These corresponding changes are usually investigated by segmenting the recorded data into epochs. In this study, the aim is to investigate brain connectivity associated to the stimulus-related changes. Therefore, epochs were segmented from -0.6 to 1sec [35] with no overlap, and baseline corrected using segment from the -0.6 to 0sec period. By passing the data to the EEGLAB toolbox, the Independent Component Analysis (ICA) algorithm was applied to the EEG data in order to minimise the eye blinks and muscle related activities [122].

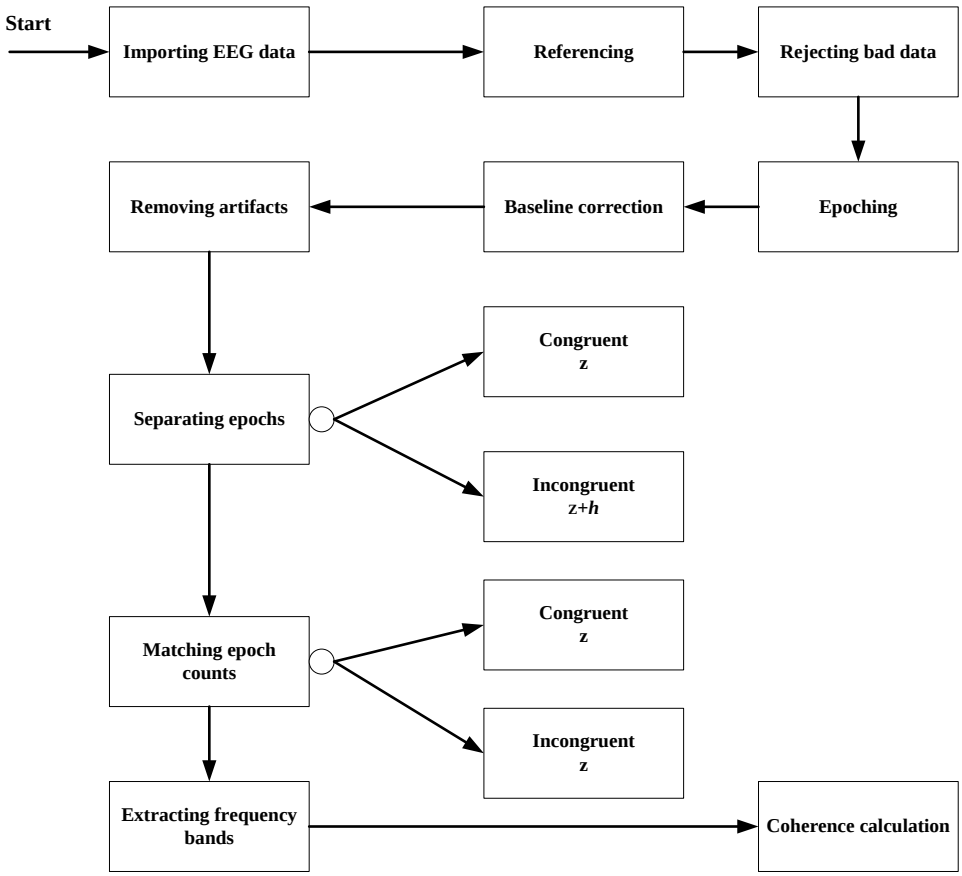

Fig. 3.6 Procedure used in the EEG pre-processing techniques.

Investigating the difference in brain correlation between different types of the Flanker stimuli requires separating the extracted epochs into two sets; the congruent and the incongruent sets. The variation in epochs count between these two sets may produce a bias in the coherency measures [16], especially the difference in our case was not trivial based on the task design (i.e. 50% of the stimuli were congruent, 25% were incongruent and 25% were reversed). This problem was solved by matching the epoch counts randomly. Stimuli set of the smallest epochs count (most likely to be from the incongruent set, z) was left with no changes, while an equal number of epochs was selected from the other set (most likely to be from the congruent set, $z + h$). Note that if coherence calculations are required to be repeated, then the randomly selected epochs should also be saved otherwise different epochs will likely to produce different coherence values.

In the last stage of the pre-processing, frequency bands were extracted from each electrode pair (x, y) because we aim to investigate the variation in the network across frequency bands. Digital bandpass filtering was applied to extract the following bands; delta band (1 to 3 Hz), theta band (4 to 7 Hz), alpha band (8 to 12 Hz) and beta band (13 to 30 Hz).

3.2.3 Procedure

As mentioned above, in each age group (seven and nine years), 45 EEG datasets (associated to the 45 subjects) were used in the current experiment. In each dataset, 33 EEG channels were involved.

Using MATLAB scripts, coherence was estimated for each possible combination (x, y) of the 33 channels over a minimum number of 25 epochs (1 sec of length). This count of epochs was selected because it minimises the bias error in coherence measure as explained in [89] [123]. With a frequency resolution of 1Hz (EEG were digitised at 250 Hz), the correlation between signals x and y was smoothed across the frequency interval of each band (delta, theta, alpha, beta). Consequently, a matrix of size 33×33 was produced within each band (delta, theta, alpha, beta) per the task condition (congruent, incongruent) for each subject k.

Fig. 3.7 (a) illustrates some of the pre-processing steps applied to each subject EEG dataset in the targeted group followed by the coherence calculation procedure. As shown two data subsets were extracted from the EEG of subject k (explained in Section 3.2.2). First subset contains EEG segments associated to the congruent stimuli while the second subset contains the segments associated to the incongruent stimuli. From each stimuli subset, four coherence matrices of size 33×33 associated to the frequency bands were generated per task condition.

First stage of the accumulation method (detailed in Section 3.1.1) was implemented by subtracting the congruent matrix from the incongruent matrix of each subject k (see Fig. 3.7(b)). As the σ threshold of the coherence deviation (explained in Section 3.1.1) varies from band to band regarding the frequency sample, σ was calculated for each frequency band (see table 3.1).

Then 45 difference matrices (dif) were generated per band. These matrices were summarised in one accumulation matrix by implementing the second stage of the proposed method (Section 3.1). Therefore, the maximum value that can be assigned to any pixel (x, y) was 45. This value is associated to the total number of the subjects involved in the present experiment, which indicates that all subjects were faced with coherence changes at this particular pixel regarding the task conflict.

The accumulation matrices were visualised and then a liberal threshold was applied to extract the subsequent graphs. As the purpose of this work is defining the common electrode pairs across the 45 subjects that were affected by the task conflict, we selected a threshold value of 30, which represents 70% of the population (45 subjects). The new subset of the extracted pixels was visualised as a colour-scale matrix and topography per band.

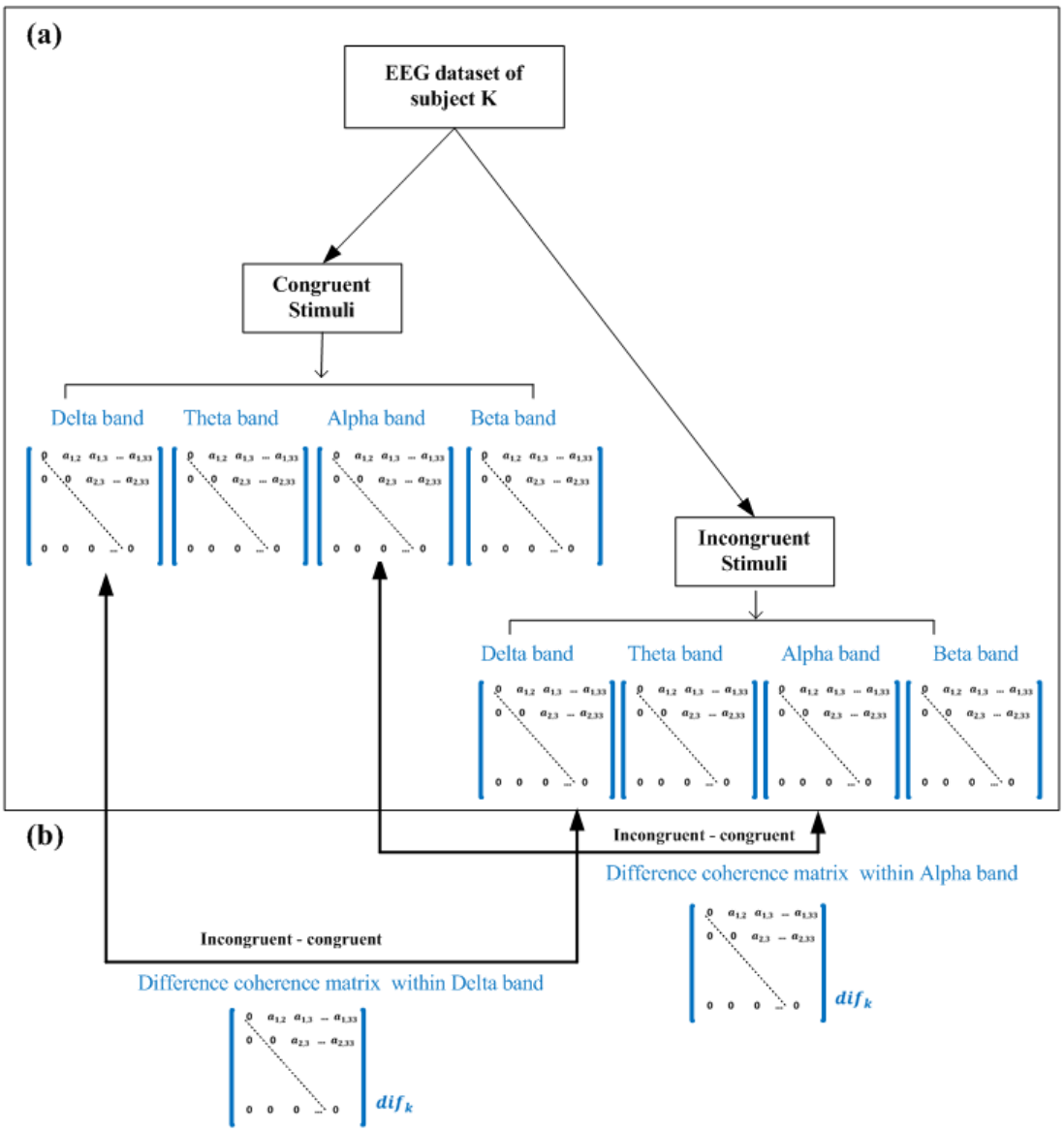

Fig. 3.7 (a) Representation of coherence matrices that were generated from EEG data of subject k. (b) Representation of how the difference matrices dif_k were computed.

TABLE 3.1

Threshold σ within frequency bands per age group

Group of age 7 years	Delta	Theta	Alpha	Beta
	0.071	0.063	0.059	0.03
Group of age 9 years	0.071	0.059	0.053	0.03

3.2.4 Results

Group Aged Seven Years

The impact of Flanker conflict on the network connectivity of the seven-year-old children was evaluated within the frequency bands by the coherence. The colour-scale graph in part (a) of Fig. 3.8 to Fig. 3.11 shows the achieved accumulation matrices within delta, theta, alpha and beta respectively. Part (b) shows the thresholded matrices while part (c) shows the topography figures of delta, theta, alpha and beta respectively.

Fig. 3.8 (c) shows that, delta band in the seven-years of age group experienced a coherence increase in the left hemisphere, specifically the parietal inter-electrode pairs (P7/CP5, P7/P3) and the parietal-central area with occipital pairs (PZ/O1). It can be seen from Fig. 3.9 (c) that, the increase in coherence measurements within theta band was concentrated in the right hemisphere, where parietal area seems to be a common factor in all occurred increases. In this frequency band, there were increase in the correlations that link the midline frontal lobe (midline frontal and midline fronto-central) to the right parietal area (FZ/P4, FCZ/P4). Increase in the correlation that links the right temporal to the right parietal (T8/P4) was observed as well. Fig. 3.10 (c) shows that the midline frontal and the midline fronto-central were both involved again in coherence increase at the alpha band in their relationship with the right frontal (FZ/F8, FCZ/F8). In addition, the intra-hemispheric coherence that maps the right frontal area to the left fronto-central (F8/FC1) faced increment in the coherence measure at the incongruent condition compared to the congruent one. Within the beta band in Fig. 3.11 (c), the right fronto-central and the right centro-parietal were confronted with coherence increase in their connection with the midline frontal (FC6/FZ, CP6/FZ). Moreover, the right fronto-central and the right motor experienced coherence increase in their connection with the midline fronto-central area (FC6/FCZ, C4/FCZ). Increase in the intra-hemispherical coherence links the left fronto-central with the right centro-parietal (FC5/CP6) areas, and the left parieto-occipital with the right occipital (PO9/O2) were observed as well.

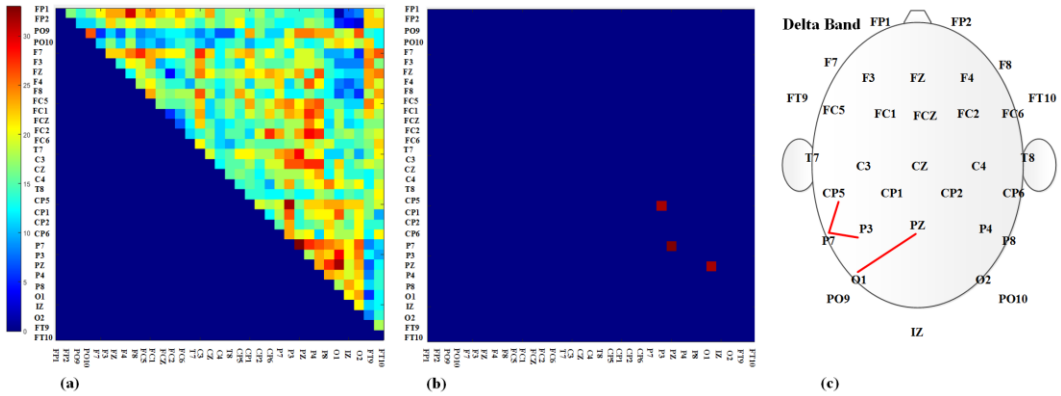

Fig. 3.8 (a) Accumulation matrix of coherence changes in the 7-year-old group within delta band. (b) High intensity pixels derived from part (a). (c) Topography figure represents electrode pairs that corresponding to the pixels in (b).

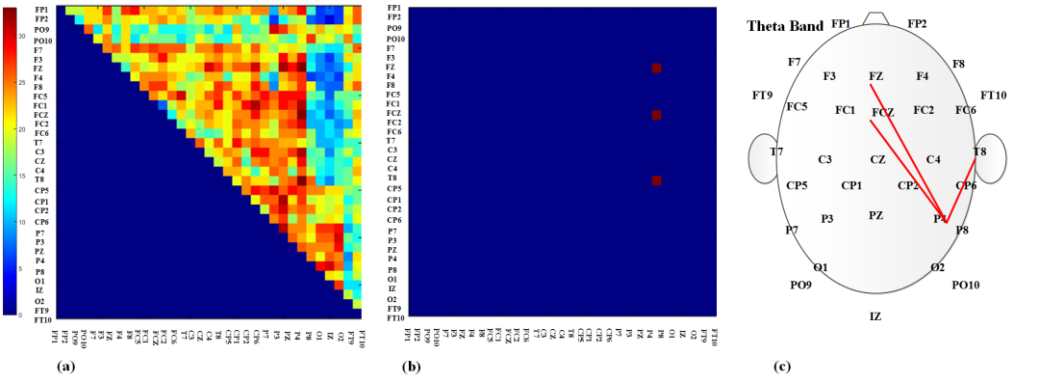

Fig. 3.9 (a) Accumulation matrix of coherence changes in the 7-year-old group within theta band. (b) High intensity pixels derived from part (a). (c) Topography figure represents electrode pairs that corresponding to the pixels in (b)

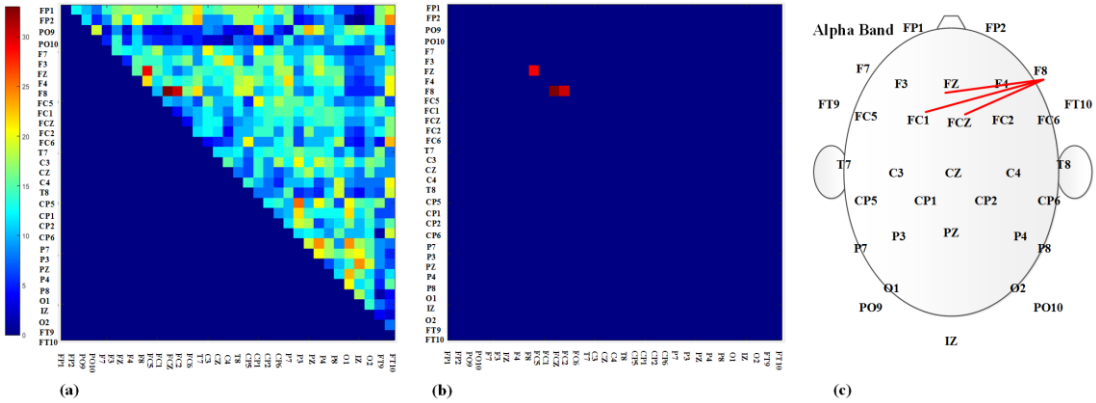

Fig. 3.10 (a) Accumulation matrix of coherence changes in the 7-year-old group within alpha band. (b) High intensity pixels derived from part (a). (c) Topography figure represents electrode pairs that corresponding to the pixels in (b).

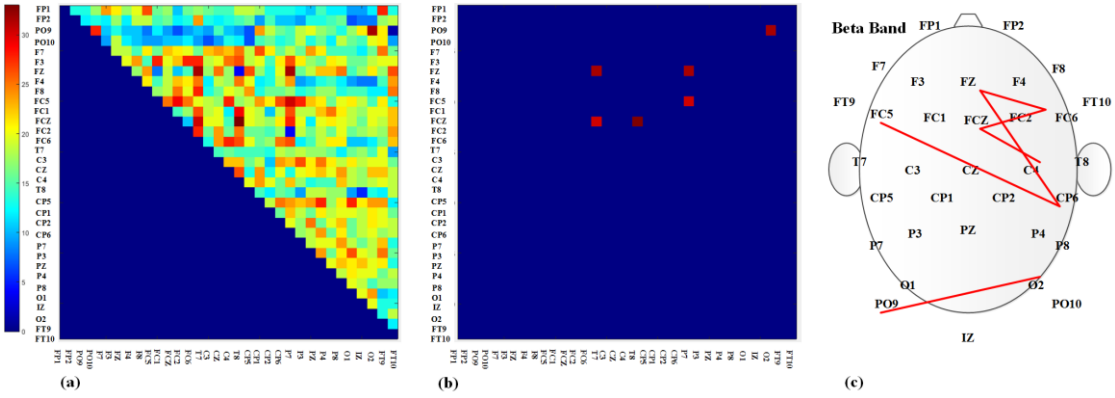

Fig. 3.11 (a) Accumulation matrix of coherence changes in the 7-year-old group within beta band. (b) High intensity pixels derived from part (a). (c) Topography figure represents electrode pairs that corresponding to the pixels in (b).

Group Aged Nine Years

In the nine-year-old age group, no coherence increase was detected within delta and theta bands at the incongruent condition compared to the congruent. The case was different within the alpha band in Fig. 3.12 (c), where this difference is represented by the increase in the correlation between the right frontal and the right fronto-central areas (F8/FC2) and between the right fronto-temporal and the right motor areas (FT10/C4). The increase in coherence measurements at beta band is depicted in Fig. 3.13 (c). This increase occurs within the right frontal area (FZ/F4) and, between the left parietal and the occipital protuberance areas (P7/IZ).

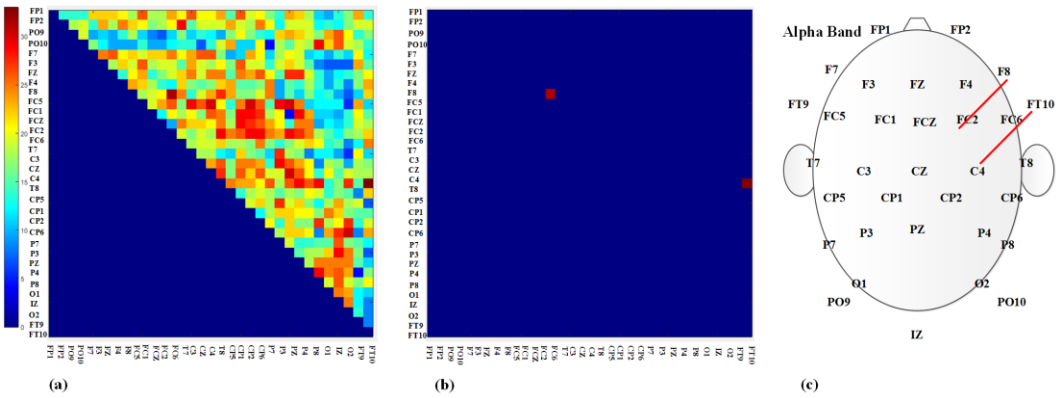

Fig. 3.12 (a) Accumulation matrix of coherence changes in the 9-year-old children within alpha band. (b) High intensity pixels derived from part (a). (c) Topography figure represents electrode pairs that corresponding to the pixels in (b).

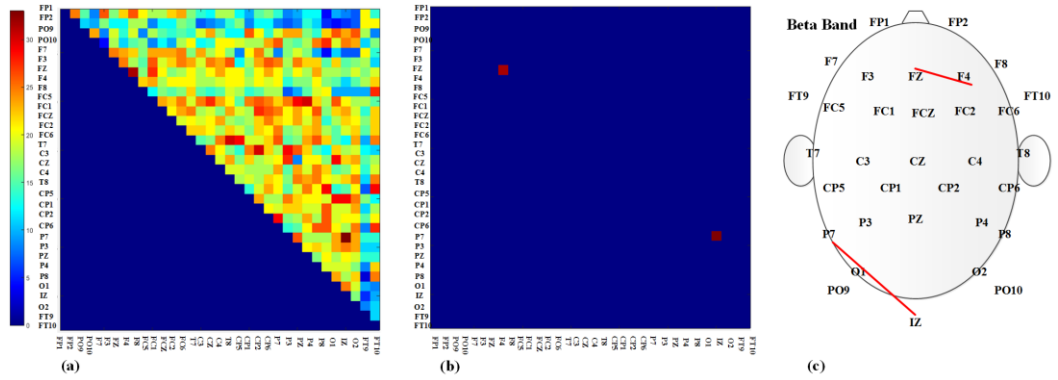

Fig. 3.13 (a) Accumulation matrix of coherence changes in the 9-year-old children within beta band. (b) High intensity pixels derived from part (a). (c) Topography figure represents electrode pairs that corresponding to the pixels in (b).

3.2.5 Discussion

Previous study by Thatcher et al. [104] suggested that the left hemisphere preceded the right hemisphere during cognitive developments. The study showed that coherence measurements of children aged four-six years (compared to that aged two months-three years) were confronted with increase concentrated in the left hemisphere. This may explain the results we achieved with the seven-year-old group, where the impact of the Flanker conflict seems to be mostly concentrated in the right hemisphere (see Fig.3.9 to Fig.3.11). Therefore, the developments that occurred earlier (from age four to six) in the left side of the brain results in determining no variations between congruent and incongruent coherence measurements in the seven-year-old group.

Flanker task conflict seems to have less effect on the same group two years later especially at delta and theta bands. The increase in the incongruent coherence compared to the congruent is still observable in the right hemisphere. This is consistent with the findings reported in [104] which states that coherence increments among the age eight to ten years are restricted in the right hemisphere.

From the outputs of the present study, we realised decrease in the effect of Flanker conflict at age nine years compared to that at age seven. For this result, our observations are similar to the finding reported in [8] and [54], in which, the efficiency of the executive attention is increased at age eight to 12 years compared to age seven years.

3.3 Statistical Validation of the Coherence Outcomes

To the best of our knowledge, coherence measure has not been used in the literature to estimate response conflict process in terms of assessing brain connectivity's changes between Flanker conditions (congruent and incongruent). Consequently, there are no explicit information about which parts in the network connectivity of the

child's brain (seven and nine-years-old) that shows significant changes associated to the induced conflict. Based on this, it is increasingly important to examine the performance of the proposed accumulation method (detailed in Section 3.1) with an appropriate statistical test.

As brain interaction to the congruent stimuli differs from its interaction to the incongruent stimuli [7], and as we adopt the same concept (Chapter 2, Section 2.2) of using brain activity at the congruent condition as a reference to its activity at the incongruent condition when the conflict process is investigated, then constructing pairs in the form $(cong, incong)$ from coherence measures of the electrode pair (x, y) across subjects does make logical sense. Based on the above details, it seems possible to interpret $cong$ and $incong$ measures as 'before' and 'after inducing the conflict' observations respectively. This can be achieved using the paired t-test.

Paired t-test is appropriate as each subject in the sample data has only two observations, referred to as 'before' and 'after' a particular change or event. Thus in this study, the difference in the network connectivity between congruent and incongruent stimuli was investigated for each frequency band separately. The null hypothesis H_0 of applying paired t-test for electrode pair (x, y) related to the deduction that the mean coherences at the congruent condition is similar to the mean coherences at the incongruent condition. In other words, the mean difference between paired observations $(cong, incong)$ is close to zero ($\mu=0$). While the alternative hypothesis H_a (left-tailed) relates to the mean coherences at the congruent condition being less than the mean coherences at the incongruent condition ($\mu<0$).

3.3.1 Procedure

To implement the statistical test on coherence values, an extra step was introduced during the calculation of the coherence measure. This step takes place before smoothing the coherences over frequency interval of each band (explained in Section 2.4.4.1). Coherence values here were first transformed using Fisher-z transformation to enforce the normality [84] and then averaged over the frequencies.

To investigate conflict-related changes in the coherence of each electrode pair (x, y) across the 45 subjects, paired t-test was implemented on coherence matrices at the level of pixels as illustrated in Fig. 3.14.

Coherence variation at each electrode pair (x, y) within the band was investigated by producing two data vectors. First vector was called the congruent vector of the electrode pair (x, y) as illustrated in Fig 3.14 (c). It gathers all coherence values located at this pixel (x, y) in the 45 congruent matrices (Fig 3.14(a)) within the band being considered. While the second vector was called the incongruent and it was produced from the incongruent matrices (Fig 3.14(b)) within the same frequency band. It contains coherence values located at the same pixel (x, y) in the 45 incongruent matrices.

An important issue to mention here is to keep subjects order identical across the two data vectors. This means if the first subject for example has been ordered as k then, the first value in the congruent vector and the first value in the incongruent vector must also come from the same subject, k.

Within each band, the paired t-test was employed 528 times (528 pixels) and the pixels that identified with significant change at incongruent condition compared to the congruent were visualised on a topographical figure.

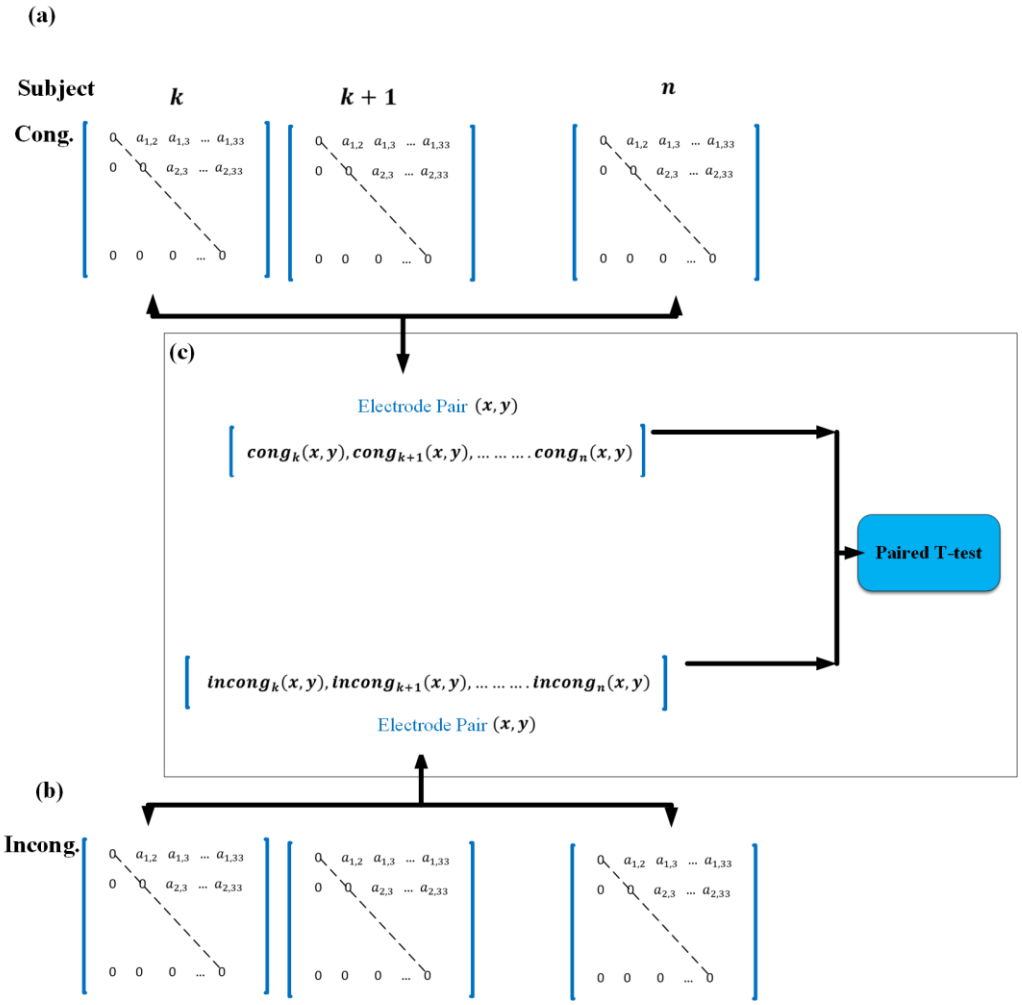

Fig. 3.14 (a& b) Procedure that followed among the analysis to produce two data vectors for each electrode pair (x, y) to be investigated by the paired t-test in part (c).

3.3.2 Results

Statistical estimation for the Flanker stimuli-related changes on the coherence was performed on the seven and nine-year-old groups. The paired t-test was utilised to validate the results of the proposed method (Section 3.2).

At the confidence level of 0.01, the test was not able to determine changes in the network connectivity of the nine-year-old children between Flanker conditions. While with the younger group (seven-year-old children), the test was successful to detect changes within the theta band.

Fig 3.15 shows the electrode pairs that were identified with significant variations within theta band. In this figure, Flanker conflict seems to have impact on the neural connection that links the left prefrontal electrode to the parieto-occipital area (FP1/PO10, FP1/PO9). Table 3.2 shows the paired t-test statistics at the electrode pairs being defined, where $tstat$ refers to the value of the test statistic, df refers to the degrees of freedom of the test and sd refers to the standard deviation of $(incong - cong)$.

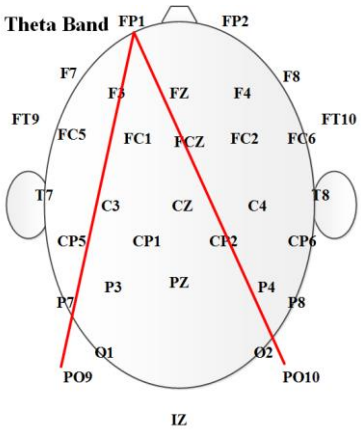

Fig. 3.15 Topography figure of coherence differences (incongruent versus congruent) in the group aged 7 years at theta band.

TABLE 3.2

Paired t-test statistics correspond to electrode pairs of interest (FP1/PO9 and FP1/PO10) investigated within theta at age 7 and 9 years old.

	age group	$tstat$	df	sd	$P\ value$
FP1/PO9	7 years	-2.4804	43	0.4148	0.0086
	9 years	0.1084	43	0.4816	0.5429
FP1/PO10	7 years	-2.5480	43	0.4328	0.0072
	9 years	0.2958	43	0.6187	0.6156

3.3.3 Discussion

By comparing Fig 3.15 of the seven-year-old group at theta band with the corresponding Figure that generated by the accumulation method (Fig 3.9 (c)), we can see that there is no similarity in localising the Flanker conflict influence. Where the accumulation method defined the right inter-hemispheric region (i.e. FZ/P4, FCZ/P4 and T8/P4) for conflict-related changes.

The variety in the results between the two methodologies (Section 3.2 and Section 3.3) in specifying the involved brain regions during the conflict process is possibly refers to a lack in consistency pattern among coherence changes. Therefore, we conclude that, if our assumption is true, which indicates that EEG coherency changes at Flanker incongruent condition can provide estimate of the generated conflict, then EEG coherence in this study was not representing a true reflection of brain network connectivity.

Volume conduction is a common factor of contamination when the connectivity network is addressed [16]. Electrical activity of a single source may be captured by multiple electrodes. Then the neighbouring electrode pair presents high connectivity increase as inter-electrode distance decreases. Special attention has been paid to this issue and inverse methods were introduced to estimate brain's true activities such as a non-optimal solution. The achieved results were not totally convincing because the dependency of the inverse method on a set of constraints which in turn requires a deep understanding of EEG underlying generators.

It is therefore important to investigate EEG processing techniques that minimising the impact of volume conduction on the network connectivity. This study will be presented in the next chapter.

3.4 Summary

A new approach to exploit the EEG coherence analysis to assess the executive attention was introduced in this chapter. It is built on finding the coherence increment

($incong - cong$) through all given EEG electrode pairs when Flanker incongruent stimuli are presented. The method based on accumulation process was proposed to evaluate the conflict level and define its corresponding spatial information in the scalp area. The results were visualised on topography maps to facilitate the comparison after which the paired t-test was implemented.

From the results of the accumulation method and the paired t-test, variation in the network connectivity between Flanker congruent and incongruent stimuli was found. It indicates that, EEG coherence measure successfully detects changes in the activity of brain regions when the conflict was generated by the Flanker incongruent stimuli.

The drop in the number of affected brain regions at age nine compared to age seven may be related to the well-known reduction of the conflict level which was discussed in [8] and [54]. Similar reduction in the conflict effect was also revealed by the paired t-test with a significance level of 1%. The paired t-test was unable to capture differences in coherence values at age nine years within the four frequency bands. Moreover, it was solely successful to detect conflict related-changes in the network connectivity within one frequency band (i.e. theta band at age seven years) across the two age groups.

Chapter 4

Eliminating Volume Conduction Impact using Imaginary Part of EEG Coherency

As addressed in the previous chapter, coherence technique (coh) was capable of detecting variations in the brain synchronisation between Flanker stimuli. In addition, it was successful in capturing a decline in the cognitive conflict, induced by the Flanker incongruent stimuli, at age nine years compared to age seven years. However, its findings were not statistically validated.

Volume conduction is the major obstacle in estimating EEG brain connectivity [16]. It may result in a false representation of the brain interactions if the two time processes x and y capture the activity of a single brain source. Distinguishing between brain underlying active neural sources from recorded EEG data is a complicated task. It involves several steps such as signal denoising, segmentation of anatomic regions from MRIs, extracting numerical solutions from the electromagnetic forward problem and maintaining consistency spanning space, time and frequency and across subjects.

In [35], a new measurement quantity was suggested to replace the magnitude-squared coherence value (coh) in representing the brain network connectivity. This new quantity emphasises the imaginary part of coherency (Chapter 2, Section 2.4.4.2). In this particular technique, Nolte et al. [35] relied on the fundamental assumption widely adopted in EEG studies, which states that the time lag between the underlying source activity and its recorded scalp potential is zero [124]. This means that scalp

signals with vanishing or zero time lag are assumed to belong to the same source neural generator. Regarding this, the value of the imaginary coherence was found to be small or vanishing when the time delay between the two signals x and y is small or vanishing [35].

In fact, the imaginary component of coherency misses an important part of the brain interactions, which is associated to the real synchronisations that occur between the non-time-lagged signals (i.e. signals of zero or minor lag). However, in the literature, it has been widely reported that the imaginary coherence between time-lagged scalp signals has achieved promising results in assessing the true neural interactions (e.g. [22] [26], [125], [126]).

In this Chapter, we will extend the previous work by investigating the use of the imaginary component of coherency in examining the variation in the brain's functional communication in response to the Flanker stimuli.

This chapter is organised as follows. In order to examine the performance of the imaginary component of coherency, Section 4.1 addresses implementing the accumulation method on this measure. Paired t-test is further applied to validate the results of the accumulation method from the statistical perspective and this will be reported in Section 4.2. Lastly, Section 4.3 summarises the study.

4.1 Experiment

In an attempt to improve the measured coherency between the EEG signals, this experiment was conducted on the imaginary component of the coherency instead of the coherence. The calculation was performed on the same EEG dataset introduced in the previous chapter (Section 3.2.1). Consequently, for each subject k, (2.10) was used on each stimuli type set (congruent, incongruent) to produce the 33×33 matrix per frequency band where the bands were defined as delta from 1 to 3 Hz, theta from 4 to 7 Hz, alpha from 8 to 12 Hz and beta from 13 to 30 Hz.

Therefore, in each age group (seven and nine-year-old children), we produced 45 matrices (associated with the 45 subjects) for each stimuli type (congruent, incongruent) per frequency band. These matrices were then accumulated in the similar fashion as described in Chapter 2 (Section 3.1).

4.1.1 Accumulation Method's Implementation on the Imaginary Part of Coherency

In order to apply the accumulation method, the $icoh$ matrices were normalised to be in the range [0, 1] instead of [-1, 1]. Afterward, method's procedure, that detailed in the previous chapter (Section 3.1), was followed on the $icoh$ matrices of each band (delta, theta, alpha, and beta). For each subject k, the congruent matrix was subtracted from the incongruent one. Total of 45 difference matrices (dif) were generated per band. Then they were summarised in one accumulation matrix. This matrix was thresholded to extract the high-intensity pixels. Lastly, topography figures for the extracted pixels were depicted.

4.1.2 Results

Group Aged Seven Years

At age seven years, the imaginary coherence found no significant changes in the network connectivity between Flanker stimuli within delta band. While it was successful within theta band (see Fig. 4.1(c)) to capture neural variations in the right hemisphere between centro-parietal and occipital areas (CP6/O2).

On the other hand, several differences were realised within the high waves (alpha and beta) as shown in Fig. 4.2 and Fig. 4.3. In Fig. 4.2 (c), the right parietal region seems to be well involved in the connectivity changes associated with the task conflict within the alpha band. In respect to the brain inter-hemispheric interactions, the connectivity of right parietal region with the frontal (P8/F4), fronto-central (P8/FC2, P8/FCZ) and middle central (P8/CZ) experienced an increase in the imaginary coherence measures. As for intra-hemispheric interactions, its connectivity with the back regions of the left

side of the brain (P8/P3, P4/P7, P8/CP5, P4/PO9) was encountered with coherency increases as well. The temporal region connectivity with the right prefrontal area (FT10/FP2) and the right fronto-central (T8/FC2) were acted differently for the incongruent condition compared with the congruent.

Fig. 4.3 (c) reveals that functional activities between the right frontal region (F8) and the back regions in the left side of the brain (i.e. parietal (P3), parieto-occipital (PO9) and occipital (O1)) were stimulated when task conflict was induced. The mentioned changes in the activity of the right frontal region (F8) were synchronised with inter-hemispheric changes in its activity with the occipital region (F8/O2). In the left part of the brain, the frontal region was faced with inter-hemispheric changes with the temporal area (F7/T7) and intra-hemispheric changes with the centro-parietal area (F7/CP6). While in the right part of the brain, it was faced with intra-hemispheric changes with the centro-parietal area (F4/CP1). Increase in the imaginary coherence between the right and left parietal regions (P8/P3) and between the right parietal and left frontal (P4/F3, P4/FC6) were observed in Fig.4.3(c).

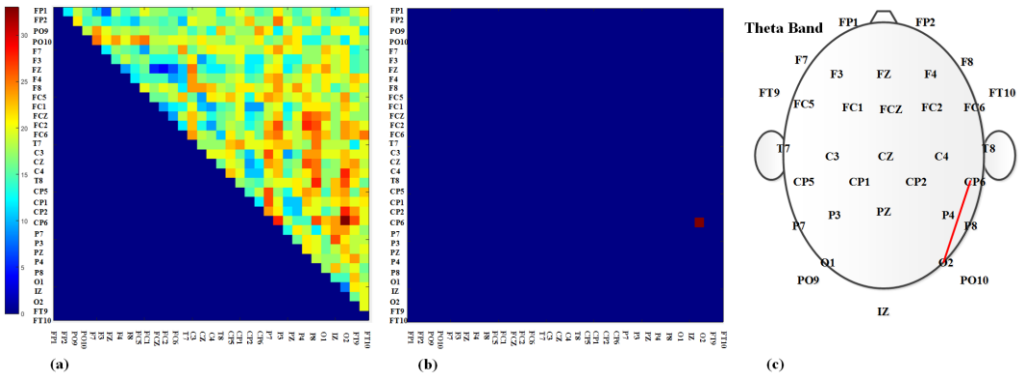

Fig. 4.1 (a) Accumulation matrix of imaginary coherence changes in the 7-year-old children within theta band. (b) High intensity pixels derived from part (a). (c) Topography figure represents electrode pairs that corresponding to the pixels in (b).

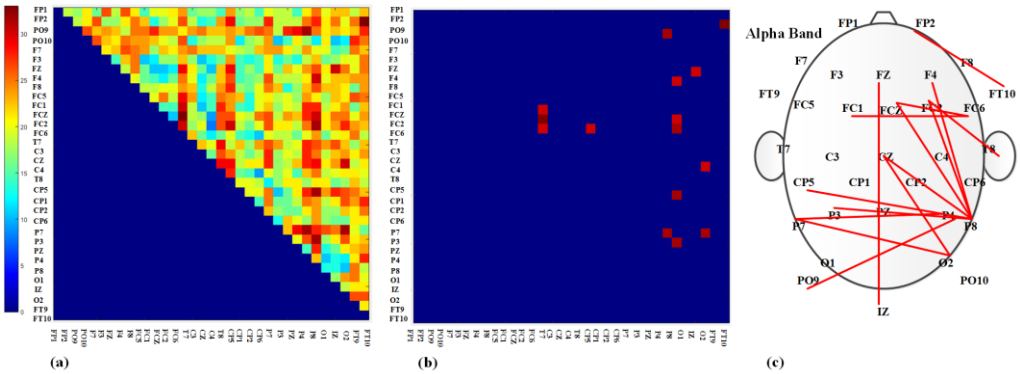

Fig. 4.2 (a) Accumulation matrix of imaginary coherence changes in the 7-year-old children within alpha band. (b) High intensity pixels derived from part (a). (c) Topography figure represents electrode pairs that corresponding to the pixels in (b).

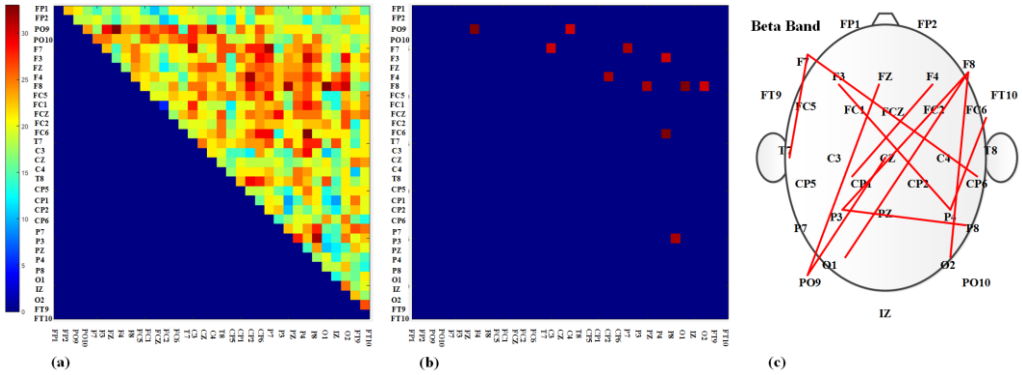

Fig. 4.3 (a) Accumulation matrix of imaginary coherence changes in the 7-year-old children within beta band. (b) High intensity pixels derived from part (a). (c) Topography figure represents electrode pairs that corresponding to the pixels in (b).

Group Aged Nine Years

Based on the accumulation method's outputs shown in Fig. 4.4, no variations in the *icoh* measure of the nine-year-old children were found between the congruent and incongruent stimuli at the delta, theta, and alpha frequency bands. Instead, significant changes in the interactions of the frontal lobe within the beta band were realised. As can be seen in Fig. 4.4 (c), the Flanker conflict seems to stimulate the functional

activity of the right fronto-central with the right and left frontal regions (FC6/F8, FC6/F7).

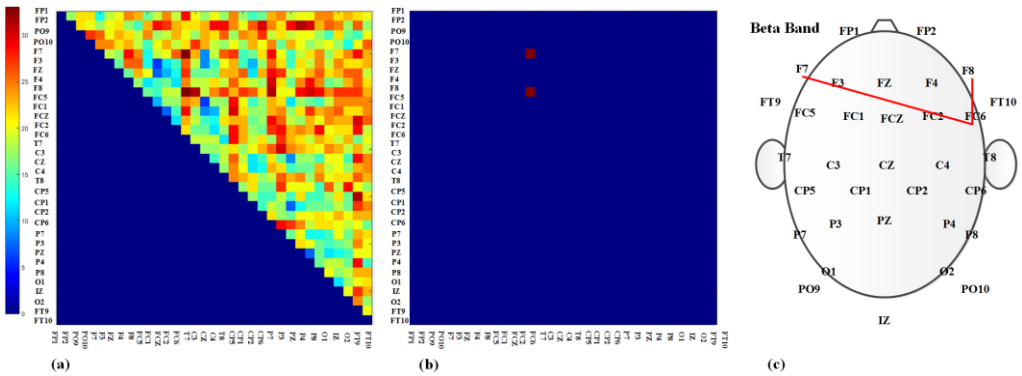

Fig. 4.4 (a) Accumulation matrix of imaginary coherence changes in the 9-year-old children within beta band. (b) High intensity pixels derived from part (a). (c) Topography figure represents electrode pairs that corresponding to the pixels in (b).

4.1.3 Discussion

To date (to our best knowledge), no prior research has been reported in the use of the imaginary coherence in studying children cognitive developments. However, the recent $icoh$ results show consistency with the coh findings reported in [104]. This, in turn, confirms that coherence and imaginary part of coherency are just two perspectives on the same concept (i.e. the coherency).

The main observation on the topographies of the seven-year-old group (Fig. 4.1 to Fig. 4.3) is the absence of the left inter-hemispheric coherency's changes. Namely, there were almost no changes regarding the incongruent stimuli in the connectivity between electrode pairs in the left hemisphere. Instead, distinct inter-hemispheric variations in the right part of the brain especially within the alpha activity were realised. Because of this and as suggested in [104], we conclude that the development of the left part of the child brain at age seven years preceded the right part.

Developments in the cognition of the nine-year-old children are revealed from the $icoh$ findings. As the $icoh$ was unable to determine changes in the network connectivity of the nine-year-old group in particular at the delta, theta and alpha

bands, a decline in the impact of the cognitive conflict is concluded. This matches the findings reported in [8] and [54].

The conflict impact that observed in the synchronisations of the right hemisphere at beta in Fig. 4.4(c) reveals that, at age nine years, the right hemisphere of the brain is not yet developed as well as the left hemisphere. This matches Thatcher et al. observation in [104], that the evolution of the right hemisphere takes place at age eight to 10 years.

4.2 Statistical Validation of the Imaginary Part of the Coherency Measure

This section reports the statistical verification of the study. The paired t-test was implemented on the imaginary part of the coherency. The procedure was identical to the one described in Chapter 3 (Section 3.3.1). Like in the previous section, the paired t-test was implemented to examine the effect of the Flanker conflict on the $icoh$ at each electrode pair (x, y) where H_0 (null hypothesis) states that the mean of the congruent $icoh$ is equal to the mean of the incongruent $icoh$, and H_a (alternative hypothesis to the left-tailed) states that the mean of the congruent $icoh$ is less than that of the incongruent $icoh$.

4.2.1 Results

Group Aged Seven Years

Fig. 4.5 (a-d) shows topography representation of the brain connectivity differences associated with the Flanker conflict at age seven years. It can be seen from Fig. 4.5 (a) that, the increase in the imaginary coherence within delta band was concentrated at the left hemisphere, where fronto-temporal area seems to be involved in all occurred interactions. At this band, there were increases in the correlations that link fronto-temporal to the central lobe (FT9/C3) and parietal lobe (FT9/P3, FT9/PZ).

Brain interactions regarding the stimuli type encountered no changes within the theta band as can be seen in Fig. 4.5(b). Alpha waves of the same recorded EEG signals were reacted differently (see Fig. 4.5 (c)). More regions in the right part of the cortex seem to be affected when the incongruent stimuli presented on the screen. An obvious increment in the functional connectivity was found between the temporal and frontal lobes in the right hemisphere (T8/FP2, T8/FZ, T8/FC2, T8/FCZ, and FT10/F4). Increment within the right central lobe (CZ/C4, CZ/CP6) and within the intra-hemispheric parietal lobe (P7/P4, P7/P8) were also realised within the same band.

The connectivity changes within the beta band is shown in Fig. 4.5 (d) which revealed changes in the longer distance connectivity primarily linking the occipital lobe to the frontal lobe (PO9/F3, PO9/FZ, O1/F8, and O2/F8). Also, change in the brain activity was observed in the right hemisphere between the parietal lobe and fronto-central area (P4/FC6), and within the parietal lobe (P3/PZ and P3/P8).

Table 4.1 shows the paired t-test statistics at the electrode pairs being defined within the four frequency bands, where $tstat$ refers to the value of the test statistic, df refers to the degrees of freedom of the test and sd refers to the standard deviation of $(incong - cong)$.

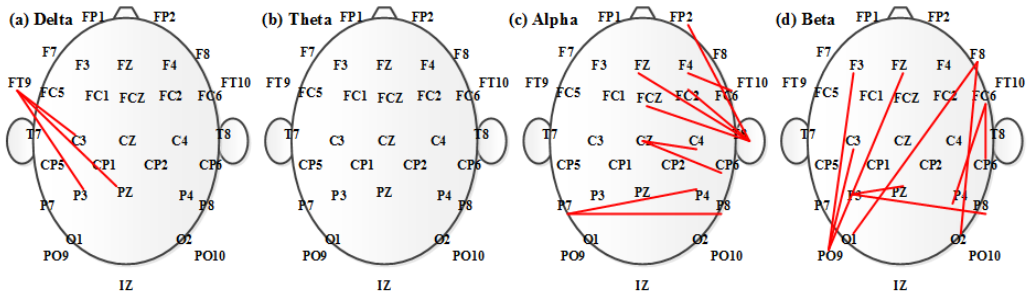

Fig. 4.5 Topography figures of the imaginary coherence's increment regarding the Flanker conflict in the group aged 7 years within (a) delta, (b) theta, (c) alpha, and (d) beta.

TABLE 4.1

Paired t-test statistics correspond to electrode pairs of interest (identified in Fig. 4.5) investigated within the frequency bands at age 7 years old

	Electrode pairs	$tstat$	df	sd	$P\ value$
Delta	FT9/C3	-2.4390	43	0.0145	0.0095
	FT9/PZ	-2.5533	43	0.0116	0.0072
	FT9/P3	-2.4742	43	0.0134	0.0087
Alpha	T8/ FP2	-2.4246	43	0.1876	0.0098
	T8/ FZ	-2.7014	43	0.1950	0.0049
	FT10/ F4	-2.9211	43	0.1186	0.0028
	T8/ FCZ	-2.6702	43	0.1873	0.0053
	T8/ FC2	-2.5066	43	0.1819	0.0080
	CZ/C4	-2.9373	43	0.1277	0.0027
	CZ/CP6	-2.6540	43	0.1633	0.0056
	P7/P4	-2.8706	43	0.1614	0.0032
	P7/P8	-2.6389	43	0.1825	0.0058
Beta	PO9/F3	-2.4724	43	0.0903	0.0087
	PO9/FZ	-2.6074	43	0.0925	0.0062
	PO9/C3	-2.4335	43	0.0897	0.0096
	O1/ F8	-3.1054	34	0.0894	0.0017
	O2/ F8	-2.4562	43	0.0843	0.0091
	FC6/CP6	-2.5276	43	0.0732	0.0076
	P4/ FC6	-2.5129	43	0.0787	0.0079
	P3/PZ	-2.8321	43	0.0438	0.0035
	P3/P8	-2.5110	43	0.0876	0.0079

Group Aged Nine Years

The results for the group aged nine years within delta band are depicted in Fig. 4.6 (a). It can be seen that the effect is represented in the changes within the temporal lobe (T7/T8) and with central lobe (T7/CZ, T7/C4, T7/CP6, T7/CP2, T7/CP1). The coherency changes were observed within the parietal lobe as well (P7/P3, P7/P4).

As shown in Fig. 4.6 (b), the paired t-test was able to detect increment in the intra-hemispheric coherency within the theta band. This is represented in the connectivity within the frontal lobe (F7/ F8) and that links the left frontal region to the right temporal (F7/ T8). Another intra-hemispheric change was observed within the central lobe (C3/ CP2). This change, in particular, was noticed to take a place within the alpha band as well as shown in Fig. 4.6 (c). In addition, pronounced increments in the right frontoparietal (F4/ P8, F8/ P8) and frontoccipital (F8/ O2) connectivity were observed.

Inter-hemispheric changes in the $icoh$ were observed within the beta band (see Fig. 4.6 (d)) on both sides of the brain between the temporal and frontal regions (FT9/FZ, T8/ FC6). In terms of the intra-hemispheric changes, increase in the $icoh$ within the frontal lobe (F7/FC6) and within the parietal lobe (P7/ CP6) were observed when the conflict was generated.

Table 4.2 shows the paired t-test statistics at the electrode pairs being defined within the four frequency bands, where $tstat$ refers to the value of the test statistic, df refers to the degrees of freedom of the test and sd refers to the standard deviation of $(incong - cong)$.

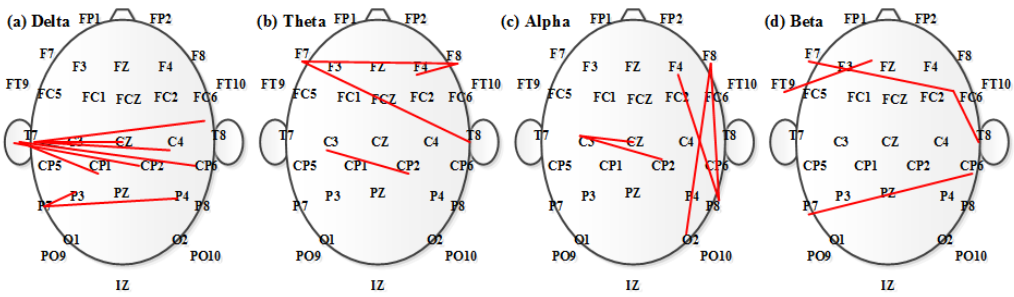

Fig. 4.6 Topography figures of the imaginary coherence's increment regarding the Flanker conflict in the group aged 9 years within (a) delta, (b) theta, (c) alpha and (d) beta.

TABLE 4.2

Paired t-test statistics correspond to electrode pairs of interest (identified in Fig. 4.6) investigated within the frequency bands at age 9 years old

	Electrode pairs	$tstat$	df	sd	$P\ value$
Delta	T7/C3	-2.8341	43	0.0104	0.0035
	T7/CZ	-2.5726	43	0.0122	0.0068
	T7/C4	-3.1564	43	0.0133	0.0015
	T7/T8	-2.6290	43	0.0135	0.0059
	T7/CP1	-2.8605	43	0.0115	0.0033
	T7/CP2	-2.6335	43	0.0138	0.0058
	T7/CP6	-2.8235	43	0.0133	0.0036
	P7/P3	-3.0788	43	0.0110	0.0018
	P7/P4	-2.7056	43	0.0138	0.0049
Theta	F7/F8	-2.4823	43	0.0826	0.0085
	F7/T8	-2.4462	43	0.0881	0.0093
	F4/F8	-2.6737	43	0.0578	0.0053
	C3/CP2	-2.4897	43	0.0584	0.0084
Alpha	F4/P8	-2.4895	43	0.1132	0.0084
	F8/P8	-3.0558	43	0.1087	0.0019
	F8/O2	-2.6360	43	0.1291	0.0058
	C3/CZ	-2.8828	43	0.0807	0.0031
	C3/CP2	-2.7897	43	0.0854	0.0039
Beta	F7/FC6	-3.1826	43	0.0763	0.0014
	FZ/FT9	-2.5668	43	0.0500	0.0069
	FC6/T8	-2.6411	43	0.0789	0.0057
	CP6/P7	-2.5758	43	0.0685	0.0068

4.2.2 Discussion

We noted that the accumulation method and the paired t-test have similar findings in common. At age seven years, conflict-related changes were observed to be more pronounced within alpha and beta bands.

Within the alpha band, common changes in the neural connectivity of the right and left sides of the parietal lobe were observed by the two methodologies (i.e. P7/P4, P3/P8 by the accumulation method as shown in Fig. 4.2(c) and P7/P4, P7/P8 by the paired t-test method as shown in Fig. 4.5(c)). In addition, another evidence of the network connectivity was verified by the statistical test to be subjected to the conflict influence; the frontal and temporal regions in the right hemisphere specifically FC2/T8. Moreover, it was verified that no differences were found in the inter-hemispheric network connectivity of the left part of the brain between the congruent and incongruent stimuli.

Within the beta band, two pieces of the network connectivity were verified by the paired t-test. The first occurs in the left hemisphere, connecting the parieto-occipital region to the frontal lobe (i.e. PO9/FZ as shown in Fig. 4.3(c) and Fig. 4.5(d)). The second occurs in the right hemisphere, connecting the fronto-central region to the parietal lobe (FC6/P4 as shown in Fig. 4.3(c) and Fig. 4.5(d)). Moreover, pronounced changes in the activity of the right frontal area and the occipital lobe (F8/O1, F8/O2) were detected by the accumulation method and subsequently verified by the statistical test.

At age nine years, the accumulation method detected conflict related-changes in the connectivity of the frontal lobe at the beta band which is reinforced by the results of the paired t-test (i.e. F7/FC6 as shown in Fig. 4.4 (c) and Fig. 4.6 (d) respectively).

Reduction in the Flanker conflict was revealed when the experiment was repeated two years later. This reduction was deduced from comparing the topography figures of the seven-year-old children with that of the nine-year-old children.

4.3 Summary

In this chapter, the imaginary component of coherency was utilised to assess the conflict-related changes in the network connectivity of the seven and nine-year-old children. Similar to the coherence method, connectivity matrices of the EEG data were calculated by the imaginary coherence at the Flanker congruent and incongruent conditions. These matrices were processed by the accumulation method to detect the Flanker conflict impact. Then they were passed to the Paired t-test for study verification.

It was found that, the paired t-test is more efficient on the imaginary component of the coherency ($icoh$) than on the coherence (coh) in verifying the conflict-related changes. Our finding demonstrates evidence for Piaget developmental staging of the brain hemispheres. Due to the suggested development of the left part of the brain at age seven years, no changes corresponding to the incongruent stimuli were found in the left inter-hemispheric connectivity.

The imaginary component of coherency demonstrates continues growth process of the brain hemispheres at age nine years. It is revealed when no coherency variations occurred regarding the task conflict within delta, theta and alpha bands, which implies that cognitive conflict decreases as children mature.

Chapter 5

Mining Coherency Data

In this chapter, we continue to investigate conflict-related changes in the network connectivity from a different perspective. We will concentrate on finding meaningful features in the coherency data (coherence, imaginary coherence) which can help to make distinction between them regarding the conflict. Extracting information from the data in such way is known as data mining or knowledge discovery from data (KDD) [107].

In this study, two different experiments were conducted to investigate the appropriate way in classifying the available coherency datasets. Section 5.1 reports the results of classifying the coherency datasets in respect to stimuli type, while 5.2 reports the results of classifying the coherency datasets in respect to age groups. Section 5.3 summarises the results and draws a conclusion.

5.1 Experiment 1

Mining Coherency Data of Flanker Stimuli per Age Group

In the first experiment, we aim to test the ability of the classifiers in discriminating the EEG coherency data (coherence, imaginary coherence) of the conflict stimuli (incongruent) from that of the non-conflict stimuli (congruent). In this experiment, we hypothesise that, conflict effect on the brain activity (e.g. [60], [7]), which is

assessed here by the EEG coherency, can be distinguished by the classification algorithms. Moreover, we hypothesise that performing the classification process on the coherency data of the seven and nine-year-old groups can reveal insights on the conflict decline that was observed after seven years of age as in [2] and [54].

Six most plausible classifiers from Weka software are examined on the coherency data (coherence, imaginary coherence) in the current study. These classifiers as detailed in Section 2.5.2 are naïve Bayes, support vector machines (SVM), multilayer perceptron (MLP), decision tree, random forests and random tree. As the aim of this study is to perform a broad assessment of the targeted classifiers, default values of the classifiers' parameters, as implemented in Weka, are used.

The classifiers are trained on the coherency values (coherence, imaginary part of coherency) to determine the Flanker stimuli type (congruent or incongruent). Consequently, coherency values that are calculated at the congruent condition are gathered with that calculated at the incongruent condition per frequency band (delta, theta, alpha and beta). The classifiers are initially examined on the entire size of the datasets and then on selected subsets. In each attempt, a comparison between the classification algorithms is performed in terms of the classification accuracy.

5.1.1 Procedure

Dataset Preparation

Four datasets associated to the frequency bands (delta, theta, alpha, beta) were generated for each age group (seven and nine-year-old) per coherency measure (coh, $icoh$). These datasets were given names to distinguish them. They were distinguished by the frequency band, age group and coherency measure such as "$delta7coh$" and "$beta9icoh$". The former dataset contains the coherence matrices at both conditions (congruent and incongruent) of the seven-year-old children within delta band and the later dataset contains the imaginary coherence matrices at both conditions (congruent and incongruent) of the nine-year-old children within beta band.

Identical procedure was followed to create the rest of the datasets. It began with gathering congruent and incongruent coherency matrices (i.e. each of the two belongs to individual participant k, where k=1,2,…, 45) of the age group within the band being addressed. Fig. 5.1 shows that the congruent and incongruent matrices (i.e. upper right triangular part which consists of 528 values) of each subject k in the group were transformed to vectors of 528 values. Labels were added to these vectors as "$cong$" for the congruent vector and "$incong$" for the incongruent vector. They were then stored in a data file that represents the training dataset. Based on this, each data file contains 90 instances and 528 attributes (features).

These data files were then transformed into the format (i.e. attribute-relation file format, ARFF) suitable for the Weka software [111]. As shown in Fig. 5.2, the ARFF file structure may begin with lines of % sign for comments describing the dataset. Dataset name must be specified in a line which starts with the definition @ relation. Instance attributes are detailed in a block of lines, each of which begins with the definition @ attribute followed by attribute's name and then its type.

In the present research, all attributes are of numeric type except the classes of nominal type. EEG electrodes that were involved in each coherency assessment were used as a distinguished name to the corresponding attribute. For example, coherency value measured between channel FP1 and FP2 was stored in the ARFF file under attribute named FP1FP2. Coherency data were added to the ARFF file after the definition *@data*. They were listed one per line with commas separating the attributes.

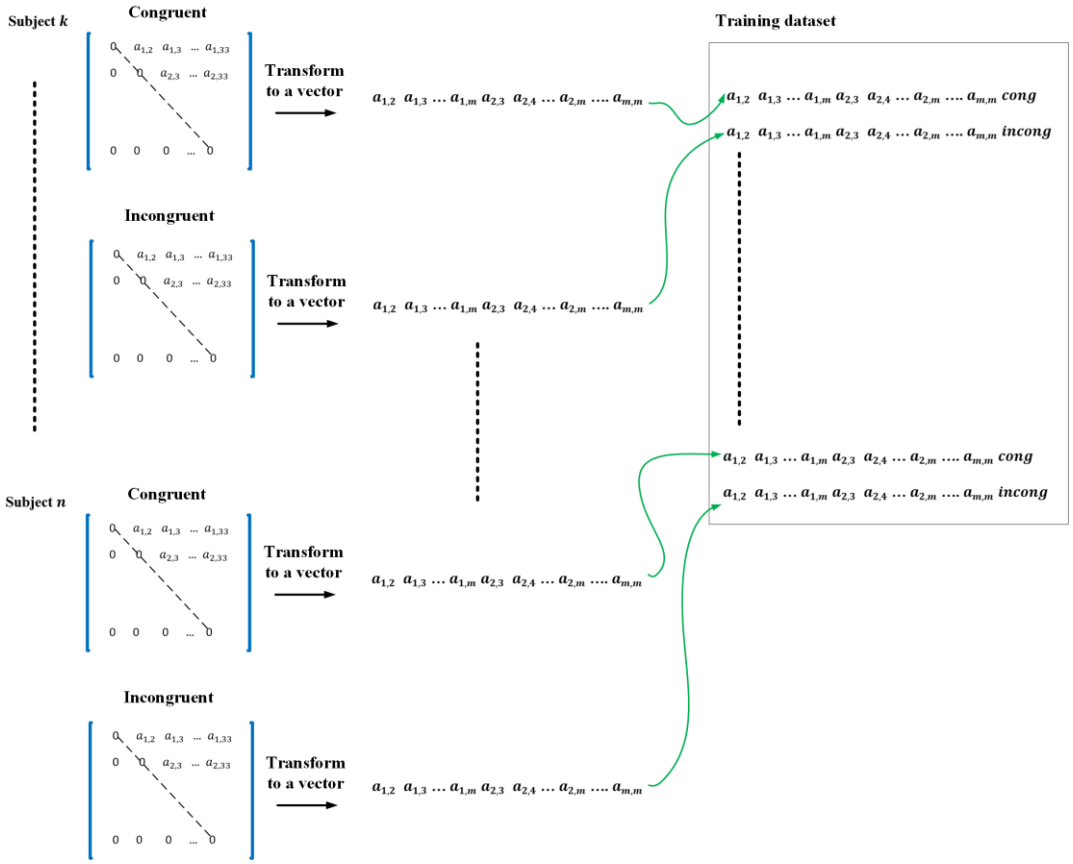

Fig. 5.1 The procedure followed among the analysis to produce data instances of experiment 1.

```
% ARFF file for the imaginary coherence of the 9-year-old children within alpha band
@relation alpha9icoh

@attribute FP1FP2    numeric
@attribute FP1PO9    numeric
@attribute FP1PO10   numeric
@attribute FP1F7     numeric
@attribute FP1F3     numeric
@attribute FP1FZ     numeric
@attribute FP1F4     numeric
@attribute FP1F8     numeric
@attribute FP1FC5    numeric
@attribute FP1FC1    numeric
@attribute FP1FCZ    numeric
@attribute FP1FC2    numeric
@attribute FP1FC6    numeric
@attribute FP1T7     numeric
@attribute FP1C3     numeric
@attribute FP1CZ     numeric
@attribute FP1C4     numeric
@attribute FP1T8     numeric
@attribute FP1CP5    numeric
@attribute FP1CP1    numeric
.
.
.
.
.
@attribute stim      {cong,incong}

@data
0.079704,0.036413,-0.13975,0.070796,-0.013636,0.062105,0.16676,0.1035,0.034495,0.022504,0.059405,0.089188,.......,cong
0.10732,0.17475,-0.0016374,0.024608,0.021157,-0.017174,0.030895,0.030327,-0.0071723,-0.063571,-0.010507,.........,incong
-0.0099263,0.015675,-0.065038,-0.16798,-0.052228,-0.1199,-0.14804,0.15817,-0.034698,-0.012744,-0.0093485,.........,cong
0.022861,-0.015366,-0.035684,0.024998,0.002082,-0.0081469,-0.046672,-0.036681,-0.033443,-0.037415,0.1079,.......,incong
-0.030793,-0.041479,-0.068598,-0.1529,-0.0073083,-0.029361,-0.070709,-0.12762,-0.021701,-0.036189,-0.056969,.......,cong
-0.087011,-0.081725,-0.065938,-0.10588,-0.070536,0.099872,-0.085048,0.062364,-0.078755,-0.010848,0.0034392,......,incong
-0.032085,0.0089673,-0.17429,-0.062483,-0.01541,-0.090085,-0.10668,-0.18112,-0.14941,-0.11802,-0.14129,.......,cong
-0.071455,-0.1971,-0.13789,-0.12803,-0.083655,-0.09827,-0.11389,-0.10018,-0.086738,0.0021142,0.1339,0.14028,......,incong
.
.
.
.
.
.
```

Fig. 5.2 Illustrations for the ARFF data file structure.

Cross Validation

The amount of instances generated from the coherency matrices within each band was 90 instances. This number is not adequate to be divided into training and testing sets. In practise, holding out part of the data for testing and using the remaining for training is the common solution [111]. This technique is known as the cross-validation, and it depends on dividing the data into a fixed number of folds. In the present work, we chose 10 because it has shown the best error minimisation through numerous tests. In practical terms, it is characterised as the standard method and is termed as tenfold cross-validation. The learning process is computed 10 times. Each time one fold (one-tenth) is held out to be the testing set after training is perform on the remaining nine-

tenths of the dataset. In each run, error estimate is evaluated on these training set. They are averaged to end up with overall classification performance.

Attributes Extraction

Initially the classifiers were trained on the complete attributes set, and then they were trained on selected subsets of the attributes. Machine learning algorithms often get distracted by the irrelevant attributes. In particular, when the attributes count is as quite large as in this study (i.e. 528 attributes). In this case, it is very common to use a subset of the attributes instated [111] [107]. Such reduction in the attributes count was found to be very useful in speeding up the learning algorithms and improving the classification performance.

This attribute selection task was performed by implementing *WrapperSubsetEval* technique from Weka data mining framework. It is based upon the Wrapper method which uses a classifier to determine an ideal attributes subset [111]. In Wrapper method, the training set is divided into several subsets of different sets of attributes. Then, cross-validation technique (explained above), that holds one subset for testing and use the rest for training the classifier, is used to find the best attributes subset to achieve the highest classification performance.

5.1.2 Results

Coherence Datasets

Classification accuracy on the coherence datasets of the seven and nine-year-old groups within the frequency bands are shown in tables 5.1 and 5.3. The six implemented classifiers (i.e. naïve Bayes, support vector machines (SVM), multilayer perceptron (MLP), decision tree, random forests and random tree) are listed in the first column. The yellow coloured columns display classification accuracy for the seven-year-old group while the blue coloured columns display classification accuracy for the nine-year-old group. The best result across each band (i.e. column) is highlighted in bold.

Table 5.1 shows the results of implementing the classifiers on the entire coh datasets (90×528). The highest accuracy in the seven-year-old group was 45.5 % within delta, 47.7% within theta, 59.1% within alpha and 46.6 % within beta. While for the nine-year-old group, it was 48.9% within delta, 47.7% within theta, 48.9% within alpha and 45.5% within beta. These significant results in the two age groups are not associated to any classifier.

Table 5.2 demonstrates attribute subsets that were extracted from the entire coh datasets (90×528) by the wrapper method. The yellow coloured columns are associated to the seven-year-old group across bands (i.e. delta, theta, alpha and beta). While the blue coloured columns are associated to the nine-year-old group.

Classification results on the extracted subsets of both groups (seven and nine-year-old) are presented in table 5.3. We note that the classification accuracies were improved compared to the previous results shown in table 5.1. In addition, the decision tree (i.e. J48) is consistently the best performing on the coh measure in both groups across the frequency bands. It achieved 73.9% within delta, 63.6 % within theta, 79.5% within alpha and 62.5 % within beta as the highest accuracy in the seven-year-old group. While it achieved 73.9% within theta, 69.3% within alpha and 54.5 % within beta in the nine-year-old group.

TABLE 5.1

Classification results on the entire coh datasets of the 7 and 9-year-old groups

	Delta		Theta		Alpha		Beta	
Classifier	*7 years*	*9 years*	*7 years*	*9 years*	*7 years*	*9 years*	*7 years*	*9 years*
NaiveBayes	35.2%	44.3%	**47.7%**	**47.7%**	43.2%	33.0%	30.7%	39.8%
LibSVM	42.1%	43.2%	44.3%	46.6%	44.3 %	43.2%	44.3%	**45.5%**
MultilayerPerceptron	36.4%	30.7%	44.3%	28.4%	45.5 %	38.6%	41.0%	21.6%
J48	**45.5%**	**48.9%**	39.8%	37.5 %	**59.1%**	42.1%	38.6%	31.8%
RandomForest	39.8%	44.32%	39.8%	27.3%	45.5 %	34.1%	26.1%	19.3%
RandomTree	**45.5%**	**48.9%**	43.2%	44.3%	40.9 %	**48.9%**	**46.6%**	34.1%

TABLE 5.2

Attribute subsets derived from the *coh* datasets

Delta		Theta		Alpha		Beta	
7 years	*9 years*	*7 years*	*9 years*	*7 years*	*9 years*	*7 years*	*9 years*
FC5P4	FP1PZ	**CP6FT9**	FP1T7	FP2F8	PO9CP5	**FP1O1**	PO9FC2
FC1FT9	PO10FT9	FP1FP2	FP1P7	FP2CP6	PO9P8	FP2C4	PO10IZ
FC6CZ	F4FT9	PO9FT10	FP2FT9	PO9F4	F7F3	PO10CP6	F3T8
T7P4	FC6IZ	F7F4	PO10FC5	PO9O1	F7FCZ	F3FC1	F3P8
T8P4	CZCP2	FZFC2	F4O1	PO10PZ	F8T8	F4FC6	FZFC5
CP1PZ	T8FT10	F4FC2	F4O2	F3CZ	FC1T7	CP1P3	FZP8
		F4CP6	FC5P4	FCZP8	FC1CP1		F4T8
		FC6CP2	FC1PZ	CP6P3	FC1IZ		F4CP2
			FCZFC2		FC2CP6		F8C3
			FCZP7		FC6T7		F8CP1
			FC2CP1		C3T8		FC1CP6
			FC2O2		CZCP1		FCZCP5
			T7CP5		CZCP2		FC2P3
			C4T8		CZO1		
			T8O1		T8PZ		
			CP1P8		CP2P3		
			CP2IZ		CP6P4		
					P7FT9		

TABLE 5.3
Classification results on the *coh* datasets of the 7 and 9-year-old groups after subset attribute selection was performed. © [2016] IEEE.

	Delta		Theta		Alpha		Beta	
Classifier	*7years*	*9years*	*7years*	*9years*	*7years*	*9years*	*7years*	*9years*
NaiveBayes	45.5 %	48.9%	55.7 %	52.3%	48.9 %	31.8 %	46.6 %	40.9%
LibSVM	39.8 %	44.3%	53.4 %	44.3%	44.3 %	43.2 %	44.3 %	43.2%
MultilayerPerceptron	59.1 %	51.1%	60.2 %	48.9%	58.0 %	35.2 %	44.3 %	36.4%
J48	**73.9%**	63.6%	**63.6%**	**73.9%**	**79.5%**	**69.3%**	**62.5%**	**54.5%**
RandomForest	61.4 %	**67.0%**	60.2 %	42.0 %	58.0 %	53.4 %	44.3 %	44.3 %
RandomTree	54.5 %	61.4%	60.2 %	59.1 %	53.4 %	59.1%	44.3 %	53.4 %

Imaginary Coherence Datasets

Like the coh datasets, the six classification algorithms were applied to the entire $icoh$ datasets (90×528). From table 5.4, we can see that naïve Bayes is the most accurate classifier in distinguishing the Flanker stimuli across the frequency bands. In the seven-year-old group, best classification accuracy was 59.1% within delta, 72.7% within theta, 78.4% within alpha and 79.5% within beta. While in the nine-year-old group, it was 60.2 % within delta, 61.4 % within theta, 54.5 % within alpha and 67 % within beta.

Table 5.5 shows the attribute subsets extracted from the $icoh$ datasets by the wrapper algorithm. Significant improvement was observed in the classifiers performance on the extracted attribute subsets as demonstrated in table 5.6.

The best performing results were obtained by the naïve Bayes classifier. It discriminated $icoh$ measures within alpha and beta bands in the seven-year-old group with 90.9% accuracy and in the nine-year-old group with 88.6% and 84.1% accuracy at beta and theta respectively.

TABLE 5.4

Classification results on the entire $icoh$ datasets of the 7 and 9-year-old groups

	Delta		Theta		Alpha		Beta	
Classifier	*7 years*	*9 years*	*7 years*	*9 years*	*7 years*	*9years*	*7years*	*9years*
NaiveBayes	**59.1%**	**60.2%**	**72.7%**	**61.4%**	**78.4%**	**54.5%**	**79.5%**	**67%**
LibSVM	46.6%	46.6%	44.3%	45.5%	46.6%	43.2%	48.9%	43.2%
MultilayerPerceptron	38.6%	48.9%	36.4%	44.3%	44.3%	39.8%	52.3%	45.5%
J48	52.3%	51.1%	60.2%	52.3%	60.2%	**54.5%**	55.7%	47.7%
RandomForest	40.9%	52.3%	59.1%	55.7%	68.2%	46.6%	61.4%	60.2%
RandomTree	50%	50%	59.1%	56.8%	60.2%	47.7%	58%	48.9%

TABLE 5.5

Attribute subsets derived from the *icoh* datasets

Delta		Theta		Alpha		Beta	
7 years	*9 years*	*7 years*	*9 years*	*7 years*	*9 years*	*7 years*	*9 years*
FP1PO9	FP2PO9	FP1FT10	FP2T8	FP2O2	FP2FT10	FP2CP2	FP2T8
FP1O2	FP2F8	FP2F7	PO10FC6	PO9T8	PO9PO10	FP2P8	PO9F4
PO9P4	PO10C3	FP2O1	FZFC5	F7FC5	PO10CP1	PO9IZ	PO10CP5
F3CP2	PO10FT9	PO9FT10	T7T8	F7FC2	PO10FT10	PO9O2	F7FC2
FC1FT10	F4FC6	F3T8	CZO1	F7CP6	F7F3	F4PZ	F7P3
C3FT9	F4P8	FC5FC1	CP1CP2	F3FC1	F7CP2	FC1CP2	FZFCZ
CZCP5	F8CP6	FC1CP5	CP6PZ	F8P4	T7C4	T7IZ	FZT8
	F8O2	FC1CP1	P7FT9	F8O2	CZO2	CP5FT10	F8T7
	FC5FC2	FCZFT10	PZFT10	FC5P7	P7O1	P7PZ	FC1FC6
	FCZC3	T7CP6		FC1T7	FT9FT10	PZP8	FCZFC6
	CP1P7	P7FT10		FC2T8		PZFT9	FCZP8
	CP6P4			FC2O1			FCZFT10
				T8CP6			T8O1
				CP6P3			
				CP6IZ			

TABLE 5.6

Classification results on the *icoh* datasets of the 7 and 9-year-old groups after subset attribute selection was performed.

	Delta		Theta		Alpha		Beta	
Classifier	*7 years*	*9 years*	*7 years*	*9 years*	*7 years*	*9 years*	*7 years*	*9 years*
NaiveBayes	**81.8 %**	**72.7%**	**83.0%**	**84.1%**	**90.9%**	**83.0 %**	**90.9 %**	**88.6 %**
LibSVM	48.9 %	43.2 %	40.9 %	47.7 %	45.5%	46.6%	43.2%	45.5 %
MultilayerPerceptron	55.7 %	60.2 %	59.1 %	58.0 %	68.2 %	71.6 %	62.5%	64.8 %
J48	65.9 %	60.2 %	65.9 %	64.8 %	72.7 %	67.0 %	67.0%	63.7 %
RandomForest	60.2 %	65.9 %	72.7 %	73.9 %	76.1 %	67.0 %	73.9%	72.7 %
RandomTree	58.0%	55.7 %	59.1 %	58.0 %	70.5%	56.8 %	68.2%	65.9%

5.1.3 Discussion

It was shown in the results above that, any attempt to use the entire attributes set of the coh data seems to distract the classification. The classification accuracy across the two age groups was not significant (it was ≤ 59.1%, slightly above chance). In addition, it was difficult to assess which learning algorithm is more efficient with such datasets. Eliminating the trivial attributes using the wrapper technique enhanced the performance of the classifiers. The J48 algorithm discriminates Flanker stimuli within delta and alpha bands with an accuracy ≥ 73.9% for the age seven years group. With a lower classification accuracy (i.e. 73.9% at theta and 69.3% at alpha), the J48 classifier was also the winner in classifying the coh datasets of the nine-year-old group at theta and alpha bands.

In contrast to the coh datasets, classifying the $icoh$ instances using the entire attributes set produced comparatively better results. This may mean that the volume conduction effect is being minimised within the $icoh$ measures. The naïve Bayes classifier showed the best performance in distinguishing the Flanker stimuli at age seven-years with an accuracy ≥ 78.4% within the alpha and beta band. It is also the best performing classifier for the age nine-year group with an accuracy ≥ 61.4% within theta and beta.

Attribute selection technique generally increased the classification performance for the $icoh$ datasets (table 5.6). Where the accuracy of Naïve Bayes classifier within alpha and beta in the seven-year-old group has increased to 90.9%, and within theta and beta in the nine-year-old group has increased to be ≥ 84.1%.

In terms of EEG conflict's spatial information, attribute subsets of the $icoh$ datasets presented in table 5.5 were depicted in topographical figures in order to make general comparisons with the results of the accumulation method presented in Chapter 4. Fig. 5.3 and Fig. 5.4demonstrate the topography of the $icoh$ attribute subsets within the frequency bands in the seven and nine-year-old groups respectively. In Fig. 5.3 (c), we observed that, the coherency between electrodes FC2 and T8 was selected by the wrapper method to distinguish between Flanker stimuli within alpha band at age seven years. This exact pair was previously identified in Chapter 4 by the accumulation

method on the *icoh* measure (page 60, line 3, Fig. 4.2 (c)). Then, it was statistically verified by the paired t-test (page 64, line 6, Fig. 4.5 (c)).

This particular area in the right hemisphere (i.e. temporal-frontal coupling) was identified in [104] to be not developed before age eight years. This may explain why its synchronisation was significantly changing when processing the conflict as identified by the current research.

Another common change in the synchronisation of the seven-year-old children was observed by the two methodologies, which may refer also to the late evolution of the right frontal lobe. It is associated to the neural activity that links right frontal with right parietal lobe within beta band. In Fig. 5.3 (d), it is represented by the connectivity that links FP2 with CP2 and F4 with PZ. In Chapter 4 (page 60, line 13, Fig. 4.3 (c)), similar finding was detected by the accumulation method in the connectivity that links F4 with CP1.

Although the development of the right hemisphere as suggested in [104] does not complete before age 10 years, the conflict seems to have no effect on the right interhemispheric synchronisation at age nine years as commonly identified by the two methodologies within beta band. Fig. 5.4 (d) presents that the neural connectivity between the left frontal and right fronto-central activity at beta was identified by the wrapper method as electrode pair F7/FC2. This variation was previously captured by the accumulation method in Chapter 4 (Page 62, Line 2 and Fig. 4.4 (c)) in the correlation of F7 and FC6. It was also verified by the paired t-test (Page 66, Line 15 and Fig. 4.6 (d)).

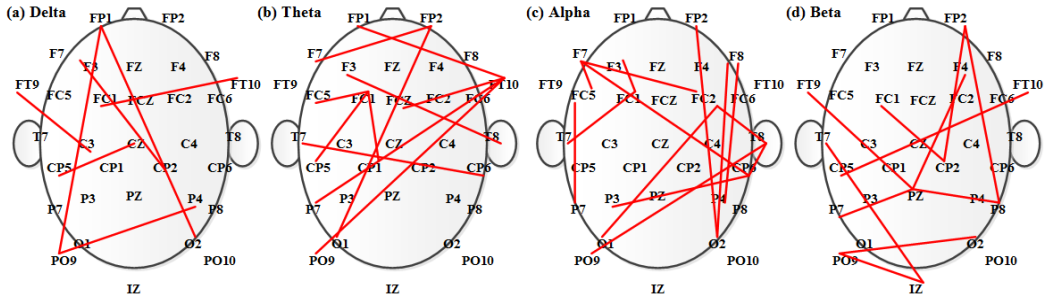

Fig. 5.3 Topography figures for the *icoh* attribute subsets demonstrated in table 5.6 at age seven years.

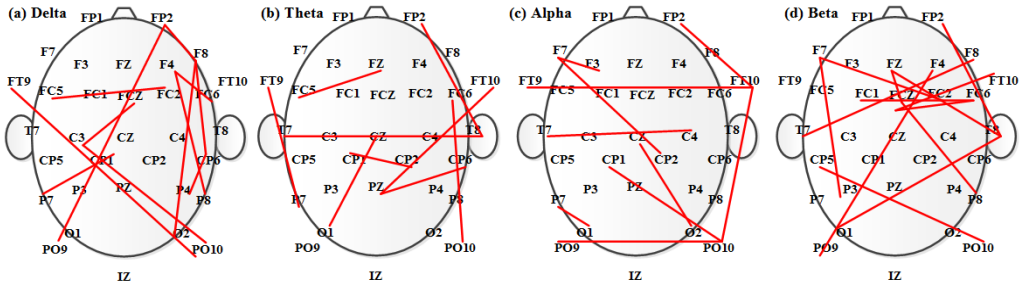

Fig. 5.4 Topography figures for the *icoh* attribute subsets demonstrated in table 5.6 at age nine.

5.2 Experiment 2

Mining Coherency Data of Age Groups per Stimuli Type

In this experiment, we investigated the ability of the classification algorithms in discriminating coherency data from different age groups (seven and nine-year-old). It is relied on checking age-related changes in the network connectivity when one type of stimuli is performed. In other words, age groups are classified based on the network connectivity reaction to one type of stimuli each time (i.e. cong (age 7) vs. cong (age 9), incong (age 7) vs. incong (age 9).

This approach can reveal which stimuli type is the best to differentiate between network connectivity of two age groups. We hypothesised that implementing the classifiers on the coherency data of different age groups (i.e. seven and nine-year-old) that assess the conflict stimuli (incongruent stimuli) will produce better accuracy than that assess non-conflict stimuli (congruent stimuli).

Classifiers set that demonstrated in Section 2.5.2 were utilised in this work as well. They were initially examined on the entire size of the datasets and then on the selected subsets.

5.2.1 Procedure

For each stimuli type (congruent, incongruent), Four datasets associated to the frequency bands (delta, theta, alpha, beta) were generated per coherency measure (coh,$icoh$). They were distinguished by names such as "*alphaCongcoh*" and "*thetaIncongicoh*". The former dataset is associated to the congruent stimuli. It contains coherence matrices of the seven and nine-year-old children within alpha band. While the later dataset is associated to the incongruent stimuli and contains the imaginary coherence matrices of the seven and nine-year-old children within theta band.

Fig. 5.5 shows how the datasets were generated for this experiment. The procedure was identical to that explained in Section 5.1.1. The only difference is which coherency matrices were targeted. As demonstrated in Fig. 5.5, for each subject k, coherency matrices of the same stimuli type from both groups (seven and nine-year-old) were involved. They were transformed to vectors of 528 elements and labelled by either "7" or "9". Then they were stored in ARFF files and passed to the Weka software. Using all of the data attributes (i.e. 528 attributes); classification algorithms that detailed in Section 2.5.2 were first implemented. In order to enhance the performance of the classifiers, the entire coherency datasets were substituted by attribute subsets, which were extracted by the Wrapper method (as explained in Section 5.1.1).

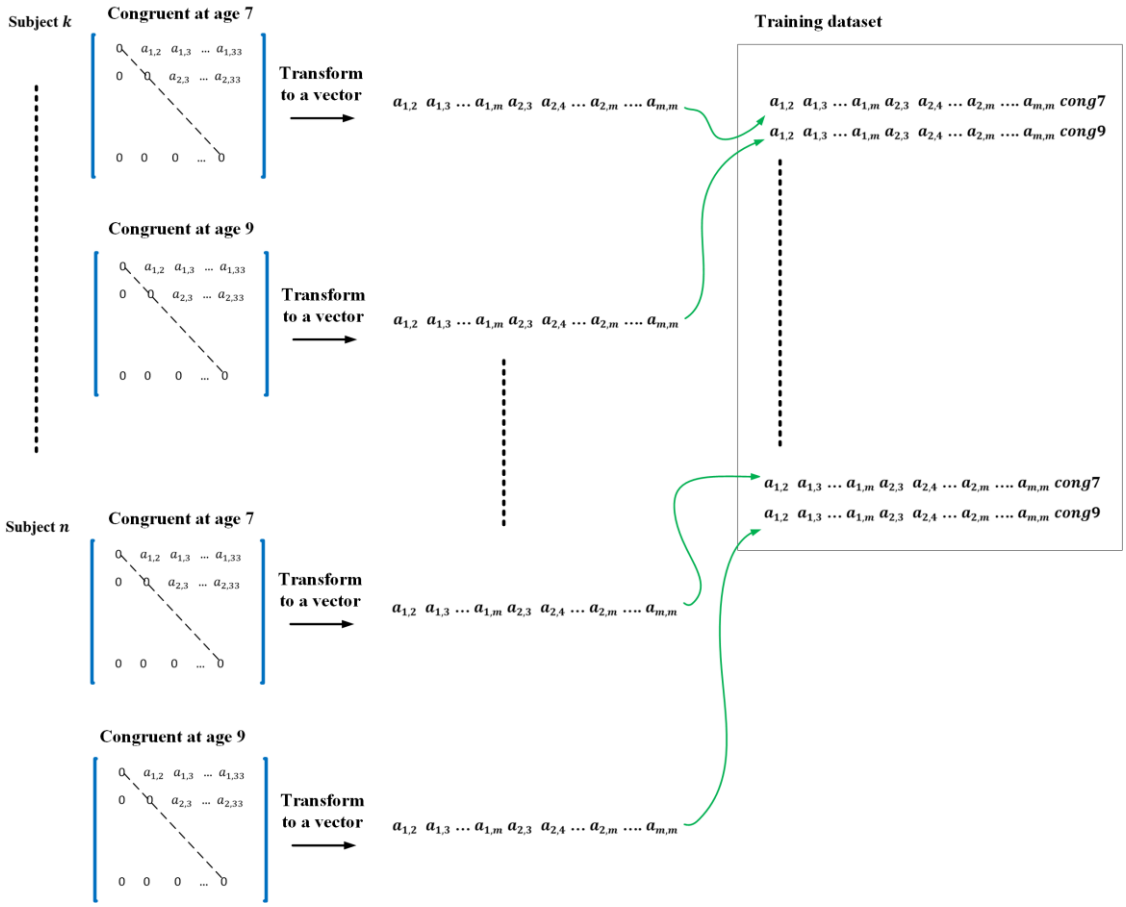

Fig. 5.5 The procedure followed among the analysis to produce data instances of experiment 2.

5.2.2 Results

Coherence Datasets

Tables 5.7 and 5.9 show classification results on the coherence measure before and after attribute selection. First column shows the six implemented classifiers. Columns coloured in yellow present the classification accuracy on the congruent stimuli and columns coloured in blue present the classification accuracy on the incongruent stimuli. The best accuracy in each column was highlighted in bold.

In table 5.7, the MultilayerPerceptron classifier provided the highest accuracy in discriminating children age groups (seven and nine year-old) at the congruent condition, which was ≥ 59.1% across all the frequency bands. As for the incongruent condition, better accuracies (≥ 61.4%) were achieved within the frequency bands compared to that at the congruent condition. However, no particular classifier performs consistently in this case.

Table 5.8 demonstrates attribute subsets that were extracted from the entire *coh* datasets (90×528) by the wrapper method. The yellow coloured columns display the subsets that are associated to the congruent stimuli across bands (i.e. delta, theta, alpha and beta). While the blue coloured columns display the subsets that are associated to the incongruent stimuli.

Attribute subsets that were extracted from the *coh* datasets by the wrapper method are shown in table 5.8. Performing machine learning algorithms on these subsets have improved the results as can be seen in table 5.9. The naïve Bayes achieved the best performance accuracy within the frequency bands at both task conditions (congruent and incongruent). Its accuracy performance at the incongruent condition (≥ 69.3%) was better than that at the congruent condition (≥ 63.6%) particularly within the theta, alpha and beta bands.

TABLE 5.7

Results of classifying the entire *coh* datasets by Flanker stimulus type

	Delta		Theta		Alpha		Beta	
Classifier	*Cong.*	*Incong.*	*Cong.*	*Incong.*	*Cong.*	*Incong.*	*Cong.*	*Incong.*
NaiveBayes	55.7%	52.3%	50%	51.1%	50%	48.9%	51.1%	48.9%
LibSVM	44.3%	45.5%	45.5%	45.5%	45.5%	45.5%	45.5%	45.5%
MultilayerPerceptron	**62.5%**	45.5%	**59.1%**	58 %	**61.4%**	**67%**	**59.1%**	**68.2%**
J48	55.7%	**62.5%**	44.3%	47.7%	48.9%	50%	58%	55.7%
RandomForest	50%	45.5%	50%	52.3%	50%	58%	52.3%	60.2%
RandomTree	54.5%	46.6%	43.2%	**61.4%**	46.6%	55.7%	50%	59.1%

TABLE 5.8

Attribute subsets derived from the *coh* datasets

Delta		Theta		Alpha		Beta	
Cong.	*Incong.*	*Cong.*	*Incong.*	*Cong.*	*Incong.*	*Cong.*	*Incong.*
F7C3	FP2FC2	FC5FC2	FP1FT10	FP1CZ	FP2F4	PO10O2	PO9O1
FC5C4	FP2C3	FC5FT9	PO9P8	FZFC1	FP2FT10	FZFCZ	F3FC1
FC5FT9	PO10CP6	FCZP4	FC1P4	F8FC1	F7FC5	F4FC2	F4F8
FCZC4	FC1CP1	P3O2	FC2CP6	F8C4	FZFC1	F8FC6	F4FC6
FC6CZ	CP1CP2	O1O2	CP5P3	T8CP6	FZFC2	FC5T7	F8FC6
FC6CP2	P7P4		CP1P4	P4P8	FZFC6	P4P8	
FC6FT10	P8O1		PZP4		FCZFC2		
CP2P3					FCZCP1		
CP2O2					FC6FT10		
CP6O2					C3P3		
P4P8					CZCP1		
					T8FT10		
					P7P3		
					IZO2		

TABLE 5.9

Results of classifying the feature subsets of *coh* datasets by Flanker stimulus type

	Delta		Theta		Alpha		Beta	
Classifier	*Cong.*	*Incong.*	*Cong.*	*Incong.*	*Cong.*	*Incong.*	*Cong.*	*Incong.*
NaiveBayes	**78.4%**	**71.6 %**	**75 %**	**76.1 %**	**63.6%**	**74%**	65.9%	**69.3 %**
LibSVM	45.5%	45.5 %	58 %	58 %	47.7%	48.9 %	54.5%	64.8 %
MultilayerPerceptron	58%	56.8 %	68.2%	65.9 %	51.1%	65.9 %	**67.0%**	69.3 %
J48	60.2%	43.2 %	64.8%	54.5 %	55.7%	55.7 %	59.1%	47.7 %
RandomForest	65.9%	58 %	64.8%	62.5 %	56.8%	63.6 %	61.4%	55.7 %
RandomTree	59.1%	52.3 %	63.6%	61.4 %	58%	60.2 %	64.8%	50 %

Imaginary Coherence Datasets

When the full *icoh* datasets (90×528) were passed into the targeted classifiers, the performance accuracy of the naïve Bayes for the incongruent condition exceeded 83% within theta, alpha and beta bands as shown in table 5.10. In contrast, the classification results by the congruent stimuli did not exceed 53.4% within the four frequency bands for all classifiers.

Table 5.12 demonstrates that passing the *icoh* features' subsets to the classifiers produced better classification accuracies. The naïve Bayes is consistently the best performing on the imaginary coherence feature subsets at all frequency bands for both conditions. It reasonably classified the connectivity measures correctly into the two age groups (seven and nine year-old children) for the congruent condition at all frequency bands with accuracy ≥ 72.7%. While its accuracy for the incongruent condition increased to 76.1% within the delta band and be ≥ 94.3% within the higher frequency bands (i.e. theta, alpha and beta).

TABLE 5.10

Results of classifying the entire *icoh* datasets by Flanker stimulus type

	Delta		Theta		Alpha		Beta	
Classifier	*Cong.*	*Incong.*	*Cong.*	*Incong.*	*Cong.*	*Incong.*	*Cong.*	*Incong.*
NaiveBayes	**53.4%**	50%	42%	**83%**	**50%**	**88.6%**	44.3%	**89.8%**
LibSVM	45.5%	45.5%	45.5%	45.5%	46.6%	47.7%	42%	46.6%
MultilayerPerceptron	50%	**54.5%**	**50%**	42%	**50%**	47.7%	48.9%	53.4%
J48	40.9%	48.9%	44.3%	68.2%	42%	69.3%	38.6%	81.8%
RandomForest	52.3%	46.6%	38.6%	77.3%	46.6%	81.8%	44.3%	**89.8%**
RandomTree	50%	52.3%	45.5%	65.9%	53.4%	72.7%	**50%**	67%

TABLE 5.11

Attribute subsets derived from the *icoh* datasets

Delta		Theta		Alpha		Beta	
Cong.	*Incong.*	*Cong.*	*Incong.*	*Cong.*	*Incong.*	*Cong.*	*Incong.*
FP2F4	PO10F7	PO10FC5	FP1FP2	FP1CP6	FP1CZ	FP1F8	F3FC1
F4CZ	F7P7	PO10T7	PO9C4	FP1FT10	FP1IZ	FP1PZ	FZCP2
CP6P4	FC5CP1	F3O2	F7T8	PO9O1	PO10CP6	F3IZ	FZP3
CP6FT9	FCZC3	F4F8	FZP7	PO10FT10	F7CP1	F4FC6	FZFT10
CP6FT10	C3CP5	FC1IZ	F4T8	F3FC1	F3T7	F8CP5	F4FC5
P3FT9	C3CP2		T7T8	F4C4	FZFT10	F8O2	C4CP6
	CP5CP6		T7FT9	F8FCZ	FC5O2	FCZCZ	
			T7FT10	F8CP5	T7CZ	FCZO2	
			T8PZ	T8CP5	T8P3	P7IZ	
				T8P7	CP1P8		
				CP1FT9			

TABLE 5.12

Results of classifying the feature subsets of *icoh* datasets by Flanker stimulus type

	Delta		Theta		Alpha		Beta	
Classifier	*Cong.*	*Incong.*	*Cong.*	*Incong.*	*Cong.*	*Incong.*	*Cong.*	*Incong.*
NaiveBayes	**78.4%**	**76.1%**	**72.7%**	**94.3%**	**76.1%**	**96.6%**	**81.8%**	**95.5%**
LibSVM	48.9%	48.9%	51.1%	48.9%	48.9%	46.6%	43.2%	45.5%
MultilayerPerceptron	69.3%	65.9%	59.1%	73.9%	61.4%	77.3%	68.2%	75%
J48	62.5 %	62.5%	68.2%	69.3%	55.7%	73.9%	60.2%	81.8%
RandomForest	63.6%	69.3%	62.5%	81.8%	71.6%	79.5%	67%	86.4%
RandomTree	58%	58%	55.7%	72.7%	65.9%	69.3%	54.5%	75%

5.2.3 Discussion

Before extracting the attribute subsets, the first assessment was to examine how efficient the machine learning algorithms are in discriminating age groups (seven and nine years) in coherency values by using total number of 528 attributes. With the coh datasets, the measures of incongruent stimuli released the best results. The classifiers discriminated the instances with an accuracy $\geq$ 61.4% across frequency bands. Similarly, with the entire $icoh$ datasets, naïve Bayes classifier was successful in classifying the incongruent instances at theta, alpha and beta with an accuracy exceeding 83%.

After implementing the classification algorithms on the selected attributes, the naïve Bayes classifier presented to be the best in classifying the incongruent coh datasets with accuracy exceeding 69.3% at the theta, alpha and beta. Its performance much improved on the $icoh$ subsets of the incongruent stimuli. It achieved accuracy $\geq$ 94.3% at theta, alpha and beta.

5.3 Summary

Classification is an important functionality in the data mining field and is extensively used for predicting data classes. This chapter made extensive use of EEG coherency (i.e., coherence, imaginary part of coherency) that is assessed in Chapters 3 and 4. In terms of supervised learning, coherency measures (coherence, imaginary part of coherency) were treated as training sets and passed to number of the Weka classifiers. The classifiers were implemented initially on the full attribute dataset comprising coherency measures (coherence, imaginary coherence). Subsequently, they were tested on attribute subsets extracted by the wrapper method.

Two different experiments were conducted in this chapter. In the first experiment, which considers mining the coherency data of Flanker stimuli per age group, the result shows that the classification results of the imaginary coherence datasets were much better than those of the coherence datasets. In particular, the Naïve Bayes classifier

was able to discriminate the Flanker congruent and incongruent stimuli at seven years of age with an accuracy of 90.9% at the alpha and beta bands. In addition, it achieved an accuracy ≥ 84.1% at nine years of age within beta and theta bands.

In the second experiment, which considers mining the coherency data of different age groups per Flanker stimuli type, the result suggests the imaginary coherence data of the incongruent stimuli for better classification. The Naïve Bayes is consistently the best classifier at all frequency bands. It reasonably classified the connectivity measures correctly as corresponding to seven or nine years of age with an accuracy ≥ 94.3% at the alpha, beta, and theta bands.

From the results of the two experiments on the coherency measures, the classification accuracy decreases on the nine-year-old datasets, possibly due to the influence of the brain development implied by the decline in the task conflict as addressed in [54] and [8].

Chapter 6

Conclusion and Future Works

6.1 Summary

This thesis considered the use of EEG coherency as a measure of brain network connectivity with the goal of detecting and localising the efficiency of the executive attention network (EAN). This novel method showed that the data-driven approach could provide significant results, which to some extent matches the previous reported findings.

In Chapter 2, the fundamental concepts of EAN were introduced. The ANT, the most widely used strategy in measuring the efficiency of the executive attention, was explained. It operationalises a conflict score based on behavioural changes that occur when the subject performs a task of conflict. The ANT findings provided insights into assessing and tracing the maturation process. Localising the conflict process is an important task, which may aid in diagnosing a variety of brain disorders. Therefore, the use of the ANT model is often combined with the use of a neuroimaging or electrophysiological technique to obtain a conflict's spatial information.

In modern theories, the integration of cerebral areas, which can be assessed by functional connectivity, is thought to underlie human cognition [12] [21] [22] [23] [24] [25]. The basics of EEG coherency as a measure of functional connectivity and some of its significant findings in this area were reviewed. Accordingly, the main contribution of this thesis is to investigate the use of EEG coherency analysis in

estimating and localising executive attention. This study examined the EEG data of seven- and nine-year-old children as they have shown significant behavioural and cognitive differences [54] [8] [127].

In Chapter 3, a new method, namely, accumulation was introduced to assess and localise the conflict process. It exploits the EEG coherence (i.e., magnitude-squared coherence) to evaluate conflict-related changes in brain synchronisation at the delta, theta, alpha and beta bands. It was built on the hypothesis that performing a task stimulus that induces a conflict causes different changes in brain network connectivity compared to a non-conflict stimulus. It also hypothesises that evaluating and localising these changes across a group of subjects can evaluate the conflict level. The results of the accumulation method showed that the EEG coherence successfully detects changes in the activity of brain regions regarding the conflict process in seven- and nine-year-old children. Regarding the topography comparison between the two age groups, a decline in the conflict effect was observed at nine-year-old group compared to seven-year-old group. However, the paired t-test was unable to associate the task conflict to particular brain regions similar to that which were identified by the accumulation method. This non-consistency in the findings are attributed to volume conduction, which refers to the possibility of capturing the activity of a single brain source by multiple EEG electrodes. Despite that, the results at this stage showed that EEG coherence is still useful since it can capture synchronisation changes regarding the induced conflict. Moreover, it presented evidence of the conflict decline as children mature.

In Chapter 4, to overcome the problem of volume conduction, the imaginary part of coherency was extracted. This quantity was found to be small or vanishing when the two signals being processed were recorded from a single brain source [35]. Applying similar methodology of employing steps such as those implemented on EEG coherence in Chapter 3, the imaginary part of coherency was utilised in assessing the efficiency of the EAN in seven- and nine-year-old children. Based on our examination, the imaginary part of coherency analysis is useful in studying cognitive conflict since the accumulation findings could be statically validated. It showed evidence of the development of the left part of the brain at seven years of age.

Furthermore, it showed that when children reach nine years of age, their cognition becomes more efficient in resolving conflict.

As discussed in Chapter 5, EEG coherency (i.e., coherence, imaginary part of coherency) assessed in Chapters 3 and 4 were mined. In particular, they were targeted by classification algorithms to investigate which measure can provide us with an excellent data source to differentiate the network connectivity. Two different experiments were conducted. In the first experiment, EEG coherency data of each age group were classified on stimuli type (i.e. congruent or incongruent). In the second experiment, they were classified on age group (i.e. seven- or nine-year-old). The results show that the measure of the imaginary coherence provided a good data source for classifying the different network connectivities. With this dataset, the classification algorithms were able to achieve significant accuracy in both experiments. Conflict effect in the imaginary coherence was discriminated with an accuracy of 90.9% at the alpha and beta bands at seven years of age. Moreover, at nine years of age, it was discriminated with an accuracy $\geq$ 84.1% at beta and theta bands. The classifiers achieved more accurate results in the second experiment. The imaginary coherence values that measured at the incongruent condition were successfully classified on the age group (i.e., seven- or nine-year-olds) with an accuracy $\geq$ 94.3% at the alpha, beta, and theta bands.

6.2 Future Works

1. Studying response-related changes

As explained in Chapter 3 (Subsection 3.2.2), EEG signals were segmented regarding the stimulus onset to investigate the effect of task conflict in the stimulus-related changes. In several developmental studies, such as [121], which was conducted on the same EEG data used in this thesis, useful neural indicators to particular cognitive developments were found in the response-related changes. In this respect, we suggest studying the conflict effect on response-related changes where we think this may reveal additional knowledge about the conflict process.

2. Matching epochs count

As discussed in Chapter 3 (Subsection 3.2.2), to compare coherency values of electrode pair at different conditions, epoch counts must be matched. Based on this, epoch counts of the task stimuli (i.e., congruent and incongruent) were matched at the level of the subject's EEG data (i.e., for each subject, congruent epochs were equalised to incongruent epochs) before calculating the coherence and the imaginary part of coherency. However, conflict-related changes in the coherency (i.e. difference matrix, dif) of each subject were thresholded by a statistical parameter (i.e. coherence deviation, σ), which was calculated based on the mean epoch counts of the age group (Chapter 3, Subsection 3.1.1). This thresholding process affects the accumulator of the proposed method, which only considers the significant values as defined by the σ. Therefore, for the future work, we suggest using a constant number of epochs from all subjects to eliminate any coherency bias regarding the σ.

3. Manipulating with classifiers parameters

In Chapter 5, as a broad assessment of the targeted classifiers, default values of the classifiers' parameters as implemented in Weka were used. However, we think extending this study to learn classifiers' parameters from the data is a potential means of increasing the efficiency of the classification algorithms.

References

[1] M. R. Rueda, P. Checa, and L. M. Combita, "Enhanced Efficiency of the Executive Attention Network after Training in Preschool Children: Immediate Changes and Effects after Two Months," *Developmental Cognitive Neuroscience*, vol. 2, pp. S192-S204, 2012.

[2] M. Rueda, M. Posner, M. Rothbart, and C. Davis-Stober, "Development of the Time Course for Processing Conflict: An Event-Related Potentials Study with 4 Year Olds and Adults," *BMC Neuroscience*, vol. 5, pp. 1-13, 2004.

[3] C. Blair and A. Ursache, "A Bidirectional Model of Executive Functions and Self-Regulation," *Handbook of self-regulation: Research, theory, and applications*, vol. 2, pp. 300-320, 2011.

[4] M. C. Welsh and B. F. Pennington, "Assessing Frontal Lobe Functioning in Children: Views from Developmental Psychology," *Developmental neuropsychology*, vol. 4, pp. 199-230, 1988.

[5] B. J. Casey, S. Durston, and J. A. Fossella, "Evidence for a Mechanistic Model of Cognitive Control," *Clinical Neuroscience Research*, vol. 1, pp. 267-282, 2001.

[6] A. Abundis-Gutiérrez, P. Checa, C. Castellanos, and M. Rosario Rueda, "Electrophysiological Correlates of Attention Networks in Childhood and Early Adulthood," *Neuropsychologia*, vol. 57, pp. 78-92, 2014.

[7] J. Fan, B. D. McCandliss, T. Sommer, A. Raz, and M. I. Posner, "Testing the Efficiency and Independence of Attentional Networks," *Journal of cognitive neuroscience*, vol. 14, pp. 340-347, 2002.

[8] M. R. Rueda, J. Fan, B. D. McCandliss, J. D. Halparin, D. B. Gruber, L. P. Lercari, *et al.*, "Development of Attentional Networks in Childhood," *Neuropsychologia*, vol. 42, pp. 1029-1040, 2004.

[9] M. R. Rueda, M. I. Posner, and M. K. Rothbart, "The Development of Executive Attention: Contributions to the Emergence of Self-Regulation," *Developmental neuropsychology*, vol. 28, pp. 573-594, 2005.

[10] M. R. Rueda, J. P. Pozuelos, and L. M. Cómbita, "Cognitive Neuroscience of Attention from Brain Mechanisms to Individual Differences in Efficiency," *AIMS Neuroscience* vol. 2, p. 20, 2015.

[11] W. Damon, R. M. Lerner, D. KUHN, and R. SIEGLER, *Handbook of Child Psychology : Cognition, Perception, and Language*, 6 ed. Hoboken: Wiley, 2006.

[12] J. O. N. Brock, C. C. Brown, J. Boucher, and G. Rippon, "The Temporal Binding Deficit Hypothesis of Autism," *Develop. Psychopathol.*, vol. 14, pp. 209-224, 2002.

[13] G. Tononi, G. M. Edelman, and O. Sporns, "Complexity and Coherency: Integrating Information in the Brain," *Trends in Cognitive Sciences*, vol. 2, pp. 474-484, 1998.

[14] H. Berger, "Über Das Elektrenkephalogramm Des Menschen," *European archives of psychiatry and clinical neuroscience*, vol. 98, pp. 231-254, 1933.

[15] L. F. Haas, "Hans Berger (1873–1941), Richard Caton (1842–1926), and Electroencephalography," *Journal of Neurology, Neurosurgery & Psychiatry*, vol. 74, p. 9, 2003.
[16] M. X. Cohen, *Analyzing Neural Time Series Data: Theory and Practice*, 1 ed. London, England: The MIT Press, 2014.
[17] W. Tatum, *Handbook of Eeg Interpretation*, 2. ed. New York: New York : Demos Medical Publishing, 2014.
[18] L. J. Otten and M. D. Rugg, "Interpreting Event-Related Brain Potentials," *Event-related potentials: A methods handbook*, pp. 3-16, 2005.
[19] B. Kopp, F. Rist, and U. Mattler, "N200 in the Flanker Task as a Neurobehavioral Tool for Investigating Executive Control," *Psychophysiology*, vol. 33, pp. 282-294, 1996.
[20] V. Van Veen and C. S. Carter, "The Timing of Action-Monitoring Processes in the Anterior Cingulate Cortex," *Journal of cognitive neuroscience*, vol. 14, pp. 593-602, 2002.
[21] V. Sakkalis, "Review of Advanced Techniques for the Estimation of Brain Connectivity Measured with Eeg/Meg," *Computers in Biology and Medicine*, vol. 41, pp. 1110-1117, 2011.
[22] J. Martino, S. M. Honma, A. M. Findlay, A. G. Guggisberg, J. P. Owen, H. E. Kirsch, *et al.*, "Resting Functional Connectivity in Patients with Brain Tumors in Eloquent Areas," *Annals of Neurology*, vol. 69, pp. 521-532, 2011.
[23] V. Francisco, L. Jean-Philippe, R. Eugenio, and M. Jacques, "The Brainweb: Phase Synchronization and Large-Scale Integration," *Nature Reviews Neuroscience*, vol. 2, p. 229, 2001.
[24] A. A. Fingelkurts and A. A. Fingelkurts, "Making Complexity Simpler: Multivariability and Metastability in the Brain," *International Journal of Neuroscience*, vol. 114, pp. 843-862, 2004.
[25] A. Pikovsky, M. Rosenblum, and J. Kurths, *Synchronization: A Universal Concept in Nonlinear Sciences* vol. 12: Cambridge university press, 2003.
[26] L. Dominguez, J. Stieben, J. Velazquez, and S. Shanker, "The Imaginary Part of Coherency in Autism: Differences in Cortical Functional Connectivity in Preschool Children: E75941," *PLoS ONE*, vol. 8, 2013.
[27] P. Flor-Henry and Z. Koles, "Eeg Studies in Depression, Mania and Normals: Evidence for Partial Shifts of Laterality in the Affective Psychoses," in *Clinical Neurophysiological Aspects of Psychopathological Conditions*, ed: Karger Publishers, 1980, pp. 21-43.
[28] P. Flor-Henry and Z. Koles, "Eeg Characteristics of Normal Subjects: A Comparison of Men and Women and of Dextrals and Sinistrals," *Research Communications in Psychology, Psychiatry & Behavior*, 1982.
[29] J. Gruzelier and P. Flor-Henry, *Hemisphere Asymmetries of Function in Psychopathology* Amsterdam: Amsterdam : Elsevier/North-Holland Biomedical Press, 1979.
[30] B. Sklar, J. Hanley, and W. W. Simmons, "An Eeg Experiment Aimed toward Identifying Dyslexic Children," *Nature*, vol. 240, p. 414, 1972.
[31] B. Sklar, J. Hanley, and W. W. Simmons, "A Computer Analysis of Eeg Spectral Signatures from Normal and Dyslexic Children," *Biomedical Engineering, IEEE Transactions on*, vol. BME-20, pp. 20-26, 1973.

[32] J. Montagu, "The Hyperkinetic Child: A Behavioural, Electrodermal and Eeg Investigation," *Developmental Medicine & Child Neurology,* vol. 17, pp. 299-305, 1975.
[33] D. M. Tucker, S. L. Dawson, D. L. Roth, and J. G. Penland, "Regional Changes in Eeg Power and Coherence During Cognition: Intensive Study of Two Individuals," *Behavioral neuroscience,* vol. 99, p. 564, 1985.
[34] E. Marosi, T. Harmony, L. Sánchez, J. Becker, J. Bernal, A. Reyes, *et al.*, "Maturation of the Coherence of Eeg Activity in Normal and Learning-Disabled Children," *Electroencephalography and clinical Neurophysiology,* vol. 83, pp. 350-357, 1992.
[35] G. Nolte, O. Bai, L. Wheaton, Z. Mari, S. Vorbach, and M. Hallett, "Identifying True Brain Interaction from Eeg Data Using the Imaginary Part of Coherency," *Clinical Neurophysiology,* vol. 115, pp. 2292-2307, 2004.
[36] B. R. Kar, *Cognition and Brain Development : Converging Evidence from Various Methodologies*. Washington, D.C.: Washington, D.C. : American Psychological Association, 2013.
[37] G. Butterworth, *Principles of Developmental Psychology : An Introduction*. Hoboken: Hoboken : Taylor and Francis, 2014.
[38] J. Piaget, "Part I: Cognitive Development in Children: Piaget Development and Learning," *Journal of research in science teaching,* vol. 2, pp. 176-186, 1964.
[39] D. H. Feldman, "Piaget's Stages: The Unfinished Symphony of Cognitive Development," *New Ideas in Psychology,* vol. 22, pp. 175-231, 2004.
[40] M. I. Posner, M. R. Rueda, and P. Kanske, "Probing the Mechanisms of Attention," in *Handbook of Psychophysiology:*, J. T. Cacioppo, L. G. Tassinary, and G. Berntson, Eds., ed Cambridge: Cambridge University Press, 2001, pp. 410-432.
[41] D. I. Shore, J. A. Burack, D. Miller, S. Joseph, and J. T. Enns, "The Development of Change Detection," *Developmental Science,* vol. 9, pp. 490-497, 2006.
[42] R. A. Rensink, "Change Detection," *Annual review of psychology,* vol. 53, pp. 245-277, 2002.
[43] M. W. Dye and D. Bavelier, "Differential Development of Visual Attention Skills in School-Age Children," *Vision research,* vol. 50, pp. 452-459, 2010.
[44] M. K. Rothbart and M. R. Rueda, "The Development of Effortful Control," *Developing individuality in the human brain: A tribute to Michael I. Posner,* pp. 167-188, 2005.
[45] M. I. Posner and S. E. Petersen, "The Attention System of the Human Brain," *Annual review of neuroscience,* vol. 13, pp. 25-42, 1990.
[46] J. T. Coull, C. D. Frith, R. S. J. Frackowiak, and P. M. Grasby, "A Fronto-Parietal Network for Rapid Visual Information Processing: A Pet Study of Sustained Attention and Working Memory," *Neuropsychologia,* vol. 34, pp. 1085-1095, 1996.
[47] R. T. Marrocco, E. A. Witte, and M. C. Davidson, "Arousal Systems," *Current Opinion in Neurobiology,* vol. 4, pp. 166-170, 1994.
[48] M. I. Posner, "Orienting of Attention," *Quarterly journal of experimental psychology,* vol. 32, pp. 3-25, 1980.

[49] G. Bush, P. Luu, and M. I. Posner, "Cognitive and Emotional Influences in Anterior Cingulate Cortex," *Trends in Cognitive Sciences,* vol. 4, pp. 215-222, 2000.
[50] A. W. Macdonald, J. D. Cohen, V. A. Stenger, and C. S. Carter, "Dissociating the Role of the Dorsolateral Prefrontal and Anterior Cingulate Cortex in Cognitive Control," *Science,* vol. 288, pp. 1835-1838, 2000.
[51] N. Akhtar and J. T. Enns, "Relations between Convert Orienting and Filtering in the Development of Visual Attention," *Journal of experimental child psychology,* vol. 48, pp. 315-334, 1989.
[52] L. M. Trick and J. T. Enns, "Lifespan Changes in Attention: The Visual Search Task," *Cognitive Development,* vol. 13, pp. 369-386, 1998.
[53] M. K. Rothbart, L. K. Ellis, M. Rosario Rueda, and M. I. Posner, "Developing Mechanisms of Temperamental Effortful Control," *Journal of personality,* vol. 71, pp. 1113-1144, 2003.
[54] J. P. Pozuelos, P. Paz-Alonso, A. Castillo, L. Fuentes, and M. Rueda, "Development of Attention Networks and Their Interactions in Childhood," *Dev. Psychol.,* vol. 50, pp. 2405-2415, 2014.
[55] J. D. Power, D. A. Fair, B. L. Schlaggar, and S. E. Petersen, "The Development of Human Functional Brain Networks," *Neuron,* vol. 67, pp. 735-748, 2010.
[56] P. Checa, R. Rodríguez-Bailón, and M. R. Rueda, "Neurocognitive and Temperamental Systems of Self-Regulation and Early Adolescents' Social and Academic Outcomes," *Mind, Brain, and Education,* vol. 2, pp. 177-187, 2008.
[57] M. R. Rueda, P. Checa, and M. K. Rothbart, "Contributions of Attentional Control to Socioemotional and Academic Development," *Early Education and Development,* vol. 21, pp. 744-764, 2010.
[58] N. Eisenberg, C. Valiente, and N. D. Eggum, "Self-Regulation and School Readiness," *Early Education and Development,* vol. 21, pp. 681-698, 2010.
[59] P. Checa and M. R. Rueda, "Behavioral and Brain Measures of Executive Attention and School Competence in Late Childhood," *Developmental Neuropsychology,* vol. 36, pp. 1018-1032, 2011.
[60] B. A. Eriksen and C. W. Eriksen, "Effects of Noise Letters Upon the Identification of a Target Letter in a Nonsearch Task," *Perception & psychophysics,* vol. 16, pp. 143-149, 1974.
[61] J. P. Lachaux, P. Fonlupt, P. Kahane, L. Minotti, D. Hoffmann, O. Bertrand, *et al.*, "Relationship between Task-Related Gamma Oscillations and Bold Signal: New Insights from Combined Fmri and Intracranial Eeg," *Human Brain Mapping,* vol. 28, pp. 1368-1375, 2007.
[62] J. P. Lachaux, P. Fonlupt, P. Kahane, L. Minotti, D. Hoffmann, O. Bertrand, *et al.*, "Relationship between Task- Related Gamma Oscillations and Bold Signal: New Insights from Combined Fmri and Intracranial Eeg," *Human Brain Mapping,* vol. 28, pp. 1368-1375, 2007.
[63] S. A. Huettel, A. W. Song, and G. McCarthy, *Functional Magnetic Resonance Imaging*: Freeman, 2009.
[64] S. H. Faro and F. B. Mohamed, *Bold Fmri : A Guide to Functional Imaging for Neuroscientists* New York, NY: New York, NY : Springer New York, 2010.

[65] D. L. Bailey, J. S. Karp, and S. Surti, "Physics and Instrumentation in Pet," in *Positron Emission Tomography : Basic Sciences* D. W. Townsend, P. E. Valk, M. N. Maisey, and SpringerLink, Eds., ed London: London : Springer London, 2005.

[66] J. Lewine and W. Orrison Jr, "Spike and Slow Wave Localization by Magnetoencephalography," *Neuroimaging clinics of north America,* vol. 5, pp. 575-596, 1995.

[67] Y. C. Okada, J. Wu, and S. Kyuhou, "Genesis of Meg Signals in a Mammalian Cns Structure," *Electroencephalography and clinical neurophysiology,* vol. 103, pp. 474-485, 1997.

[68] E. S. Schwartz, J. C. Edgar, W. C. Gaetz, and T. P. L. Roberts, "Magnetoencephalography," *Pediatric Radiology,* vol. 40, pp. 50-58, January 01 2010.

[69] K. Eggers, L. F. De Nil, and B. R. H. Van den Bergh, "The Efficiency of Attentional Networks in Children Who Stutter," *Journal of Speech, Language and Hearing Research (Online),* vol. 55, pp. 946-959, 2012.

[70] J. R. Evans and A. Abarbanel, *Introduction to Quantitative Eeg and Neurofeedback*: Elsevier, 1999.

[71] J. D. Kropotov, *Quantitative Eeg, Event-Related Potentials and Neurotherapy*. San Diego: Academic Press, 2009.

[72] W. R. Adey, D. O. Walter, and C. E. Hendrix, "Computer Techniques in Correlation and Spectral Analyses of Cerebral Slow Waves During Discriminative Behavior," *Experimental neurology,* vol. 3, pp. 501-24, 1961-Jun 1961.

[73] C. J. Stam, "Nonlinear Dynamical Analysis of Eeg and Meg: Review of an Emerging Field," *Clin Neurophysiol,* vol. 116, pp. 2266-301, Oct 2005.

[74] L. M. Pecora and T. L. Carroll, "Synchronization in Chaotic Systems," *Physical Review Letters,* vol. 64, pp. 821-824, 1990.

[75] M. G. Rosenblum, "Phase Synchronization of Chaotic Oscillators," *Physical review letters,* vol. 76, p. 1804, 1996.

[76] V. Sakkalis, C. D. Giurcaneanu, P. Xanthopoulos, M. E. Zervakis, V. Tsiaras, Y. Yang, *et al.*, "Assessment of Linear and Nonlinear Synchronization Measures for Analyzing Eeg in a Mild Epileptic Paradigm," *Ieee Transactions on Information Technology in Biomedicine,* vol. 13, pp. 433-441, Jul 2009.

[77] J. P. Lachaux, E. Rodriguez, J. Martinerie, and F. J. Varela, "Measuring Phase Synchrony in Brain Signals," *Human Brain Mapping,* vol. 8, pp. 194-208, 1999.

[78] A. Pikovsky, M. Rosenblum, and J. Kurths, *Synchronization : A Universal Concept in Nonlinear Sciences* Cambridge: Cambridge : Cambridge University Press, 2001.

[79] E. Pereda, R. Q. Quiroga, and J. Bhattacharya, "Nonlinear Multivariate Analysis of Neurophysiological Signals," *Progress in Neurobiology,* vol. 77, pp. 1-37, 2005.

[80] V. Sakkalis, "Review of Advanced Techniques for the Estimation of Brain Connectivity Measured with Eeg/Meg," *Comput Biol Med,* vol. 41, pp. 1110-7, Dec 2011.

[81] J. Arnhold, P. Grassberger, K. Lehnertz, and C. E. Elger, "A Robust Method for Detecting Interdependences: Application to Intracranially Recorded Eeg," *Physica D: Nonlinear Phenomena,* vol. 134, pp. 419-430, 1999.

[82] V. Sakkalis and M. Zervakis, "Linear and Nonlinear Synchronization Analysis and Visualization During Altered States of Consciousness," in *Recent Advances in Biomedical Engineering*, ed: InTech, 2009.

[83] M. A. Brazier and J. U. Casby, "Cross-Correlation and Autocorrelation Studies of Electroencephalographic Potentials," *Electroencephalogr Clin Neurophysiol,* vol. 4, pp. 201-11, May 1952.

[84] J. C. Shaw, "An Introduction to the Coherence Function and Its Use in Eeg Signal Analysis," *Journal of medical engineering & technology,* vol. 5, pp. 279-88, 1981.

[85] P. Stoica and R. L. Moses, *Spectral Analysis of Signals* Upper Saddle River, NJ: Upper Saddle River, NJ : Pearson Education, 2005.

[86] P. Welch, "The Use of Fast Fourier Transform for the Estimation of Power Spectra: A Method Based on Time Averaging over Short, Modified Periodograms," *Audio and Electroacoustics, IEEE Transactions on,* vol. 15, pp. 70-73, 1967.

[87] R. M. Lehembre, M.-A. P. Bruno, A. P. Vanhaudenhuyse, C. M. Chatelle, V. M. Cologan, Y. M. Leclercq, *et al.*, "Resting-State Eeg Study of Comatose Patients: A Connectivity and Frequency Analysis to Find Differences between Vegetative and Minimally Conscious States," *Functional Neurology,* vol. 27, pp. 41-7, 2014-03-07 2012.

[88] W. v. Drongelen, *Signal Processing for Neuroscientists : Introduction to the Analysis of Physiological Signals* Burlington, MA, USA Academic Press 2007.

[89] P. L. Nunez, R. Srinivasan, A. F. Westdorp, R. S. Wijesinghe, D. M. Tucker, R. B. Silberstein, *et al.*, "Eeg Coherency: I: Statistics, Reference Electrode, Volume Conduction, Laplacians, Cortical Imaging, and Interpretation at Multiple Scales," *Electroencephalography and Clinical Neurophysiology,* vol. 103, pp. 499-515, 1997.

[90] C. C. French and J. G. Beaumont, "A Critical Review of Eeg Coherence Studies of Hemisphere Function," *International Journal of Psychophysiology,* vol. 1, pp. 241-254, 1984.

[91] P. L. Nunez and R. Srinivasan, *Electric Fields of the Brain: The Neurophysics of Eeg*: Oxford University Press, USA, 2006.

[92] APA, *Diagnostic and Statistical Manual of Mental Disorders : Dsm-Iv-Tr*, 4th ed., text revision. ed. Washington, DC: Washington, DC : American Psychiatric Association, 2000.

[93] P. Barttfeld, B. Wicker, S. Cukier, S. Navarta, S. Lew, and M. Sigman, "A Big-World Network in Asd: Dynamical Connectivity Analysis Reflects a Deficit in Long-Range Connections and an Excess of Short-Range Connections," *Neuropsychologia,* vol. 49, pp. 254-263, 2011.

[94] M. Murias, S. J. Webb, J. Greenson, and G. Dawson, "Resting State Cortical Connectivity Reflected in Eeg Coherence in Individuals with Autism," *Biological psychiatry,* vol. 62, pp. 270-273, 2007.

[95] P. Sauseng, W. Klimesch, M. Schabus, and M. Doppelmayr, "Fronto-Parietal Eeg Coherence in Theta and Upper Alpha Reflect Central Executive Functions of Working Memory," *Int J Psychophysiol*, vol. 57, pp. 97-103, Aug 2005.

[96] B. Schack, W. Klimesch, and P. Sauseng, "Phase Synchronization between Theta and Upper Alpha Oscillations in a Working Memory Task," *International Journal of Psychophysiology*, vol. 57, pp. 105-114, 2005.

[97] J. I. Fleck, J. Kuti, J. Brown, J. R. Mahon, and C. Gayda-Chelder, "Frontal-Posterior Coherence and Cognitive Function in Older Adults," *International Journal of Psychophysiology*, vol. 110, pp. 217-230, 2016.

[98] J. M. Ford, M. Gray, W. O. Faustman, T. H. Heinks, and D. H. Mathalon, "Reduced Gamma-Band Coherence to Distorted Feedback During Speech When What You Say Is Not What You Hear," *International Journal of Psychophysiology*, vol. 57, pp. 143-150, 2005.

[99] S. Weiss and H. M. Mueller, "The Contribution of Eeg Coherence to the Investigation of Language," *Brain and Language*, vol. 85, pp. 325-343, 2003.

[100] M.-c. Cheung, A. S. Chan, and S. L. Sze, "Increased Theta Coherence During Chinese Reading," *International Journal of Psychophysiology*, vol. 74, pp. 132-138, 2009.

[101] C. Babiloni, F. Babiloni, F. Carducci, S. F. Cappa, F. Cincotti, C. Del Percio, *et al.*, "Human Cortical Rhythms During Visual Delayed Choice Reaction Time Tasks: A High-Resolution Eeg Study on Normal Aging," *Behavioural Brain Research*, vol. 153, pp. 261-271, 2004.

[102] H. Kondo, M. Morishita, N. Osaka, M. Osaka, H. Fukuyama, and H. Shibasaki, "Functional Roles of the Cingulo-Frontal Network in Performance on Working Memory," *Neuroimage*, vol. 21, pp. 2-14, 2004.

[103] F. Collette, E. Salmon, M. Van Der Linden, C. Chicherio, S. Belleville, C. Degueldre, *et al.*, "Regional Brain Activity During Tasks Devoted to the Central Executive of Working Memory," *Cognitive Brain Research*, vol. 7, pp. 411-417, 1999.

[104] R. W. Thatcher, R. A. Walker, and S. Giudice, "Human Cerebral Hemispheres Develop at Different Rates and Ages," *Science*, vol. 236, pp. 1110-1113, 1987.

[105] J. J. González, S. Mañas, L. De Vera, L. D. Méndez, S. López, J. M. Garrido, *et al.*, "Assessment of Electroencephalographic Functional Connectivity in Term and Preterm Neonates," *Clinical Neurophysiology*, vol. 122, pp. 696-702, 2011.

[106] T. Sander, A. Bock, S. Leistner, A. Kühn, and L. Trahms, "Coherence and Imaginary Part of Coherency Identifies Cortico-Muscular and Cortico-Thalamic Coupling," in *Engineering in Medicine and Biology Society (EMBC), 2010 Annual International Conference of the IEEE*, 2010, pp. 1714-1717.

[107] J. Han, *Data Mining : Concepts and Techniques*, 3rd ed.. ed. Burlington: Burlington : Elsevier Science, 2011.

[108] M. Bramer, *Principles of Data Mining* 2nd ed. 2013.. ed. London: London : Springer London : Imprint: Springer, 2013.

[109] S. Bandyopadhyay, *Classification and Learning Using Genetic Algorithms : Applications in Bioinformatics and Web Intelligence* Berlin, Heidelberg: Berlin, Heidelberg : Springer Berlin Heidelberg, 2007.

[110] O. Maimon and L. Rokach, *Data Mining and Knowledge Discovery Handbook*, 2nd ed.. ed. New York: New York : Springer, 2010.
[111] I. H. Witten, E. Frank, and M. A. Hall, *Data Mining : Practical Machine Learning Tools and Techniques.*, 3 ed. United States: Burlington, MA : Morgan Kaufmann, 2011.
[112] R. Rojas, *Neural Networks: A Systematic Introduction*: Springer Science & Business Media, 2013.
[113] V. N. Vapnik, *The Nature of Statistical Learning Theory* New York: New York : Springer, 1995.
[114] J. R. Quinlan, *C4.5 : Programs for Machine Learning* San Mateo, Calif.: San Mateo, Calif. : Morgan Kaufmann Publishers, 1993.
[115] X. Wu, *The Top Ten Algorithms in Data Mining*. Hoboken: Hoboken : Chapman & Hall/CRC, 2009.
[116] S. R. Safavian and D. Landgrebe, "A Survey of Decision Tree Classifier Methodology," 1990.
[117] G. Williams, *Data Mining with Rattle and R : The Art of Excavating Data for Knowledge Discovery*. New York, NY: New York, NY : Springer New York, 2011.
[118] L. Breiman, "Random Forests," *Machine learning,* vol. 45, pp. 5-32, 2001.
[119] T. K. Ho, "Random Decision Forests," in *Document Analysis and Recognition, 1995., Proceedings of the Third International Conference on*, 1995, pp. 278-282.
[120] B. Saltzbertg, W. D. Burton Jr, N. R. Burch, J. Fletcher, and R. Michaels, "Electrophysiological Measures of Regional Neural Interactive Coupling. Linear and Non-Linear Dependence Relationships among Multiple Channel Electroencephalographic Recordings," *International Journal of Bio-Medical Computing,* vol. 18, pp. 77-87, 1986.
[121] C. Richardson, M. Anderson, C. L. Reid, and A. M. Fox, "Neural Indicators of Error Processing and Intraindividual Variability in Reaction Time in 7 and 9 Year-Olds," *Developmental Psychobiology,* vol. 53, pp. 256-265, 2011.
[122] A. Delorme and S. Makeig, "Eeglab: An Open Source Toolbox for Analysis of Single-Trial Eeg Dynamics Including Independent Component Analysis," *Journal of Neuroscience Methods,* vol. 134, pp. 9-21, 2004.
[123] J. S. Bendat and A. G. Piersol, "Random Data Analysis and Measurement Procedures," *Measurement Science and Technology,* vol. 11, p. 1825, 2000.
[124] J. Stinstra and M. Peters, "The Volume Conductor May Act as a Temporal Filter on the Ecg and Eeg," *Medical and Biological Engineering and Computing,* vol. 36, pp. 711-716, 1998.
[125] T. H. Sander, A. Bock, S. Leistner, A. Kuhn, and L. Trahms, "Coherence and Imaginary Part of Coherency Identifies Cortico-Muscular and Cortico-Thalamic Coupling," *Conference proceedings : Annual International Conference of the IEEE Engineering in Medicine and Biology Society. ,* pp. 1714-1717, 2010.
[126] A. Ewald, L. Marzetti, F. Zappasodi, F. C. Meinecke, and G. Nolte, "Estimating True Brain Connectivity from Eeg/Meg Data Invariant to Linear and Static Transformations in Sensor Space," *NeuroImage,* vol. 60, pp. 476-488, 2012.

[127] M. Anderson, C. Reid, and J. Nelson, "Developmental Changes in Inspection Time: What a Difference a Year Makes," *Intelligence*, vol. 29, pp. 475-486, 2001.

Every reasonable effort has been made to acknowledge the owners of copyright material. I would be pleased to hear from any copyright owner who has been omitted or incorrectly acknowledged.